National Library of Canada | Bibliothèque nationale du Canada

CANADIAN THESES ON MICROFICHE | ***THÈSES CANADIENNES SUR MICROFICHE***

NAME OF AUTHOR *NOM DE L'AUTEUR* Thompson Andrew McMath

TITLE OF THESIS *TITRE DE LA THÈSE* Transmission measurement of the optical constants of thin solid films.

UNIVERSITY *UNIVERSITÉ* SIMON FRASER UNIVERSITY

DEGREE FOR WHICH THESIS WAS PRESENTED *GRADE POUR LEQUEL CETTE THÈSE FUT PRÉSENTÉE* Doctor of Philosophy

YEAR THIS DEGREE CONFERRED *ANNÉE D'OBTENTION DE CE GRADE* 1978

NAME OF SUPERVISOR *NOM DU DIRECTEUR DE THÈSE* Dr. J.C. Irwin

Permission is hereby granted to the NATIONAL LIBRARY OF CANADA to microfilm this thesis and to lend or sell copies of the film.

The author reserves other publication rights, and neither the thesis nor extensive extracts from it may be printed or otherwise reproduced without the author's written permission.

L'autorisation est, par la présente, accordée à la BIBLIOTHÈQUE NATIONALE DU CANADA de microfilmer cette thèse et de prêter ou de vendre des exemplaires du film.

L'auteur se réserve les autres droits de publication, ni la thèse ni de longs extraits de celle-ci ne doivent être imprimés ou autrement reproduits sans l'autorisation écrite de l'auteur.

DATED *DATÉ* August 16, 1978 SIGNED *SIGNÉ* _____

PERMANENT ADDRESS *RÉSIDENCE FIXE* [redacted]

NOTICE

The quality of this microfiche is heavily dependent upon the quality of the original thesis submitted for microfilming. Every effort has been made to ensure the highest quality of reproduction possible.

If pages are missing, contact the university which granted the degree.

Some pages may have indistinct print especially if the original pages were typed with a poor typewriter ribbon or if the university sent us a poor photocopy.

Previously copyrighted materials (journal articles, published tests, etc.) are not filmed.

Reproduction in full or in part of this film is governed by the Canadian Copyright Act, R.S.C. 1970, c. C-30. Please read the authorization forms which accompany this thesis.

THIS DISSERTATION
HAS BEEN MICROFILMED
EXACTLY AS RECEIVED

AVIS

La qualité de cette microfiche dépend grandement de la qualité de la thèse soumise au microfilmage. Nous avons tout fait pour assurer une qualité supérieure de reproduction.

S'il manque des pages, veuillez communiquer avec l'université qui a conféré le grade.

La qualité d'impression de certaines pages peut laisser à désirer, surtout si les pages originales ont été dactylographiées à l'aide d'un ruban usé ou si l'université nous a fait parvenir une photocopie de mauvaise qualité.

Les documents qui font déjà l'objet d'un droit d'auteur (articles de revue, examens publiés, etc.) ne sont pas microfilmés.

La reproduction, même partielle, de ce microfilm est soumise à la Loi canadienne sur le droit d'auteur, SRC 1970, c. C-30. Veuillez prendre connaissance des formules d'autorisation qui accompagnent cette thèse.

LA THÈSE A ÉTÉ
MICROFILMÉE TELLE QUE
NOUS L'AVONS REÇUE

TRANSMISSION MEASUREMENT OF THE OPTICAL CONSTANTS OF THIN SOLID FILMS

by

THOMPSON ANDREW MCMATH
B.Sc. QUEEN'S UNIVERSITY 1965
M.Sc. MCMASTER UNIVERSITY 1967

A THESIS SUBMITTED IN PARTIAL FULFILLMENT
OF THE REQUIREMENTS FOR THE DEGREE OF
DOCTOR OF PHILOSOPHY
in the Department
of
Physics

SIMON FRASER UNIVERSITY
JULY 1978

APPROVAL

Name: Thompson Andrew McMath

Degree: Doctor of Philosophy

Title of Thesis: Transmission Measurement of the Optical Constants of Thin Solid Films

Examining Committee:

Chairman: S. Gygax

J. C. Irwin
Senior Supervisor

J. F. Cochran
Examining Committee

R. F. Frindt
Examining Committee

A. E. Curzon
Examining Committee

J. L. Brebner
External Examiner
Professor of Physics
Universite de Montreal
Montreal, Que.

Date Approved: July 28, 1978

PARTIAL COPYRIGHT LICENSE

I hereby grant to Simon Fraser University the right to lend my thesis or dissertation (the title of which is shown below) to users of the Simon Fraser University Library, and to make partial or single copies only for such users or in response to a request from the library of any other university, or other educational institution, on its own behalf or for one of its users. I further agree that permission for multiple copying of this thesis for scholarly purposes may be granted by me or the Dean of Graduate Studies. It is understood that copying or publication of this thesis for financial gain shall not be allowed without my written permission.

Title of Thesis/Dissertation:

Transmission Measurement of the Optical Constants of Thin Solid Films

Author: _____

(signature)

Thompson Andrew McMATH

(name)

Aug 16 '78

(date)

ABSTRACT

A transmission interferometric technique has been developed for the measurement of the optical constants of thin solid films. A laser is used as the light source, and the phase shift and attenuation of light transmitted through a set of samples of different thickness are measured. Values of the refractive index n and extinction coefficient k are determined by fitting expressions for the phase shift and optical density as functions of thickness to the data. By using samples thick enough that the effects of multiple internal reflections can be neglected and fitting as a function of thickness, surface effects can be eliminated, and the results are representative of the bulk material.

The technique has been evaluated by measuring the optical constants of gold in the spectral range 459.7 to 632.8 nm, using several lines from an Ar ion laser and a HeNe laser. Evaporated films of thickness 41 to 241 nm were used. The measurements were in good agreement with previous results, and the technique is shown to be sufficiently accurate that it could be used to investigate the effects of surface layers.

Interferometer measurements were also made on thin crystals of GaSe, a weakly absorbing layer structure material which is optically uniaxial, with the optic axis perpendicular to the surfaces. GaSe has an absorption edge at 620 nm, and a tuneable dye laser was used for a detailed study of the optical constants in the vicinity of this edge. Both the ordinary and extraordinary constants were determined. The results were in excellent agreement with previous work. The dispersion curves of GaSe were also determined by the Butler fringe technique over a wide wavelength range. The refractive indices are obtained from the wavelengths of the maxima of fringes due to multiple internal reflections seen in transmission as the wavelength of the incident light is scanned. These measurements were made to corroborate previous work and provide a basis for comparison for the interferometer measurements.

ACKNOWLEDGEMENTS

I would like to thank my supervisor, Dr. J.C. Irwin, for his for his continued support, technical, moral, and financial. I thank the other members of my research committee, Dr. J.F. Cochran and Dr. R.F. Frindt, for their suggestions and advice, and I thank the other members of the group, particularly Dr. P.A.D. Hewko, for interference that was usually constructive. I thank Mr. Frank Wick and the others in the machine shop for making sense and reality out of my designs, and Mr. Wally Hall and the others in the electronics shop for their fast and efficient service. I thank Wylbur IBM 740-158 for assistance in typing the manuscript.

The financial support of the National Research Council of Canada and of Simon Fraser University are greatfully acknowledged.

Most of all, I thank Sharon, for the good times.

TABLE OF CONTENTS

LIST OF TABLES

LIST OF FIGURES

CHAPTER 1
INTRODUCTION

The interaction between electromagnetic radiation and matter is characterized by the optical constants of the material, the refractive index and extinction coefficient, or equivalently the real and imaginary parts of the dielectric constant. A detailed measurement of the values and variation of the optical constants over some range of energy provides information on such fundamental properties as the band structure of a material or the effects of impurities in crystals. Detailed and accurate knowledge of the optical constants is also required in such practical applications as the design of lens systems, fiber optics, and second harmonic generation.

Measurement of the optical properties can be difficult, particularly for highly absorbing materials such as metals and semiconductors for energies above the fundamental absorption edge. Many techniques for their measurement have evolved: see for example Abelès[1] or Heavens[2]. Reflection techniques are commonly used in all spectral ranges. A measurement of reflectivity as a function of energy at near normal incidence can yield both the real and imaginary parts through the Kramers-Kronig relations[3], but this requires measurements to be taken over a very wide (in principle infinite) spectral range. If the sample thickness is known, this requirement can be avoided by making simultaneous measurement of reflectivity and transmissivity at oblique incidence[2-5] but the analysis is considerably more involved. Ellipsometric techniques[2,3,6-9] involve irradiation of the sample with plane polarized light at a known angle of incidence and polarizing angle, and measurment of the elliptical polarization of the reflected light which results from the different reflectivities of the light components parallel and perpendicular to the plane of incidence.

The main difficulty with reflection techniques is their extreme sensitivity to the surface conditions of the sample. Small amounts of

oxidation or very thin adsorbed layers can produce spurious results, and great care must be taken in the preparation, handling, and storage of samples. In contrast, transmission measurements are very much less sensitive to surface conditions. The extinction coefficient is easily obtained from a measurement of the transmissivity of light through a sample of known thickness[10,11]. The refractive index can also be obtained easily from the wavelength and interference order of the multiple internal reflection fringes (Butler fringes) which result when white light is incident on a thin parallel-sided sample[11]. Until the advent of the laser, such measurements were restricted to transparent or very weakly absorbing materials, or to very thin metal films[12-15].

One of the most accurate techniques developed to date is that of Nestell and Christy[4], in which values of transmissivity at different angles of incidence are used in conjunction with reflectivity measurements to determine the optical constants. It does not take surface effects into account, but because of the use of transmission measurements this is not critical. This technique has been used by Johnson and Christy[16] to measure the optical constants of the noble metals. Very thin films evaporated on quartz substrates were used, and thus corrections for the substrates were required.

This thesis describes the development of a transmission interferometric technique[17-19] which is suitable for measuring the optical constants of fairly thick films (up to 250 nm) of highly absorbing materials. A tuneable dye laser is used as the light source, and thus detailed information can be obtained in the spectral range determined by the available dye. The amplitude reduction and the change in phase on transmission through the sample are measured simultaneously, and both the refractive index and extinction coefficient are determined. Data is collected for a set of samples of different thickness, and by fitting the data as a function of thickness, surface effects can be eliminated provided that these effects are consistant from sample to sample. Data is collected and processed on line by a PDP-11 computer.

Measurements with accuracy better than 1% for the refractive index values and a few percent for the extinction coefficients are achieved. The operation of the interferometer has been verified by comparison of measurements on gold films with measurements reported in the literature[16,20-22].

Measurements were also made on films of GaSe, a weakly absorbing layer structure with uniaxial anisotropy. The optical constants for both the ordinary and extraordinary rays were obtained as a function of wavelength through the fundamental absorption edge, as a test of the technique in a spectral range where the constants vary rapidly with wavelength. The refractive indices of GaSe were also measured over a wide spectral range using the Butler fringe technique[23,24]. These measurements were made to provide reference values for assessing the interferometer performance under these conditions and to confirm and extend the range of measurements reported in the literature[11,25-28]. Although the Butler fringe technique is much simpler in theory and practice than the interferometric technique, it can only be used with weakly absorbing materials, and it cannot provide detailed information in spectral regions where the optical properties vary rapidly.

In Chapter II, theoretical expressions are developed for the transmissivity, reflectivity, and phase changes on reflection and transmission when light is normally incident on a thin parallel-sided isotropic film. Propagation in anisotropic media is considered, and the expressions are extended for the special case of oblique incidence with polarization in the plane of incidence on a uniaxial film with the optic axis perpendicular to the surfaces. It is shown that these expressions lead to the much simpler equations used in analysing the Butler fringes. In Chapter III the techniques for the preparation and measurement of the samples are discussed. The principles and design of the interferometer and its operating procedure are described in detail. The handling of Butler fringe data is also discussed.

Methods of analysing the data are discussed in Chapter IV, and the results are compared with values reported in the literature. It is shown

that surface effects are not negligible for strongly absorbing films, and this is taken into account in the analysis on the assumption that the effects are consistent from sample to sample. The method is shown to be sufficiently accurate that a detailed study of surface effects could be undertaken on this basis. The techniques are assessed in Chapter V.

CHAPTER 2

TRANSMISSION OF LIGHT THROUGH A THIN FILM

2-1 Propagation of Electromagnetic Radiation in an Isotropic Medium

When electromagnetic radiation propagates in an unbounded medium, the electric and magnetic fields are related by Maxwell's equations: in Gaussian units,

$$\text{div } \vec{B} = 0 \qquad (1)$$

$$\text{div } \vec{D} = 4\pi\rho \qquad (2)$$

$$\text{curl } \vec{E} = -\frac{1}{c}\frac{\partial B}{\partial t} \qquad (3)$$

$$\text{curl } \vec{H} = \frac{1}{c}\frac{\partial D}{\partial t} + \frac{4\pi}{c}J \qquad (4)$$

The symbols have their usual meanings[2,29,30]. In an isotropic medium, the permeability, susceptibility, and conductivity are scalars, and thus $\vec{B} = \mu\vec{H}$, $\vec{D} = \epsilon\vec{E}$, and $\vec{J} = \sigma\vec{E}$. In a metal or a semiconductor with reasonably high carrier concentration we can also set the divergence of $\vec{D}$ equal to zero, since charge density variations induced by the fields will be neutralized with a relaxation time shorter than the period of oscillation at optical frequencies[30].

After substituting for $\vec{D}$, $\vec{B}$, and $\vec{J}$, $\vec{H}$ can be eliminated between equations (3) and (4) by taking the curl of (3) and then substituting from (4):

$$\nabla\times\nabla\times\vec{E} = -\frac{\mu}{c}\frac{\partial}{\partial t}(\nabla\times\vec{H})$$

$$\nabla^2\vec{E} = \frac{\mu\epsilon}{c^2}\frac{\partial^2\vec{E}}{\partial t^2} + \frac{4\pi\sigma\mu}{c^2}\frac{\partial\vec{E}}{\partial t} \qquad (5)$$

By eliminating $\vec{E}$ an identical equation in $\vec{H}$ results.

In a non-conducting medium ($\sigma = 0$) this reduces to the wave equation. The quantity $\frac{c}{\sqrt{\mu\epsilon}}$ is a constant which is characteristic of of the medium, with dimensions of velocity; $\sqrt{\mu\epsilon}$ is the refractive index n, the ratio of the velocity of the wave in vacuum to its velocity in the medium. The wave equation has the well-known plane wave solutions of the form

$$E = E_o e^{i(\omega t \pm \vec{q}\cdot\vec{r})} \qquad (6)$$

where the magnitude of the propagation vector $\vec{q}$ and the frequency ω are related by

$$q = \frac{\omega}{v} = \sqrt{\mu\epsilon}\frac{\omega}{c} = n\frac{\omega}{c} \qquad (7)$$

We assume that for a conducting medium equation (5) still has plane wave solutions of the form of (6). Substituting (6) in (5) and cancelling the common terms, we get

$$-q^2 = -\mu\epsilon\frac{\omega^2}{c^2} + i\frac{4\pi\sigma\mu\omega}{c^2} \qquad (8)$$

Thus it is seen that plane wave solutions for equation (5) still result provided that a complex propagation vector $\vec{q}$ is used. We can express this in terms of a complex dielectric constant:

$$\begin{aligned} q^2 &= \frac{\omega^2}{c^2}\mu\left(\epsilon - i\frac{4\pi\sigma}{\omega}\right) \\ &= \frac{\omega^2}{c^2}\mu\hat{\epsilon} \\ &= \frac{\omega^2}{c^2}\mu(\epsilon_1 - i\epsilon_2) \end{aligned} \qquad (9)$$

By analogy the complex refractive index is defined as

$$\hat{n} = n - ik = \sqrt{\mu\hat{\epsilon}} \qquad (10)$$

where n and k are real and non-negative. It is a good approximation to set $\mu = 1$ at optical frequencies, and thus $\hat{\epsilon} = \hat{n}^2$ or

$$\begin{aligned} \epsilon_1 &= n^2 - k^2 \\ \epsilon_2 &= 2nk \end{aligned} \qquad (11)$$

A wave propagating in the positive z-direction can now be described by

$$\begin{aligned} E &= E_0 e^{i(\omega t - q_z z)} \\ &= E_0 e^{-\frac{2\pi}{\lambda}kz}\, e^{i(\omega t - \frac{2\pi}{\lambda}nz)} \end{aligned} \qquad (12)$$

since $\hat{q} = \frac{\omega\hat{n}}{c} = \frac{2\pi}{\lambda}(n - ik)$

where λ is the wavelength of the radiation in vacuum.

Thus it is seen that the propagation of electromagnetic radiation in a material can be described in terms of a complex refractive index for the material. Although n and k are called the optical constants of the material, in general their values are dependent on the wavelength of the radiation. The real part n of the complex refractive index (often just called the refractive index) is the ratio of the wavelength of the radiation in vacuum to its wavelength in the material, the same relationship satisfied by the real refractive index for a transparent material. The imaginary part k is called the extinction coefficient and describes the damping of the wave: the amplitude is attenuated by a factor of $\exp(2\pi k)$ after traversing a distance of one vacuum wavelength in the medium. The reduction of intensity on passing through a thickness d is often described by the absorption coefficient α:

$$I = I_0 e^{-\alpha d} \qquad (13)$$

By comparison with (11) it is seen that α and k are related by

$$\alpha = \frac{4\pi k}{\lambda} \qquad (14)$$

So far the presence of boundaries between media has been ignored. When a wave encounters a boundary, part is reflected and part is refracted. If both media are transparent, the directions of the reflected and refracted waves are given by the law of reflection ($\theta_r = \theta_i$) and Snell's law ($n_1 \sin\theta_1 = n_2 \sin\theta_2$). However if one of the media is absorbing, the situation is more complicated. The attenuation of the wave is determined by the distance travelled in the medium, and thus planes of constant amplitude are parallel to the interface. Planes of constant phase are perpendicular to the direction of propagation. In general the two sets of planes are not parallel, and the wave is inhomogeneous. The angle of refraction is not given simply by using Snell's law with the real part of the complex refractive index[2,31]. A complex angle of refraction is sometimes defined by using Snell's law with the complex refractive index, which is equivalent to saying that $(\vec{q} \cdot \vec{r})$ is conserved at the interface. This approach is useful for calculating the field quantities, and is used below. Also in

general the relationship between α and k is much more complicated than that given by (14). For the special case of normal incidence the planes of constant amplitude are parallel to the planes of constant phase, and the simplicity is restored.

2-2 Light Normally Incident on a Thin Isotropic Film

We are primarily interested in calculating two quantities, the transmissivity (fraction of incident intensity transmitted) and the phase change on transmission for monochromatic light of wavelength normally incident on a thin parallel-sided film of thickness d which is suspended in air. We assume that the film is isotropic and is characterized by a complex refractive index $\hat{n}$, and that the interfaces between the film and air are mathematical planes.

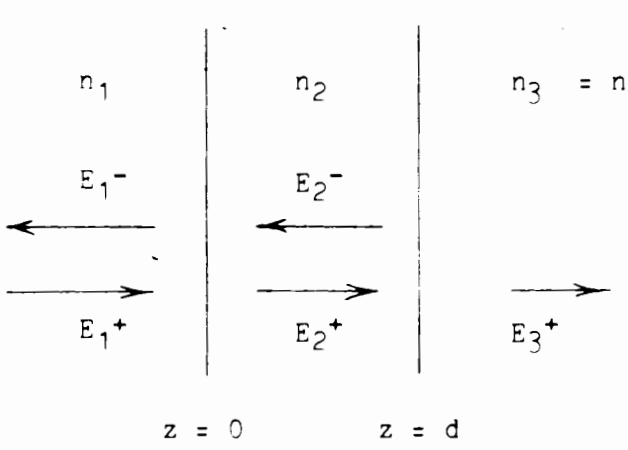

Fig. 1. The electric fields for light normally incident on a parallel-sided film of thickness d.

The notation and approach of Heavens[2] is followed, with some attention to Hadley and Dennison[32]. The system is shown schematically in Fig. 1. The surfaces divide the system into three regions, and the properties of particular regions are identified by the subscripts 1 to 3. The coordinate system is chosen such that the surfaces are perpendicular to the z-direction, with one surface at

$z = 0$ and the other at $z = d$. The incident light is travelling in the positive z-direction. Waves travelling to the right or left are indicated by + or - superscripts respectively. Although the refractive index of air is close to 1, it is left in explicitly for generality. The refractive index in region 2 is referred to as $\hat{n}$ without a subscript.

$$\text{Let } \frac{2\pi n_1}{\lambda} = \frac{\omega n_1}{c} = q_1 \tag{15}$$

$$\frac{2\pi \hat{n}}{\lambda} = \frac{\omega}{c}(n - ik) = \hat{q}_2 \tag{16}$$

Using the relationship $H = \frac{c}{\omega}\vec{q} \times \vec{E}$ the z-dependent parts of the fields $\vec{E}$ and $\vec{H}$ in the three regions can be written as

$$E_1 = E_1^{+}e^{-iq_1z} + E_1^{-}e^{+iq_1z} \tag{17}$$

$$H_1 = n_1\left(E_1^{+}e^{-iq_1z} - E_1^{-}e^{+iq_1z}\right) \tag{18}$$

$$E_2 = E_2^{+}e^{-i\hat{q}_2z} + E_2^{-}e^{+i\hat{q}_2z} \tag{19}$$

$$H_2 = \hat{n}\left(E_2^{+}e^{-i\hat{q}_2z} - E_2^{-}e^{+i\hat{q}_2z}\right) \tag{20}$$

$$E_3 = E_3^{+}e^{-iq_1z} \tag{21}$$

$$H_3 = n_1E_3^{+}e^{-iq_1z} \tag{22}$$

The conditions that the tangential components of $\vec{E}$ and $\vec{H}$ must be continuous across the boundaries are now applied:

at $z = 0$

$$E_1 = E_2 \implies E_1^{+} + E_1^{-} = E_2^{+} + E_2^{-} \tag{23}$$

$$H_1 = H_2 \implies n_1(E_1^{+} - E_1^{-}) = \hat{n}(E_2^{+} - E_2^{-}) \tag{24}$$

at $z = d$

$$E_2 = E_3 \implies E_2^{+}e^{-i\hat{q}_2d} + E_2^{-}e^{+i\hat{q}_2d} = E_3^{+} \tag{25}$$

$$H_2 = H_3 \implies \hat{n}\left(E_2^{+}e^{-i\hat{q}_2d} - E_2^{-}e^{+i\hat{q}_2d}\right) = n_1E_3^{+} \tag{26}$$

The phase in region 3 is determined by the sum of waves in region 2 at the second interface. Thus no explicit phase term is included in the field in region 3; this is just a choice of origin.

The amplitude reflection coefficient r and amplitude transmission coefficient t can now be obtained by solving the determinants of coefficients:

$$r = \frac{E_1^-}{E_1^+} = \frac{(\hat{n}^2 - n_1^2)\left(e^{-i\hat{q}_2 d} - e^{+i\hat{q}_2 d}\right)}{(\hat{n}+n_1)^2 e^{+i\hat{q}_2 d} - (\hat{n}-n_1)^2 e^{-i\hat{q}_2 d}} \qquad (27)$$

$$t = \frac{E_3^+}{E_1^+} = \frac{4\hat{n}n_1}{(\hat{n}+n_1)^2 e^{+i\hat{q}_2 d} - (\hat{n}-n_1)^2 e^{-i\hat{q}_2 d}} \qquad (28)$$

Using (16) the exponential term can be written as

$$e^{\pm i\hat{q}_2 d} = e^{\pm i\frac{2\pi nd}{\lambda}} \; e^{\pm\frac{2\pi kd}{\lambda}}$$

$$= e^{\pm K}(\cos N \pm i \sin N) \qquad (29)$$

where $K = \frac{2\pi kd}{\lambda}$ and $N = \frac{2\pi nd}{\lambda}$

It is seen that e^{-K} is the attenuation and N the phase change for a ray traversing the sample, not including any internal reflections or any phase change which may occur at a surface.

It is convenient to express r and t as complex numbers in the form

$$r = \frac{A + iB}{C + iD} = \frac{AC + BD}{C^2 + D^2} + i\,\frac{BC - AD}{C^2 + D^2} \qquad (30)$$

$$t = \frac{4n_1(n - ik)}{C + iD} = \frac{4n_1(nC - kD)}{C^2 + D^2} - i\,\frac{4n_1(nD + kC)}{C^2 + D^2} \qquad (31)$$

From these equations, the phase changes on reflection and transmission are

$$\phi_r = \arctan\left[\frac{BC - AD}{AC + BD}\right] \qquad (32)$$

$$\phi_t = \arctan\left[\frac{-nD - kC}{nC - kD}\right] \qquad (33)$$

The signs are left as they are to make the part of the computer program which tests for the quadrant of the phase angle more obvious.

Solving for A, B, C, and D, we obtain

$$A = \left[(n_1^2 - n^2 + k^2)\cos N - 2nk \sin N\right] e^{K} - \left[(n_1^2 - n^2 + k^2)\cos N + 2nk \sin N\right] e^{-K} \quad (34)$$

$$B = \left[(n_1^2 - n^2 + k^2)\sin N + 2nk \cos N\right] e^{K} + \left[(n_1^2 - n^2 + k^2)\sin N - 2nk \cos N\right] e^{-K} \quad (35)$$

$$C = \left\{\left[(n + n_1)^2 - k^2\right]\cos N + 2(n + n_1)k \sin N\right\} e^{K} - \left\{\left[(n - n_1)^2 - k^2\right]\cos N - 2(n - n_1)k \sin N\right\} e^{-K} \quad (36)$$

$$D = \left\{\left[(n + n_1)^2 - k^2\right]\sin N - 2(n + n_1)k \cos N\right\} e^{K} + \left\{\left[(n - n_1)^2 - k^2\right]\sin N + 2(n - n_1)k \cos N\right\} e^{-K} \quad (37)$$

The reflectivity and transmissivity are

$$R = rr^{*} = \frac{A^2 + B^2}{C^2 + D^2}$$

$$= \frac{(F_5^2 + 4n^2k^2)(e^{2K} + e^{-2K} - 2\cos 2N)}{F_1^2 e^{2K} + F_2^2 e^{-2K} + 8n_1 k F_3 \sin 2N - F_4 \cos 2N} \quad (38)$$

$$T = \frac{n_3}{n_1} tt^{*} = \frac{16n_1^2(n^2 + k^2)}{C^2 + D^2}$$

$$= \frac{16n_1^2(n^2 + k^2)}{F_1^2 e^{2K} + F_2^2 e^{-2K} + 8n_1 k F_3 \sin 2N - F_4 \cos 2N} \quad (39)$$

$$= \frac{16n_1^2(n^2 + k^2)}{P_o} \quad (39a)$$

where the F coefficients are defined in terms of n and k:

$$F_1 = (n + n_1)^2 + k^2 \quad (40)$$

$$F_2 = (n - n_1)^2 + k^2 \quad (41)$$

$$F_3 = n^2 - n_1^2 + k^2 \quad (42)$$

$$F_4 = 2(F_3^2 - 4n_1^2k^2) \quad (43)$$

$$F_5 = n^2 - n_1^2 - k^2 \quad (44)$$

These expressions for R and T are equivalent to those worked out by Hadley and Dennison[32]. They show, particularly for T, the exponential dependence on k, d, and $1/\lambda$, and the sinusoidal variation with n, d, and $1/\lambda$. The phase shifts can also be expressed in terms

of the F's to facilitate computer programming:

$$\phi_r = \arctan\left[\frac{2n_1kF_1e^{2K} - 2n_1kF_2e^{-2K} - 4nn_1F_3\sin 2N - 8nn_1^2k\cos 2N}{-F_1F_3e^{2K} - F_2F_3e^{-2K} - 2n_1k(F_1+F_2)\sin 2N + 2(n^2+k^2)^2\cos 2N}\right] \quad (45)$$

$$\phi_t = \arctan\left[\frac{-(nF_1+2n_1k^2)e^{K}\sin N-(nF_2-2n_1k^2)e^{-K}\sin N+kF_3(e^{K}-e^{-K})\cos N}{(nF_1+2n_1k^2)e^{K}\cos N-(nF_2-2n_1k^2)e^{-K}\cos N+kF_3(e^{K}+e^{-K})\sin N}\right] \quad (46)$$

$$= \arctan(P_1/P_2) \quad (46a)$$

We have now established the desired formulas for R, T, ϕ_r, and ϕ_t for light normally incident on a suspended film in terms of the film thickness d and refractive index $\hat{n} = n - ik$, and the incident wavelength λ. The optical constants n and k can be determined from measurements of these quantities. The approach has differed slightly from that of Heavens[2] and Born and Wolf[30], in that we have determined r and t directly from the ratio of fields without introducing the Fresnel coefficients for reflection and transmission at a single interface. That approach permits easier extension of the calculations to multiple layer systems; however, in both of these references the final expressions are for fields within a transparent substrate, i.e. they have not been extended to include the emergence of the light into the ambient. The present expression is the full solution for a single suspended film.

2-3 Transmission in the Thick Film Limit

The expressions developed above are considerably simplified if the absorption in the film is sufficiently strong that the effects of multiple internal reflections can be neglected. This will be true if the portion of the beam which is reflected from the back surface is very much weaker on returning to the back surface (i.e. after two additional traversals of the film) than the transmitted portion of the original beam. Mathematically the condition is that the product kd is sufficiently large that $\exp(-4\pi kd/\lambda) \ll 1$. At the front surface the field component E_2^- is now much smaller than E_2^+

so equations (23) and (24) reduce to

$$E_1^+ + E_1^- = E_2^+ \tag{47}$$

$$n_1(E_1^+ - E_1^-) = \hat{n}E_2^+ \tag{48}$$

Solving the determinants of coefficients now gives

$$t = \frac{E_3^+}{E_1^+} = \frac{4\hat{n}n_1}{(\hat{n}+n_1)^2} e^{-i\frac{2\pi\hat{n}d}{\lambda}}$$

$$= \frac{4\hat{n}n_1}{(\hat{n}+n_1)^2} e^{-\frac{2\pi kd}{\lambda}} e^{-i\frac{2\pi nd}{\lambda}} \tag{49}$$

and $$T = \frac{16n_1(n^2+k^2)}{F_1^2} e^{-\frac{4\pi kd}{\lambda}} \tag{50}$$

Now if t is rewritten as

$$t = Ae^{i\phi} e^{-\frac{2\pi kd}{\lambda}} e^{-i\frac{2\pi nd}{\lambda}}$$

then the phase shift can be written as

$$\phi_t = \phi - \frac{2\pi nd}{\lambda} \tag{51}$$

We also define the optical density of a film as

$$O.D. = \log_{10}\left(\frac{1}{T}\right) = \log_{10}(\text{const.}) - \frac{4\pi kd}{\lambda}\log_{10}e \tag{52}$$

From (51) and (52) it is seen that the variations with sample thickness of phase shift and optical density are $-\frac{2\pi d}{\lambda}$ and $-\frac{4\pi d}{\lambda}\log_{10}e$ respectively. Thus by measuring the phase shift and optical density on transmission for a set of samples which are sufficiently thick that multiple internal reflections are negligible, the optical constants n and k are easily obtained.

2-4 Propagation in an Anisotropic Medium

The propagation of electromagnetic radiation in anisotropic media is considerably more complicated. Maxwell's equations (1) to (4) still apply, but since the properties of the medium depend on the direction of propagation the permeability and conductivity must be written in tensor notation ϵ_{ij} and σ_{ij} (we assume that $\mu = 1$ at optical frequencies). The tensors are symmetric even for anisotropic materials[33]; thus they can be put in diagonal form, and the material is characterized by three

principal values. The principal axes of the conductivity and permeability tensors are not generally the same, but they coincide for materials with orthorhombic or higher symmetry[30]. We thus write

$$D_\ell = \epsilon_\ell E_\ell \quad \text{and} \quad J_\ell = \sigma_\ell E_\ell \tag{53}$$

or by including the conductivity terms in a complex dielectric constant as above,

$$\hat{D}_\ell = \hat{\epsilon}_\ell E_\ell \tag{54}$$

It is convenient to use $\vec{\hat{n}}$ as a modified propagation vector (recall $\vec{q} = \frac{\omega}{c}\vec{\hat{n}}$). Assuming plane wave solutions of the form (6) still hold for Maxwell's equations, in this notation equations (3) and (4) can be expressed (for propagation in the +z direction)

$$\vec{n} \times \vec{H} = -\vec{D} \tag{55}$$

$$\vec{n} \times \vec{E} = \vec{H} \tag{56}$$

These equations show that $\vec{n}$, $\vec{H}$, and $\vec{D}$ are mutually perpendicular, and that $\vec{H}$ and $\vec{E}$ are perpendicular, but $\vec{\hat{n}}$ is not necessarily perpendicular to $\vec{E}$. Also $\vec{n}$, $\vec{E}$, and $\vec{D}$ are coplanar since they are all perpendicular to $\vec{H}$. To determine the relationship between $\hat{\epsilon}_\ell$ and $\hat{n}$ we first eliminate $\vec{H}$ from (55) and (56) to get

$$\vec{D} = \hat{n}^2\vec{E} - (\vec{\hat{n}}.\vec{E})\vec{\hat{n}} \tag{57}$$

By writing (57) in component form using (54), and eliminating the field components $\vec{E}_\ell$ the complex Fresnel equation is obtained:

$$\hat{n}^2\left(\hat{\epsilon}_x\hat{n}_x^2 + \hat{\epsilon}_y\hat{n}_y^2 + \hat{\epsilon}_z\hat{n}_z^2\right) + \hat{\epsilon}_x\hat{\epsilon}_y\hat{\epsilon}_z - \hat{n}_x^2\hat{\epsilon}_x(\hat{\epsilon}_y+\hat{\epsilon}_z) - \hat{n}_y^2\hat{\epsilon}_y(\hat{\epsilon}_x+\hat{\epsilon}_z) - \hat{n}_z^2\hat{\epsilon}_z(\hat{\epsilon}_x+\hat{\epsilon}_y) = 0 \tag{58}$$

where $\hat{n}_x$, $\hat{n}_y$, and $\hat{n}_z$ are complex components of the wave vector $\vec{\hat{n}}$. This equation defines the complex wave vector surface, and contains the dispersion since the components $\hat{\epsilon}_\ell$ are functions of frequency. It is quadratic in $\hat{n}^2$, and thus there are two different complex values of $\hat{n}^2$ for each direction of propagation (solutions corresponding to +n and -n represent identical waves propagating in opposite directions). A quadrant cross-section of a general wave surface for a transparent material is shown in Fig. 2a. The distances from the origin to the two parts of the surface give the two values of n. The surface is symmetric about planes defined by any two principal axes.

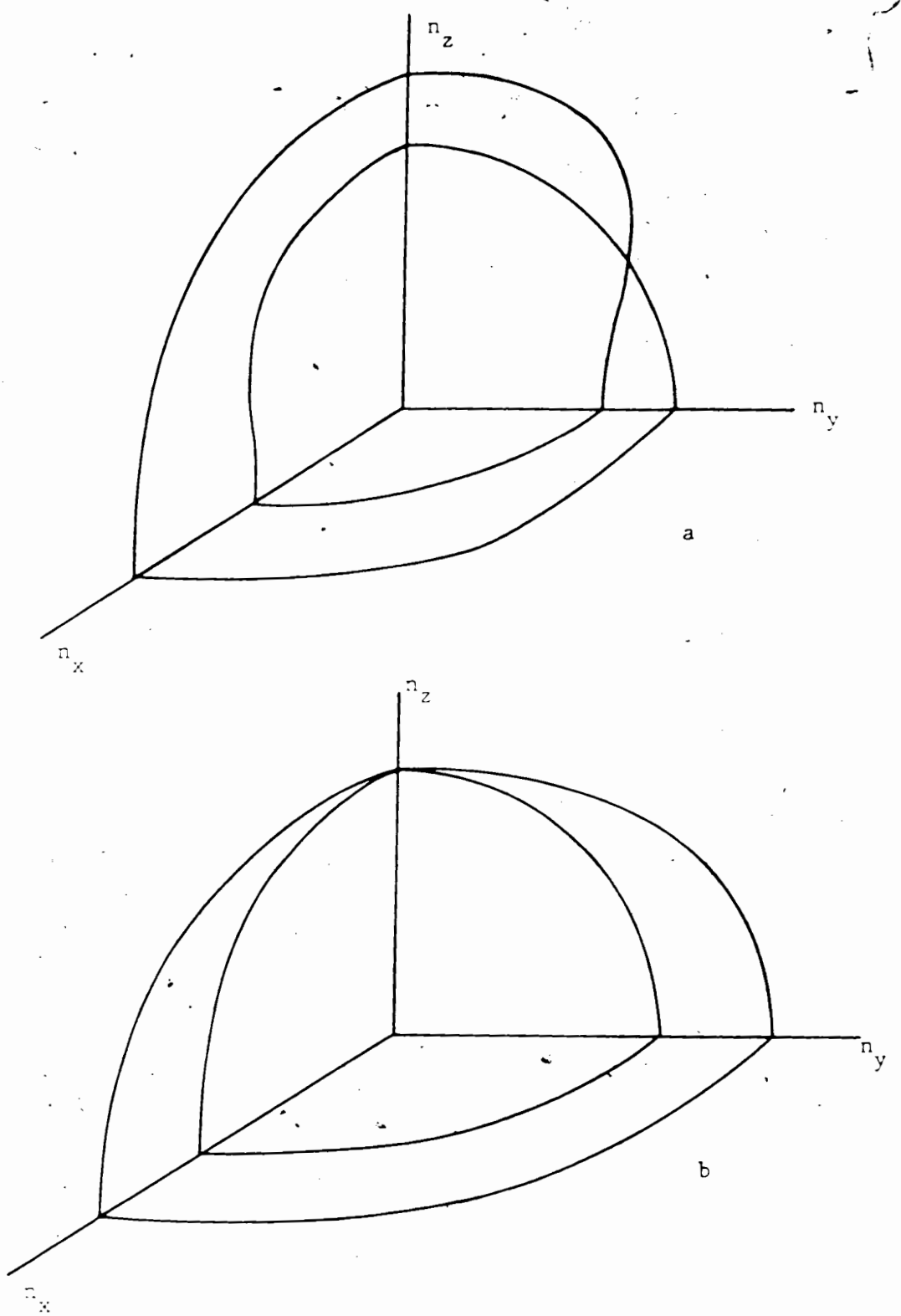

Fig. 2. Quadrant cross-sections of (a) a general wave surface, (b) the wave surfaces for a uniaxial crystal. These surfaces are for transparent materials, and are shown here as a visual aid.

It is also convenient to introduce the complex ray vector $\vec{s}$, whose direction is that of the Poynting vector (coplanar with $\vec{E}$, $\vec{D}$, and $\vec{n}$) and whose magnitude is given by $\vec{n}.\vec{s} = 1$. The length of $\vec{s}$ is proportional to the phase of the wave, and if all vectors $\vec{s}$ are considered, their tips generate a surface of constant phase. The utility of this surface comes from the fact that the direction of the wave normal is the direction of the maximum rate of change of phase, i.e. $\vec{n}$ is parallel to the normal to the ray surface at the point where the associated ray vector $\vec{s}$ intersects the surface. The converse is also true: the ray vector $\vec{s}$ is parallel to the normal to the wave surface at the point where $\vec{n}$ intersects it. This can be seen from the derivative of the condition $\vec{n}.\vec{s} = 1$, which is $\vec{n}.d\vec{s} + \vec{s}.d\vec{n} = 0$. Since the ray vector increment $d\vec{s}$ must lie in the tangent plane to the ray surface at $\vec{s}$, and this is perpendicular to $\vec{n}$, both terms must be zero. It can also be shown that if we interchange $\vec{E}$ with $\vec{D}$, $\vec{n}$ with $\vec{s}$, and $\hat{\epsilon}$ with $1/\hat{\epsilon}$ then any equation valid in one set of quantities is also valid in the other set[31,33]. This property is used to define the complex ray surface as the analogue of equation (58). It is quadratic in $\hat{s}^2$, implying that two complex roots correspond to each direction of $\vec{s}$. Thus in general two rays with different wave vectors propagate in any direction through the crystal. The orientation of the vectors and the relation between a section of the wave surface and the ray surface in coordinates $\hat{n}_x$, $\hat{n}_y$, and $\hat{n}_z$ for a transparent material are shown in Fig. 3.

For any direction in a transparent medium these two waves are completely linearly polarized[30,33], and the directions of polarization are perpendicular to each other. This in not strictly true in an absorbing medium, but is a very good approximation if the absorption is weak[30]. If the wave propagates with $\vec{n}$ in a principal plane defined by any two of the principal axes $\hat{\epsilon}_i$, then the $\vec{D}$ vectors of the two waves will be in or perpendicular to the principal plane; similarly if the ray vector $\vec{s}$ is in a principal plane then one wave will have $\vec{E}$ in the principal plane and the other wave will have $\vec{E}$ perpendicular to it.

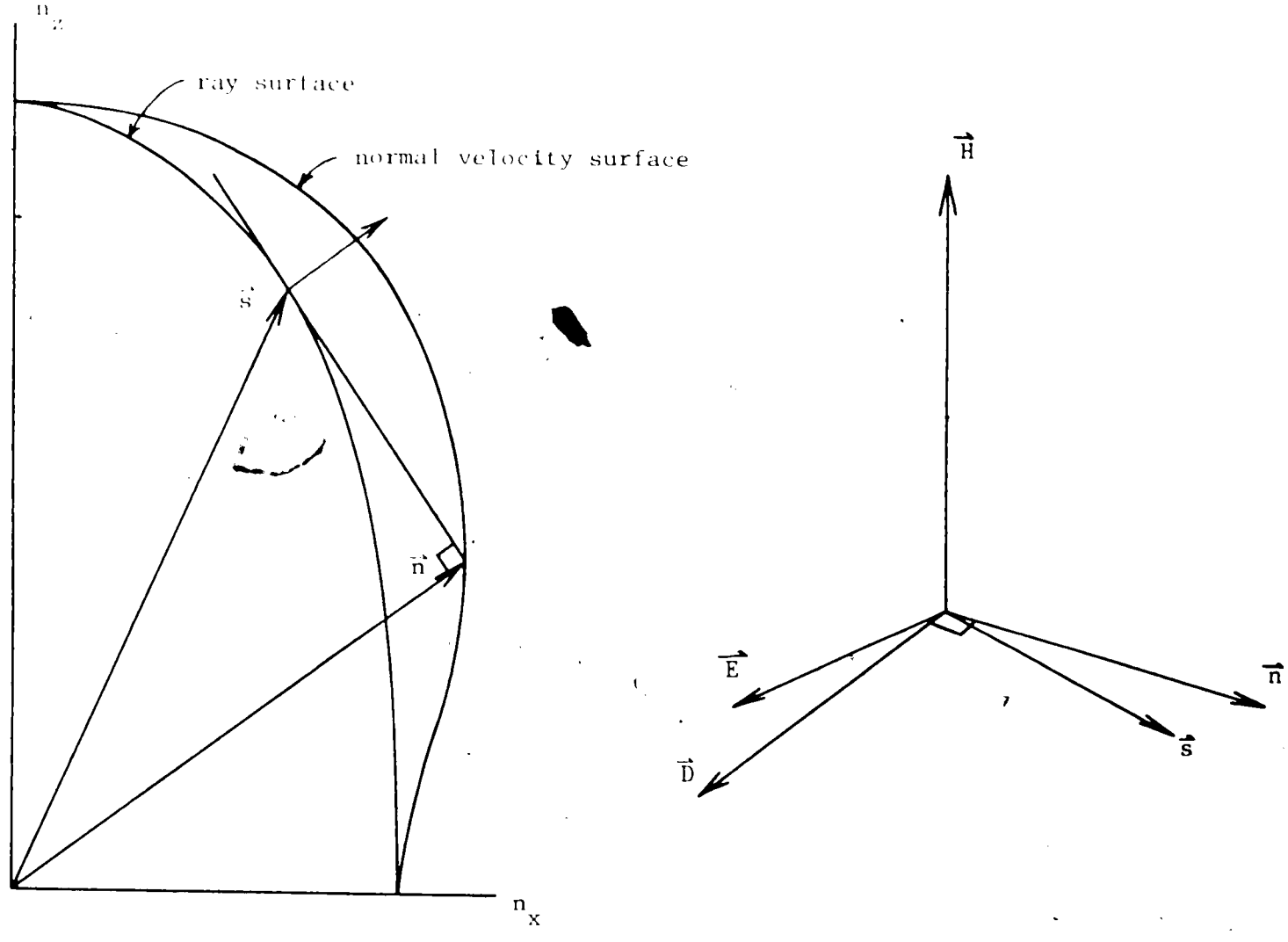

Fig. 3. The relation between a section of the wave surface and ray surface, and the orientation of the vectors

2-4-1 Uniaxial Crystals

The optical properties of a crystal depend on the symmetry of the dielectric tensor, which must remain unchanged by those symmetry operations which leave the crystal structure unchanged. Crystals with two or more crystallographically equivalent directions in one plane (other than cubic crystals) are optically uniaxial; they have a preferred direction, the optic axis, which is parallel to the axis of 3-, 4-, or 6-fold symmetry[30,33]. Thus trigonal, tetragonal, and hexagonal crystals are optically uniaxial.

If the z-axis is taken along the optic axis, and the x-axis in the principal plane defined by $\vec{\hat{n}}$ and the optic axis, then we can set $\hat{\epsilon}_x = \hat{\epsilon}_y = \hat{\epsilon}_\perp$ and $\hat{\epsilon}_z = \hat{\epsilon}_\parallel$. Now Fresnel's equation (58) becomes

$$(\hat{n}^2 - \hat{\epsilon}_\perp)\left[\hat{\epsilon}_\parallel \hat{n}_z^2 + \hat{\epsilon}_\perp(\hat{n}_x^2 + \hat{n}_y^2) - \hat{\epsilon}_\parallel \hat{\epsilon}_\perp\right] = 0 \qquad (59)$$

From this equation it is seen that the two complex values for $\hat{n}$ are given by the equations

$$\hat{n}^2 = \hat{\epsilon}_\perp \qquad (60)$$

$$\frac{\hat{n}_z^2}{\hat{\epsilon}_\perp} + \frac{(\hat{n}_x^2 + \hat{n}_y^2)}{\hat{\epsilon}_\parallel} = 1 \qquad (61)$$

Thus for a uniaxial crystal the fourth-order wave surface becomes two separate surfaces, a complex sphere and a complex ellipsoid, as shown in Fig. 2b. The two surfaces intersect on the z-axis at the same value of $\hat{n}_z$. Two types of wave propagate:

-- The ordinary wave, corresponding to equation (60), is independent of direction. The ordinary ray vector is given by the analogous equation to (60); $\hat{s}_o^2 = 1/\hat{\epsilon}_\perp$, and $\hat{n}_o \hat{s}_o = 1 = \vec{\hat{n}}_o \cdot \vec{\hat{s}}_o$. Thus $\vec{\hat{n}}$ and $\vec{\hat{s}}$ are collinear for the ordinary wave, which implies that $\vec{E}$ and $\vec{D}$ are also collinear; the wave behaves like a wave propagating in an isotropic medium. For any direction of propagation this wave is polarized perpendicular to the principal plane defined by n and the optic axis, since it depends only on $\hat{\epsilon}_\perp$.

-- The extraordinary wave, corresponding to equation (61), depends on both $\hat{\epsilon}_\perp$ and $\hat{\epsilon}_\parallel$, and on the angle θ_t that $\hat{n}_e$ makes with the optic axis. Dividing (61) by $\hat{n}_e^2$ we get

$$\frac{1}{\hat{n}_e^2} = \frac{\sin^2\theta_t}{\hat{\epsilon}_\parallel} + \frac{\cos^2\theta_t}{\hat{\epsilon}_\perp} \qquad (62)$$

For the extraordinary wave $\vec{D}$ must be polarized in the principal plane, and therefore $\vec{s}_e$ and $\vec{E}_e$ must also be in this plane since they are coplanar with $\vec{D}$ and perpendicular to $\vec{H}$. Also $\vec{s}_e$ and $\vec{E}_e$ do not coincide with $\vec{n}_e$ and $\vec{D}_e$ except for the special case of propagation along the optic axis, in which case the ordinary and extraordinary waves are indistinguishable.

2-5 Light Obliquely Incident on a Uniaxial Film

We wish to obtain the ordinary and extraordinary refractive indices and extinction coefficients for a uniaxial crystal. We will consider only the case of a thin parallel-sided crystal with the optic axis perpendicular to the surfaces, thus the plane of incidence coincides with the principal plane defined by the direction of propagation and the optic axis. It was shown above that a wave propagating with $\vec{E}$ perpendicular to the principal plane is the ordinary wave. This wave depends only on the ordinary parameters n_o and k_o. Since the optic axis is perpendicular to the surface, measurements made at normal incidence always correspond to the ordinary wave, and no further information can be gained by making measurements at oblique incidence with the radiation polarized perpendicular to the plane of incidence. We thus restrict our attention to radiation polarized in the plane of incidence, corresponding to the extraordinary wave. To simplify the notation, we omit the e subscript. We will also assume that the medium in which the film is suspended has a refractive index of 1 rather than leaving it general.

We define refractive indices $\hat{n}_\perp$ and $\hat{n}_\parallel$ by

$$\hat{n}_\perp^2 = \hat{\epsilon}_\perp \quad \text{and} \quad n_\parallel^2 = \hat{\epsilon}_\parallel \qquad (63)$$

Note that these refractive indices refer to specific directions in the

crystal, i.e. with the $\vec{D}$-vector perpendicular or parallel to the optic axis. In contrast, $\hat{n}_x$, $\hat{n}_y$, and $\hat{n}_z$ are complex components of the propagation vector $\vec{\hat{n}} = \frac{c}{\omega} q$ and they therefore depend on the direction of propagation in the crystal. The ordinary index $\hat{n}_o$ is often used interchangeably with $\hat{n}_\perp$, and the extraordinary index $\hat{n}_e$ with $\hat{n}_{//}$. This is permissable for the ordinary index, but is misleading for the extraordinary index, whose value changes with the direction of propagation. The index $\hat{n}_{//}$ refers to the specific case of propagation in a direction perpendicular to the optic axis with the $\vec{D}$-vector parallel to the axis, and is the limiting case of the extraordinary index $\hat{n}_e$. Incorrect terminology is usually obvious from the context.

2-5-1 Refraction at an Interface

It was shown above that $\vec{\hat{n}}$, $\vec{\hat{s}}$, $\vec{E}$, and $\vec{D}$ are coplanar for the extraordinary wave. By considering Huygen's construction (Fig. 4) and the symmetry of the ray surface as viewed along the plane of incidence, it is seen that if any two principal axes of the dielectric tensor are in the plane of incidence then both $\vec{\hat{n}}$ and $\vec{\hat{s}}$ will also be in this plane. Thus for a uniaxial crystal with the optic axis perpendicular to the surface, if the incident radiation is polarized in the plane of incidence the refracted wave will also be polarized in this plane; this is not true in general. The reflected wave is also polarized in this plane. Since $(\vec{\hat{q}}.\vec{r})$ must be continuous, the arguments of the exponential factors in the incident, reflected, and refracted waves must be the same at the interface. This leads to the laws of reflection and refraction:

$$\sin\theta_i = \sin\theta_r$$
$$\sin\theta_i = \hat{n} \sin\theta_t = \hat{n}_x \qquad (64)$$

For an absorbing medium, Snell's law includes a complex refractive index and angle of refraction.

We also need to know the angle that the ray vector makes with the optic axis, since $\vec{E}$ is perpendicular to $\vec{\hat{s}}$ rather than to $\vec{\hat{n}}$. This angle will be denoted θ_s. To find it we make use of the fact that the ray direction is parallel to the normal of the wave velocity

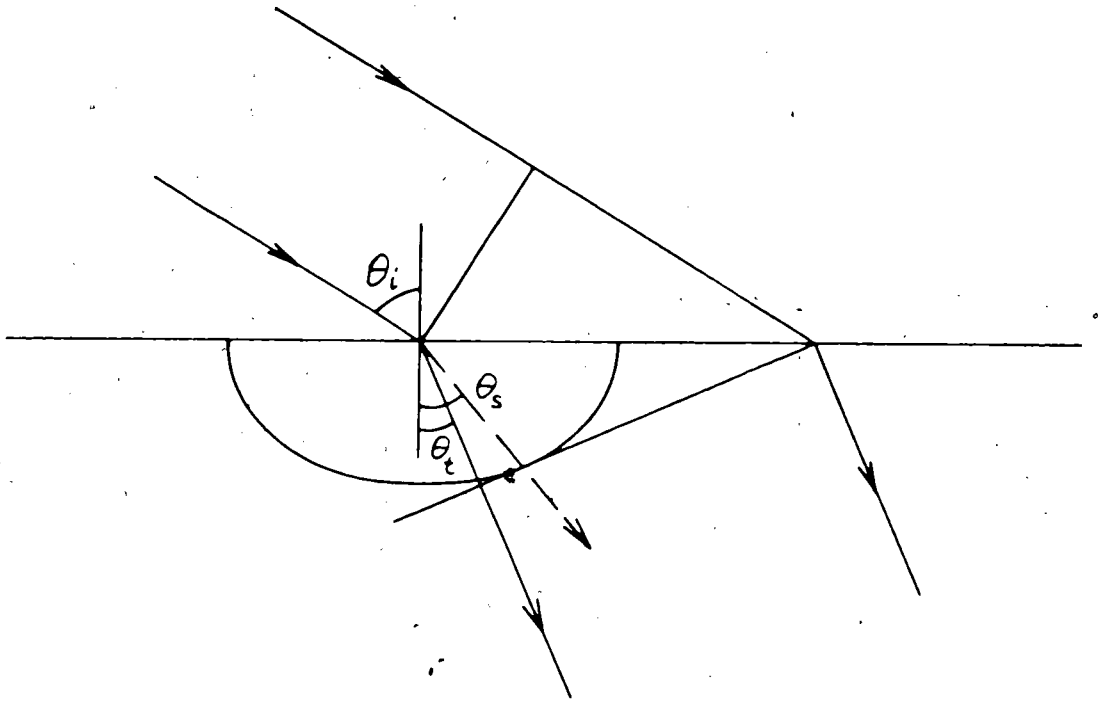

Fig. 4. Huygens' construction, showing the extraordinary wave and ray directions for a uniaxial crystal with the optic axis perpendicular to the surface.

surface at the point where the wave normal vector $\vec{\hat{n}}$ intersects it. The wave velocity surface is given by equation (61), and its normal by the gradient of (61):

$$\vec{i}\,\frac{2\hat{n}_x}{\hat{\epsilon}_{\parallel}} + \vec{j}\,\frac{2\hat{n}_y}{\hat{\epsilon}_{\parallel}} + \vec{k}\,\frac{2\hat{n}_z}{\hat{\epsilon}_{\perp}} \;/\!/\; \vec{i}\,\hat{s}_x + \vec{j}\,\hat{s}_y + \vec{k}\,\hat{s}_z \qquad (65)$$

Thus if the plane of incidence is the x-z plane,

$$\tan\theta_s = \frac{\hat{s}_x}{\hat{s}_z} = \frac{\hat{\epsilon}_{\perp}\hat{n}_x}{\hat{\epsilon}_{\parallel}\hat{n}_z} = \frac{\hat{\epsilon}_{\perp}}{\hat{\epsilon}_{\parallel}}\tan\theta_t \qquad (66)$$

The angle θ_s can be expressed in terms of the angle of incidence: using (61) and (64)

$$\hat{n}_z = \sqrt{\frac{\hat{\epsilon}_{\parallel} - \hat{n}_x^2}{\hat{\epsilon}_{\parallel}}\hat{\epsilon}_{\perp}} = \sqrt{\frac{\hat{\epsilon}_{\perp}}{\hat{\epsilon}_{\parallel}}(\hat{\epsilon}_{\parallel} - \sin^2\theta_i)} \qquad (67)$$

$$\text{thus} \quad \tan\theta_s = \sqrt{\frac{\hat{\epsilon}_{\perp}\sin^2\theta_i}{\hat{\epsilon}_{\parallel}^2 - \hat{\epsilon}_{\parallel}\sin^2\theta_i}} \qquad (68)$$

From this we also obtain

$$\sin\theta_s = \sqrt{\frac{\hat{\epsilon}_{\perp}\sin^2\theta_i}{\hat{\epsilon}_{\parallel}^2 + (\hat{\epsilon}_{\perp} - \hat{\epsilon}_{\parallel})\sin^2\theta_i}} \qquad (69)$$

$$\cos\theta_s = \sqrt{\frac{\hat{\epsilon}_{\parallel}^2 - \hat{\epsilon}_{\parallel}\sin^2\theta_i}{\hat{\epsilon}_{\parallel}^2 + (\hat{\epsilon}_{\perp} - \hat{\epsilon}_{\parallel})\sin^2\theta_i}} \qquad (70)$$

2-5-2 Transmission of the Extraordinary Wave

We wish to calculate the transmissivity and phase change on transmission of a wave incident on a thin uniaxial film (whose optic axis is perpendicular to the surfaces) at an oblique angle, when the wave is polarized in the plane of incidence. The transmitted portion of the wave will propagate in the crystal as the extraordinary wave. The system is shown schematically in Fig. 5. The coordinates are chosen with the z-axis perpendicular to the surface (parallel to the optic axis) and the x-axis in the plane of incidence.

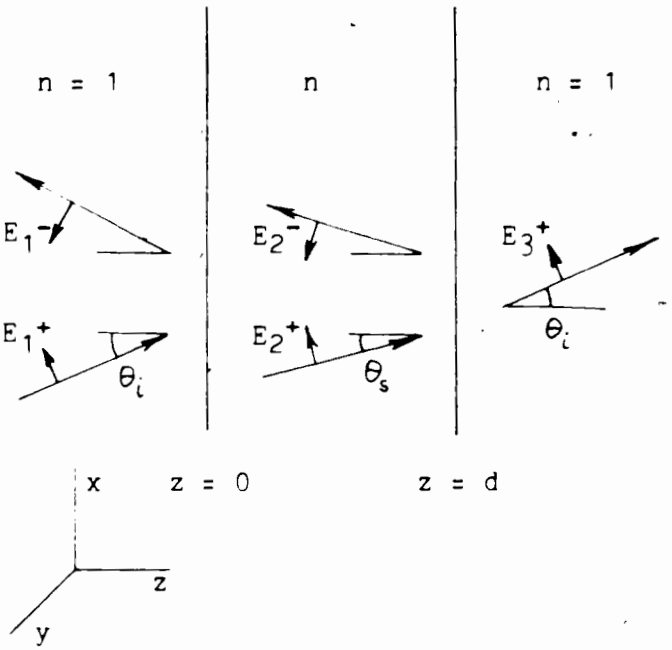

Fig. 5. The configuration of electric fields for light obliquely incident on a parallel-sided film of thickness d, polarized in the plane of incidence.

We assume plane wave solutions of the form (6). The z-dependent parts of the x- and z-components of the resultant fields in each of the three regions are given by

$$E_{1x} = \left(E_1^+ e^{-iq_{1z}z} - E_1^- e^{+iq_{1z}z}\right) \cos\theta_i \tag{71}$$

$$D_{1z} = E_{1z} = \left(-E_1^+ e^{-iq_{1z}z} - E_1^- e^{+iq_{1z}z}\right) \sin\theta_i \tag{72}$$

$$E_{2x} = \left(E_2^+ e^{-i\hat{q}_{2z}z} - E_2^- e^{+i\hat{q}_{2z}z}\right) \cos\theta_s \tag{73}$$

$$D_{2z} = \left(-D_2^+ e^{-i\hat{q}_{2z}z} - D_2^- e^{+i\hat{q}_{2z}z}\right) \sin\theta_t$$

$$= \hat{\epsilon}_{\perp} E_{2z} = \hat{\epsilon}_{\perp}\left(-E_2^+ e^{-i\hat{q}_{2z}z} - E_2^- e^{+i\hat{q}_{2z}z}\right) \sin\theta_s \tag{74}$$

$$E_{3x} = E_3^+ e^{-iq_{1z}z} \cos\theta_i \tag{75}$$

$$D_{3z} = E_{3z} = -E_3^+ e^{-iq_{1z}z} \sin\theta_i \tag{76}$$

Now applying the boundary conditions that $\vec{E}$ tangential and $\vec{D}$ normal are

continuous across the interfaces,

at z = 0

$$\left(E_1^+ - E_1^-\right)\cos\theta_i = \left(E_2^+ - E_2^-\right)\cos\theta_s \tag{77}$$

$$\left(-D_1^+ - D_1^-\right)\sin\theta_i = \left(-D_2^+ - D_2^-\right)\sin\theta_t$$

or

$$\left(E_1^+ + E_1^-\right)\sin\theta_i = \hat{\epsilon}_{\prime\prime}\left(E_2^+ + E_2^-\right)\sin\theta_s \tag{78}$$

at z = d

$$\left(E_2^+ e^{-i\hat{q}_{2z}d} - E_2^- e^{+i\hat{q}_{2z}d}\right)\cos\theta_s = E_3^+\cos\theta_i \tag{79}$$

$$\hat{\epsilon}_{\prime\prime}\left(E_2^+ e^{-i\hat{q}_{2z}d} + E_2^- e^{+i\hat{q}_{2z}d}\right)\sin\theta_s = E_3^+\sin\theta_i \tag{80}$$

As above the phase in region 3 is determined by the conditions in region 2 and no explicit phase term has been included with E_3^+. Again solving the determinant of coefficients using Cramer's rule the amplitude reflection and transmission coefficients for polarization in the plane of incidence are obtained:

$$r_{\prime\prime} = \frac{\left(\cos^2\theta_s\sin^2\theta_i - \hat{\epsilon}_{\prime\prime}^2\sin^2\theta_s\cos^2\theta_i\right)\left(e^{-i\hat{q}_{2z}d} - e^{+i\hat{q}_{2z}d}\right)}{\left(\hat{\epsilon}_{\prime\prime}\sin\theta_s\cos\theta_i + \cos\theta_s\sin\theta_i\right)^2 e^{+i\hat{q}_{2z}d} - \left(\hat{\epsilon}_{\prime\prime}\sin\theta_s\cos\theta_i - \cos\theta_s\sin\theta_i\right)^2 e^{-i\hat{q}_{2z}d}} \tag{81}$$

$$t_{\prime\prime} = \frac{4\,\hat{\epsilon}_{\prime\prime}\sin\theta_s\cos\theta_s\sin\theta_i\cos\theta_i}{\left(\hat{\epsilon}_{\prime\prime}\sin\theta_s\cos\theta_i + \cos\theta_s\sin\theta_i\right)^2 e^{+i\hat{q}_{2z}d} - \left(\hat{\epsilon}_{\prime\prime}\sin\theta_s\cos\theta_i - \cos\theta_s\sin\theta_i\right)^2 e^{-i\hat{q}_{2z}d}} \tag{82}$$

If we substitute for $\sin\theta_s$ and $\cos\theta_s$ using equations (68) and (69) then all angles are expressed in terms of the incident angle θ_i. To simplify the notation the subscript i will be dropped. We now obtain for the amplitude reflection and transmission coefficients

$$r_{//} = \frac{\left(\hat{n}_\perp^2\cos^2\theta - 1 + \frac{\sin^2\theta}{\hat{n}_{//}^2}\right)\left(e^{-i\hat{q}_{2z}d} - e^{+i\hat{q}_{2z}d}\right)}{\left[2\cos\theta\left(\frac{\hat{n}_\perp}{\hat{n}_{//}}\right)\sqrt{\hat{n}_{//}^2 - \sin^2\theta} + \left(\hat{n}_\perp^2\cos^2\theta + 1 - \frac{\sin^2\theta}{n_{//}^2}\right)\right] e^{+i\hat{q}_{2z}d}} \quad (83)$$
$$+ \left[2\cos\theta\left(\frac{\hat{n}_\perp}{\hat{n}_{//}}\right)\sqrt{n_{//}^2 - \sin^2\theta} - \left(\hat{n}_\perp^2\cos^2\theta + 1 - \frac{\sin^2\theta}{n_{//}^2}\right)\right] e^{-i\hat{q}_{2z}d}$$

$$t_{//} = \frac{4\cos\theta\left(\frac{\hat{n}_\perp}{\hat{n}_{//}}\right)\sqrt{n_{//}^2 - \sin^2\theta}}{\left[2\cos\theta\left(\frac{\hat{n}_\perp}{\hat{n}_{//}}\right)\sqrt{\hat{n}_{//}^2 - \sin^2\theta} + \left(\hat{n}_\perp^2\cos^2\theta + 1 - \frac{\sin^2\theta}{\hat{n}_{//}^2}\right)\right] e^{+i\hat{q}_{2z}d}} \quad (84)$$
$$+ \left[2\cos\theta\left(\frac{\hat{n}_\perp}{\hat{n}_{//}}\right)\sqrt{\hat{n}_{//}^2 - \sin^2\theta} - \left(\hat{n}_\perp^2\cos^2\theta + 1 - \frac{\sin^2\theta}{\hat{n}_{//}^2}\right)\right] e^{-i\hat{q}_{2z}d}$$

From the definition of $\vec{\hat{q}}$ the exponent can be expressed

$$\hat{q}_{2z}d = \frac{2\pi\hat{n}_z d}{\lambda} = \frac{2\pi d}{\lambda}\left(\frac{\hat{n}_\perp}{\hat{n}_{//}}\right)\sqrt{\hat{n}_{//}^2 - \sin^2\theta} \quad (85)$$

At this point to simplify further calculations it is convenient to define some complex numbers:

$$\left.\begin{matrix}\alpha - i\beta \\ \gamma - i\delta\end{matrix}\right\} = \hat{n}_\perp^2\cos^2\theta \left\{\begin{matrix}+ \\ -\end{matrix}\right\} \left(1 - \frac{\sin^2\theta}{\hat{n}_{//}^2}\right) \quad (86)$$

$$\eta - i\nu = \frac{\hat{n}_\perp}{\hat{n}_{//}}\sqrt{\hat{n}_{//}^2 - \sin^2\theta} \quad (87)$$

The exponential term now becomes

$$e^{\pm i q_{2z}d} = e^{\pm i\frac{2\pi d}{\lambda}(\eta - i\nu)}$$
$$= e^{\pm K_{//}}(\cos N_{//} \pm i\sin N_{//}) \quad (88)$$

where $N_{//} = \frac{2\pi\eta d}{\lambda}$ and $K_{//} = \frac{2\pi\nu d}{\lambda}$

Substituting $\hat{n}_\perp = n_\perp - ik_\perp$ and $\hat{n}_{//} = n_{//} - ik_{//}$ and solving for the real and imaginary parts of the complex numbers, we obtain

$$\left.\begin{matrix}\alpha \\ \gamma\end{matrix}\right\} = (n_\perp^2 - k_\perp^2)\cos^2\theta \left\{\begin{matrix}+ \\ -\end{matrix}\right\} \left(1 - \frac{(n_{//}^2 - k_{//}^2)\sin^2\theta}{(n_{//}^2 + k_{//}^2)^2}\right) \quad (89)$$

$$\left.\begin{matrix}\beta \\ \delta\end{matrix}\right\} = 2n_\perp k_\perp\cos^2\theta \left\{\begin{matrix}+ \\ -\end{matrix}\right\} \frac{2n_{//}k_{//}\sin^2\theta}{(n_{//}^2 + k_{//}^2)^2} \quad (90)$$

$$\eta = \frac{a(n_\perp n_{//} + k_\perp k_{//}) + b(n_\perp k_{//} - n_{//} k_\perp)}{n_{//}^2 + k_{//}^2} \qquad (91)$$

$$\nu = \frac{a(-n_\perp k_{//} + n_{//} k_\perp) + b(n_\perp n_{//} + k_\perp k_{//})}{n_{//}^2 + k_{//}^2} \qquad (92)$$

$$\text{with } \left.\begin{matrix} a \\ b \end{matrix}\right\} = \frac{1}{\sqrt{2}}\left[\sqrt{(n_{//}^2 - k_{//}^2 - \sin^2\theta)^2 + 4n_{//}^2 k_{//}^2}\left\{\begin{matrix} + \\ - \end{matrix}\right\}(n_{//}^2 - k_{//}^2 - \sin^2\theta)\right]^{\frac{1}{2}} \qquad (93)$$

The terms α, β, γ, δ, η, ν, a, and b are all real, and are defined in terms of the (real) refractive indices and extinction coefficients and the angle of incidence. As above we can express $r_{//}$ and $t_{//}$ as complex numbers in the form

$$r_{//} = \frac{A_{//} + iB_{//}}{C_{//} + iD_{//}} = \frac{A_{//} C_{//} + B_{//} D_{//}}{C_{//}^2 + D_{//}^2} + i\frac{B_{//} C_{//} - A_{//} D_{//}}{C_{//}^2 + D_{//}^2} \qquad (94)$$

$$t_{//} = \frac{4\cos\theta(\eta - i\nu)}{C + iD}$$

$$= \frac{4\cos\theta(\eta C_{//} - \nu D_{//})}{C_{//}^2 + D_{//}^2} - i\frac{4\cos\theta(\eta D_{//} + \nu C_{//})}{C_{//}^2 + D_{//}^2} \qquad (95)$$

The phase changes on reflection and transmission are

$$\phi_{r_{//}} = \arctan\left[\frac{B_{//} C_{//} - A_{//} D_{//}}{A_{//} C_{//} + B_{//} D_{//}}\right] \qquad (96)$$

$$\phi_{t_{//}} = \arctan\left[\frac{-\eta D_{//} - \nu C_{//}}{\eta C_{//} - \nu D_{//}}\right] \qquad (97)$$

Solving for $A_{//}$, $B_{//}$, $C_{//}$, and $D_{//}$ we get

$$A_{//} = -\left[\gamma\cos N_{//} + \delta\sin N_{//}\right]e^{K_{//}} + \left[\gamma\cos N_{//} - \delta\sin N_{//}\right]e^{-K_{//}} \qquad (98)$$

$$B_{//} = \left[\delta\cos N_{//} - \gamma\sin N_{//}\right]e^{K_{//}} - \left[\gamma\cos N_{//} + \delta\sin N_{//}\right]e^{-K_{//}} \qquad (99)$$

$$C_{//} = \left[(2\eta\cos\theta + \alpha)\cos N_{//} + (2\nu\cos\theta + \beta)\sin N_{//}\right]e^{K_{//}}$$
$$+ \left[(2\eta\cos\theta - \alpha)\cos N_{//} - (2\nu\cos\theta - \beta)\sin N_{//}\right]e^{-K_{//}} \qquad (100)$$

$$D_{//} = \left[-(2\nu\cos\theta + \beta)\cos N_{//} + (2\eta\cos\theta + \alpha)\sin N_{//}\right]e^{K_{//}}$$
$$- \left[(2\nu\cos\theta - \beta)\cos N_{//} + (2\eta\cos\theta - \alpha)\sin N_{//}\right]e^{-K_{//}} \qquad (101)$$

The reflectivity and transmissivity can now be written

$$R_{//} = r_{//} r_{//}^{*} = \frac{A_{//}^2 + B_{//}^2}{C_{//}^2 + D_{//}^2}$$

$$= \frac{(\gamma^2 + \delta^2)[e^{2K_{//}} + e^{-2K_{//}} - 2\cos 2N_{//}]}{G_1 e^{2K_{//}} + G_2 e^{-2K_{//}} + G_3 \sin 2N_{//} + G_4 \cos 2N_{//}} \quad (102)$$

$$T_{//} = \frac{16\cos^2\theta\,(\eta^2 + \nu^2)}{G_1 e^{2K_{//}} + G_2 e^{-2K_{//}} + G_3 \sin 2N_{//} + G_4 \cos 2N_{//}} \quad (103)$$

$$= \frac{16\cos^2\theta\,(\eta^2 + \nu^2)}{P_{o//}} \quad (103a)$$

where $G_1 = 4\cos^2\theta\,(\eta^2 + \nu^2) + 4\cos\theta\,(\alpha\eta + \beta\nu) + (\alpha^2 + \beta^2)$ (104)

$= 4J_1\cos^2\theta + 4J_3\cos\theta + J_2$

$G_2 = 4\cos^2\theta\,(\eta^2 + \nu^2) - 4\cos\theta\,(\alpha\eta + \beta\nu) + (\alpha^2 + \beta^2)$ (105)

$= 4J_1\cos^2\theta - 4J_3\cos\theta + J_2$

$G_3 = 8\cos\theta\,(\beta\eta - \alpha\nu)$ (106)

$= 8J_4\cos\theta$

$G_4 = 8\cos^2\theta\,(\eta^2 + \nu^2) - 2(\alpha^2 + \beta^2)$ (107)

$= 8J_1\cos^2\theta - 2J_2$

with $J_1 = \eta^2 + \nu^2$ (108)

$J_2 = \alpha^2 + \beta^2$ (109)

$J_3 = \alpha\eta + \beta\nu$ (110)

$J_4 = \beta\eta - \alpha\nu$ (111)

Also defining $J_5 = \alpha\gamma + \beta\delta$ (112)

$J_6 = \beta\gamma - \alpha\delta$ (113)

$J_7 = \gamma\eta + \delta\nu$ (114)

$J_8 = \delta\eta - \gamma\nu$ (115)

we can write the phase changes as

$$\phi_{r//} = \arctan\left[\frac{(J_6 - 2J_8\cos\theta)e^{2K_{//}} + (J_6 + 2J_8\cos\theta)e^{-2K_{//}} + 2J_7\cos\theta\sin 2N_{//} - 2J_6\cos 2N_{//}}{(J_5 + 2J_7\cos\theta)e^{2K_{\perp}} + (J_5 - 2J_7\cos\theta)e^{-2K_{\perp}} + 2J_8\cos\theta\sin 2N_{\perp} - 2J_5\cos 2N_{\perp}}\right] \quad (116)$$

$$\phi_{t_{//}} = \arctan\left[\frac{(-2J_1\cos\theta\sin N_{//} + J_4\cos N_{//} - J_3\sin N_{//})e^{K_{//}} + (2J_1\cos\theta\sin N_{//} - J_4\cos N_{//} - J_3\sin N_{//})e^{-K_{//}}}{(2J_1\cos\theta\cos N_{//} + J_3\cos N_{//} + J_4\sin N_{//})e^{K_{//}} + (2J_1\cos\theta\cos N_{//} - J_3\cos N_{//} + J_4\sin N_{//})e^{-K_{//}}}\right] \quad (117)$$

$$= \arctan(P_{1//}/P_{2//}) \quad (117a)$$

We have now established the desired expressions for $R_{//}$, $T_{//}$, $\phi_{r_{//}}$, and $\phi_{t_{//}}$ for light of wavelength λ incident at angle θ polarized in the plane of incidence on a uniaxial crystal of thickness d with the optic axis perpendicular to the surface, in terms of the complex refractive indices $\hat{n}_\perp = n_\perp - ik_\perp$ and $\hat{n}_{//} = n_{//} - ik_{//}$. The expressions are complete solutions for parallel-sided crystals suspended in a non-absorbing medium whose refractive index is 1.

As the angle of incidence is reduced to zero, η and ν go to $n_\perp$ and $k_\perp$ respectively; all the $n_{//}$ and $k_{//}$ terms drop out of the α, β, γ, and δ expressions, and the equations for $R_{//}$ and $T_{//}$ revert to the forms obtained at normal incidence.

A more general matrix approach to the problem of reflectivity and transmissivity is presented in Ref. [34]. The solutions presented there are not expressed explicitly in terms of the optical constants, so no direct comparisons with the present solutions can be made.

2-6 Transmission Maxima as Wavelength Is Varied (Butler Fringes)

If white light is incident on the sample and either reflectivity or transmissivity is measured as a function of wavelength, the observed intensity shows a fringe pattern because of the superposition of multiple internally reflected rays in the sample. This oscillation is apparent from the terms sin2N and cos2N in equations (38), (39), (102), and (103). The fringe maxima or minima can be located by setting the derivative of T or R with respect to λ equal to zero.

For a transparent film, k = 0, and the sine term in the denominator disappears. The transmissivity at normal incidence then becomes

$$T = \frac{8n^2}{n^4 + 6n^2 + 1 - (n^2-1)^2 \cos 2N} \qquad (118)$$

Taking the derivative with respect to λ

$$T' = 0 = n'(n^2+1)(1-\cos 2N) + N(n^2-1)(n'-n/\lambda)\sin 2N \qquad (119)$$

For the derivative to be zero, either the two terms must cancel or both must be equal to zero. If cos2N = 1 then sin2N = 0 and both terms are zero (this corresponds to a maximum in T). This gives the condition that

$$4\pi nd/\lambda = m2\pi$$

or

$$m\lambda = 2nd' \qquad (120)$$

where m is the order of interference. This is the same condition that is derived from the simple geometric consideration that for a maximum in the interference pattern the path length difference between successive reflected rays must be an integral number of wavelengths. However if cos2N = -1 then sin2N = 0 but the first term in (119) is not zero unless n' = 0. Thus the simple path length condition for the minima in the fringe pattern is not rigorously valid unless the material is dispersionless, although numerical calculations show that it is still a reasonable approximation. Similar results are obtained for R' = 0: equation (120) is obtained as the condition for reflected fringe minima, but the simple path length condition is not strictly true for maxima in R.

Similar conclusions are reached for light obliquely incident on the sample. The condition for maxima in T or minima in R is that cos2N = 1, or

$$m\lambda = 2n_\perp d\sqrt{1 - \frac{\sin^2\theta}{n_*^2}} \qquad (121)$$

where n_* is either $n_{//}$ or $n_\perp$ depending on whether the incident light is polarized in or perpendicular to the plane of incidence. Again the condition is the same as would be obtained by path length considerations, and again the path length condition for minima in T or maxima in R is not rigorously true unless the material is dispersionless.

Using equations (120) or (121) the refractive indices can be obtained by measuring the wavelengths corresponding to maxima in T or

minima in R if the sample thickness and order of interference are known. For oblique incidence the angle of incidence must also be known, and the ordinary refractive index must be known to obtain the extraordinary refractive index.

For an absorbing film the extinction coefficient is nonzero, and the sin term does not drop out of the denominator of the expressions for R or T. A sin and cos term of the same argument can be combined into a cos term with the same argument plus a phase shift which depends on the amplitudes of the sin and cos terms. As k is increased the size of the phase shift increases, but at the same time the fringe contrast is reduced as the amplitude of the internally reflected wave is attenuated. Calculating the size of the phase shift using reasonable estimates of the values of n and k for the materials studied led to the feeling that if the fringes could be observed the conditions (120) and (121) were accurate to a good approximation.

CHAPTER 3
EXPERIMENTAL TECHNIQUE

3-1 Introduction

Two techniques have been used for the measurement of the optical constants n and k of materials by studying the light transmitted through thin parallel-sided films. A Mach-Zehnder interferometer is used to measure the phase shift of transmitted light for a set of samples of different thickness, using a laser as a light source. Transmissivity is measured simultaneously, and n and k are determined from the variation of the measured quantities with sample thickness at the wavelength of the laser. In the second technique, transmission is measured using a white light source, and the dispersion curves are obtained from the fringes caused by multiple internal reflections in the sample.

The development of interferometric technique was of prime interest. Experiments to test the technique were performed on two materials with quite different optical properties. Gold is a highly absorbing, isotropic material, and and is relatively stable against oxidation. Several measurements of the optical constants have been reported[16,20-22], and there is general agreement on the shape of the dispersion and absorption curves but less agreement on the actual values. Gold films were also used in the preliminary studies on the interferometric technique[17,18]. The phase shift and transmissivity were measured at normal incidence for a set of thin films in the wavelength range from 459.7 to 632.8 nm using the lines from an argon ion laser and a helium-neon laser. The results were compared to measurements in the literature, to confirm both the technique and the measured values.

Interferometric measurements were also made on thin single crystals of GaSe. GaSe is a layer structure material; it is uniaxial, with the optic axis perpendicular to the layer surface. This material is relatively weakly absorbing, and has its fundamental absorption edge at

620 nm. There was agreement in the literature[10,11,26-28] on the general shape of the ordinary dispersion curve, but only poor agreement on the extraordinary dispersion curve and on the structure on either curve near the band edge. Measurements were made using a tuneable dye laser to study in detail the region near the absorption edge. The dyes Rhodamine 6G (range 555 to 620 nm) and Rhodamine B (range 600 to 650 nm) were used. Measurements were made both at normal incidence and at oblique incidence, and both the ordinary and extraordinary refractive indices and extinction coefficients were determined.

GaSe was also studied using the Butler fringe technique, to confirm and extend the range of measurements available, and to provide a reference for the interferometer measurements. In this technique, transmissivity is measured as a function of wavelength over a wide range (limited by the system response: photomultiplier tube, light source, and spectrometer). In principle, the full expressions (39) or (103) can be used to extract n and k at any wavelength. The dispersion curves can be obtained very simply by measuring the wavelengths corresponding to the transmission peaks and using equation (120) or (121). This gives values of n at discrete wavelengths, determined by the thickness of the samples, and from these the dispersion curve can be drawn. This technique breaks down in a region where the optical constants change rapidly, such as at an absorption edge. If the material becomes absorbing, thin films are required, but this results in widely spaced fringes. Thus the method gives the least detail where it is most needed.

3-2 Samples

3-2-1 Gold films

The gold films used in this study were prepared by Dr. Onkar Singh using a standard vacuum evaporator equipped with a liquid nitrogen trap. A very thin layer of NaCl was first evaporated onto a microcsope slide, then the slide was weighed on a Cahn G2 Electrobalance (maximum sensitivity 5×10^{-8} gm). A layer of gold was then evaporated on top of the NaCl at a rate of about 4 nm/sec, keeping the pressure below 10^{-5} torr, then the sample was weighed again. The starting material was better than 99.99% pure. The film was scribed, dividing it into several segments, then the slide was slowly lowered into water. The NaCl dissolved, leaving the gold film segments floating on the surface, supported by surface tension. A clean glass slide in which a hole 1 to 1.5 mm diameter had been drilled ultrasonically was slowly brought up under each segment, and the gold adhered to the glass slide by surface tension, leaving the film suspended over the hole. As much as possible of the water was drained off as the slide was removed. Most of the remaining water was blotted away, and the rest evaporated. Removal of the water from the hole was particularly important, as its weight would cause the film to sag. The films were examined under a microscope, and any with defects such as pinholes or wrinkles were rejected. All measurements were made on the suspended parts of the films.

Films with thicknesses of 41 to 240 nm were prepared. Two methods were used to determine the film thickness. During evaporation, the quartz crystal head of a Sloan DTM-4 thickness monitor was placed in the evaporator beside the substrate, at the same distance from the filament. The mass of gold deposited on the crystal causes its resonant frequency to change. The variation with mass is linear, and thus thickness can be determined by monitoring the resonant frequency during the evaporation. Thickness was also determined from the difference in weight of the substrate before and after evaporation, using the value of the bulk density of gold[35] 19.3 g/cm^3. The assumption of bulk values has been shown to be valid for films of thickness greater than ~20 nm[5].

The two values of thickness were in good agreement, and the uncertainty on the thickness values of the gold films was estimated to be 2%.

Similar films were prepared by the same technique for the preliminary tests of the interferometer[17,18]. Transmission electron diffraction measurements at oblique incidence were made at that time, and showed that the films were polycrystalline, with crystallite sizes from 10 to 100 nm. No anisotropy was detected. These measurements were not repeated, but were assumed to be valid for the present films.

3-2-2 GaSe Samples

GaSe crystallizes in a layer structure, with bonding between layers much weaker than the bonding between atoms of the same layer. The unit crystal layer is comprised of four atomic layers (Se, Ga, Ga, Se), as shown in Fig. 6. Within the unit layer, each Ga atom is bonded tetragonally to one Ga atom in the neighbouring layer, and to three Se atoms in the neighbouring outer layer. Each Se atom is bonded to three Ga atoms from the adjacent atomic layer. There is no direct bonding between the unit layers. Within the unit layer, the Ga atoms and the Se atoms from the different atomic layers are arranged in columns parallel to the surface normal. If the layer is viewed along the normal, the atoms are seen in a hexagonal array. The space group symmetry of the unit layer is D_{3h}^{1} ($P\bar{6}m2$)[36].

Several different crystal polytypes differing only in the stacking sequence of identical layers have been identified[37]. All of the samples studied are of the ϵ polytype[38], in which alternate layers are aligned with each other, forming a two layer unit cell. If the two sets of layers are labelled A and B, the B layers are translated with respect to the A layers, so that the B-Ga atoms are in line with the A-Se atoms. The B-Se atoms are then over the centers of the A hexagonal openings, and the A-Ga atoms are similarly in line with the B hexagonal openings. A top view of a single layer and a side view with two layers in the ϵ stacking sequence are shown in Fig. 7. The crystal symmetry is

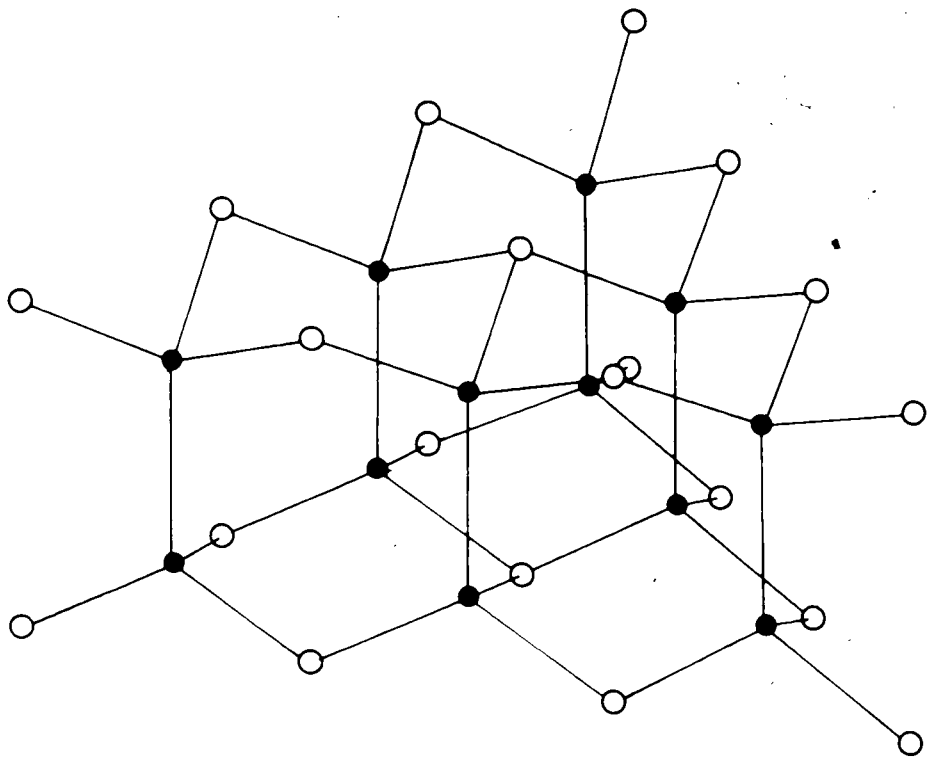

Fig. 6. The arrangement of atoms in a unit layer of GaSe. The open circles represent the Se atoms, the filled circles the Ga atoms.

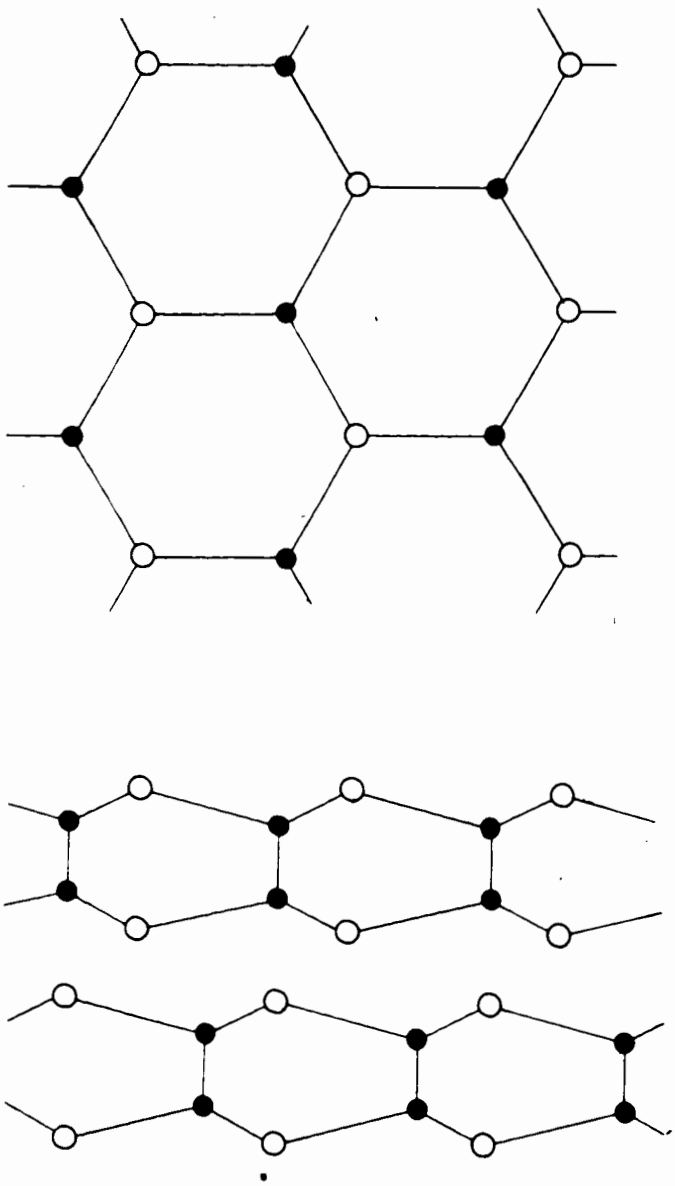

Fig. 7. A top view of one unit layer of GaSe, and a side view showing two layers in the ϵ stacking sequence.

the same as that of the unit layer, although the unit cell extends over two unit layers. As discussed above, with this crystal structure the material is optically uniaxial, with the optic axis perpendicular to the layers.

The crystals cleave easily between the layers, and thus parallel-sided samples are easily obtained. The thickest samples were cleaved from Bridgeman-grown single crystals, and the thinnest ones were grown by vapour transport in the form of very thin parallel-sided flags. Some of the crystals were provided by Dr. J.L. Brebner of the Université de Montréal and others were grown by Mr. G. Jackle in our laboratories at Simon Fraser University.

GaSe crystals are transparent in the red. Potential samples were examined under a microscope, using oblique lighting. When an area of about $1mm^2$ with no visible defects such as a crack, scratch, or surface step was found, the sample was taped onto a brass foil over one of two small holes, so that all but the choice area was masked out. This permited easy handling of the samples. Samples with thickness from 0.5 to 320 μm were prepared.

Three techniques were used to determine sample thickness. The first (thick) samples were weighed on the Cahn Electrobalance, and the lengths of the sides and all diagonals were measured on a travelling microscope. The area was then determined using the formula for the area of a triangle

$$A = \sqrt{s(s-a)(s-b)(s-c)} \qquad (122)$$

where a, b, and c are the lengths of the sides and s is the semiperimeter. A value of 5.03 g/cm^3 for the mass density[35] was used in calculating the thickness. Several factors reduced the accuracy of this method: the edges were not always straight, the corners tended to be rounded, and there were often steps on the samples so that the thickness was not uniform. Accuracy was estimated to be a few percent.

Two variations of the Butler fringe technique provided a more satisfactory determination of thickness, and also provided a means of finding the order of interference of a given fringe. Equation (121) describes the condition for transmission fringe maxima:

$$m\lambda = 2n_o d\sqrt{1-\frac{\sin^2\theta}{n_e^2}} \qquad (121)$$

For a given sample, an interference fringe pattern can be obtained by varying either the wavelength of the incident light or the angle of incidence. The loci of fringe maxima on a λ,θ plane is plotted in Fig. 8. The transmission pattern for light at a fixed wavelength was recorded as a function of the angle of incidence, using polarization perpendicular to the plane of incidence so that only the ordinary refractive index was involved, and the angles corresponding to fringe maxima were determined. Equation (121) can be written as

$$(M-x_i)\lambda = 2d\sqrt{n_o^2 - \sin^2\theta} \qquad (123)$$

where M is the interference order of the nearest fringe at normal incidence and the relative order x_i is known simply by counting the fringes from normal incidence. The refractive index is constant, and can be eliminated from Equation (123) using any two data points: rearranging, this gives

$$(x_i^2 - x_j^2)\frac{1}{d^2} - (x_i - x_j)\frac{2M}{d^2} = \frac{4}{\lambda^2}(\sin^2\theta_j - \sin^2\theta_i) \qquad (124)$$

Using all pairs of data at the fixed wavelength, this equation can be least squares fitted to provide values of M and the sample thickness d. A satisfactory result cannot be obtained from a single run at fixed wavelength, since a small change in M can almost exactly be compensated for by a change in d. Runs at two fixed wavelengths must be used. The

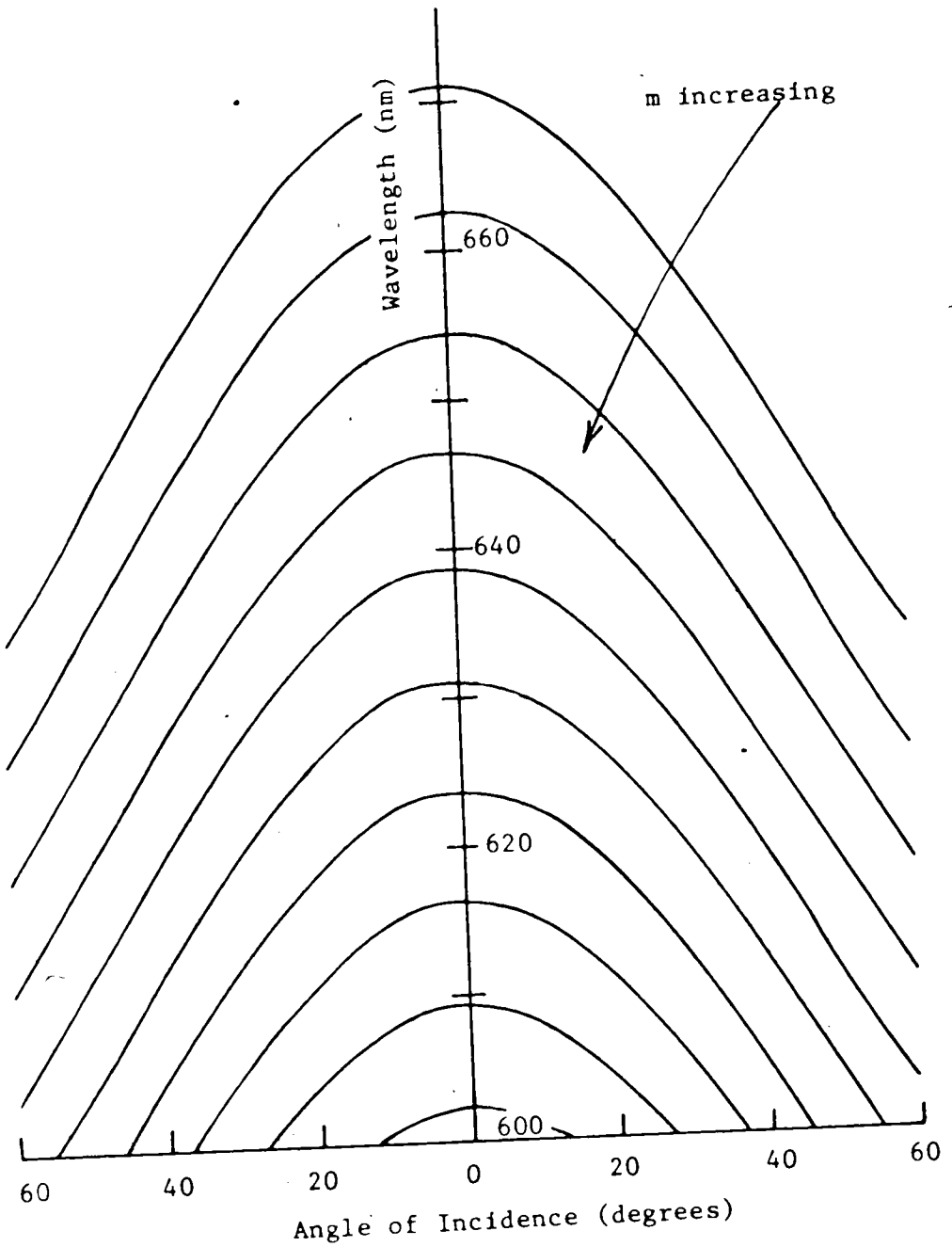

Fig. 8. The loci of Butler fringe maxima

relative shift in interference order between the data sets is obtained from a scan of transmission as a function of wavelength at normal incidence, and of course n can only be eliminated between data points taken at the same wavelength. The standard deviations of the means of the resulting values of interference order are 0.5 to 2 fringes for M = 100 to 2000 fringes, and of thickness are 0.02 to .2 μm for d = 20 to 320 μm.

This technique does not work well for GaSe samples with thickness less than about 10 μm, as very few fringes are obtained when the sample is rotated. The thicknesses of the thinnest films were determined by comparison with thick film measurements. The ordinary dispersion curve was determined from normal incidence scans of transmission as a function of wavelength, using the thicker samples. Similar runs were done on the thin films, and the data were fitted to the established dispersion curve to obtain d. Films of thickness 0.5 to 2.6 μm were measured in this way, with an accuracy of about 1%.

3-3 The Interferometer

3-3-1 Principle of Operation

The transmissivity and phase change of light on transmission through a sample can be measured by observing the change in intensity and phase of the recombined beam as the sample is moved alternately in and out of one arm of a Mach-Zehnder interferometer. The interferometer is shown schematically in Fig. 9. Light from a laser source is divided at beam splitter BS1. The two components travel separate paths through the interferometer, and are recombined at BS2, and the recombined beam is observed with the photomultiplier tube PM. A fringe pattern is generally seen on the output beam because of beam divergence. This pattern is enlarged by the beam-expanding telescope, and a pinhole with diameter much less than the fringe width is placed in front of the photomultiplier so that it sees a small part of the fringe pattern.

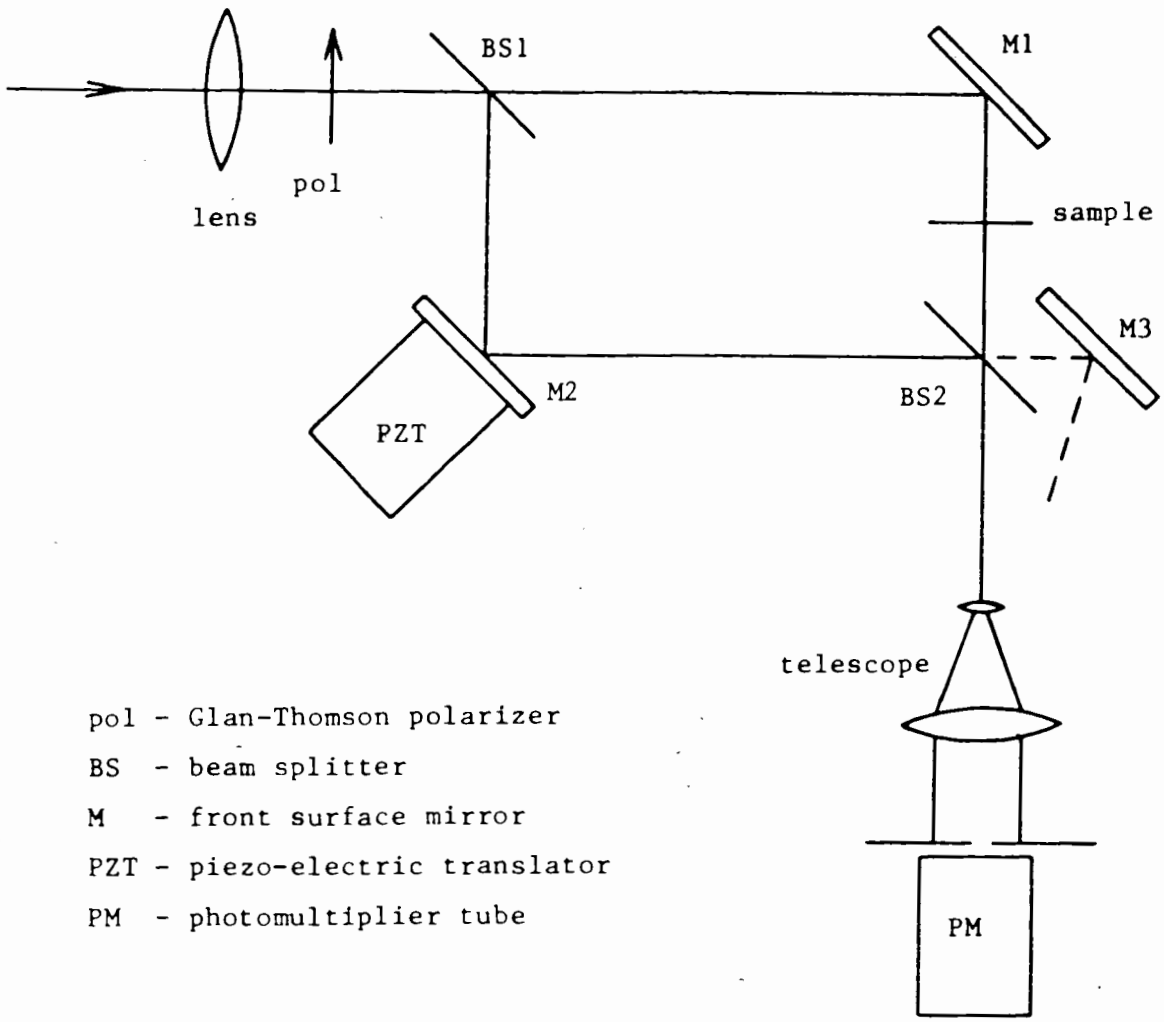

pol - Glan-Thomson polarizer
BS - beam splitter
M - front surface mirror
PZT - piezo-electric translator
PM - photomultiplier tube

Fig. 9. A schematic diagram of the interferometer.

Mirror M1 is fixed. Mirror M2 is mounted on a Burleigh PZ-81 piezo-electric translation unit, which is driven by a ramp generator. As M2 changes position the path length of the reference beam is varied: thus the phase of the reference beam is changed with respect to the sample beam, with the result that the fringe pattern on the recombined beam is scanned past the pinhole. If the position of M2 changes linearly with time, the signal from the photomultiplier will vary sinusoidally. This signal is viewed on an oscilloscope, triggered from the start of the ramp generator signal.

As the sample is inserted or withdrawn, the phase of the sample beam is changed by a fixed amount relative to the reference beam. This results in a shift in phase of the sine wave signal from the PM tube relative to the ramp generator trigger pulse: it is this phase shift which is measured.

To describe the operation mathematically, we assume plane waves of the form $\exp i(\omega t - qz)$. If M2 moves at velocity v, then the change in path length is proportional to vt, and the reference beam can be described at the point of recombination by the expression

$$\begin{aligned} r &= R\, e^{i[\omega t - q(z-pvt)]} \\ &= R\, e^{i(\omega t - qz - \omega_1 t)} \end{aligned} \qquad (125)$$

where ω_1 is the frequency at which the fringe pattern scans past the pinhole and R is the amplitude of the reference beam. Similarly the sample beam is described by

$$s = S\, e^{i(\omega t - qz + \delta_s)} \qquad (126)$$

or

$$a = A\, e^{i(\omega t - qz + \delta_a)} \qquad (127)$$

where S, A, δ_s, and δ_a are the amplitudes and (constant) phase shifts relative to the reference beam with the sample inserted or withdrawn respectively. The intensities of the recombined beam with the sample

inserted or withdrawn are

$$I_s \propto |s+r|^2 = S^2 + R^2 + 2SR\cos(\omega_1 t + \delta_s) \qquad (128)$$

$$I_a \propto |a+r|^2 = A^2 + R^2 + 2AR\cos(\omega_1 t + \delta_a) \qquad (129)$$

Now if we measure only the AC component of the signal, the ratio of intensities observed with the sample inserted or withdrawn gives the ratio of amplitudes of the light before and after passing through the sample. The difference in phase

$$(\delta_a - \delta_s) = -\frac{2\pi d}{\lambda}\cos\theta - \phi_t \qquad (130)$$

is the difference in changes of phase of light on passing through the sample or through an equivalent thickness of air, where ϕ_t is given by Equation (46) or (117). Since only the z-dependant part of the wave was considered in developing the expressions for the transmissivity and phase change, ϕ_t is for a wave emerging from a point directly opposite the point of entry in the sample, rather than along the path of the ray or along q. Thus the equivalent air path is the projection of the sample thickness onto the direction of the incident wave.

The phase difference can only be measured modulo 2π. The expression $\frac{2\pi d}{\lambda}$ gives the full phase shift through an equivalent thickness of air. The expression for ϕ_t involves an arctangent, which repeats every π radians. The quadrant for the phase shift ϕ_t must be determined from the signs of the numerator and denominator, and right hand side of equation (130) must be put modulo 2π so that it can be compared with the experimental value.

Two paths are shown for the recombined beam in Fig. 9. The best signal to noise ratio is obtained if the sample and reference beams have approximately equal amplitudes. The beam splitters are uncoated quartz, so about 7% of the beam is reflected at the first surface and 87% transmitted. If the samples to be tested are weakly absorbing, the dashed path and mirror M3 are used, so that both beams undergo one

reflection and one transmission in the beam splitters. If the material is highly opaque, the best balance is achieved by using the solid line path, so the sample beam undergoes two transmissions and the reference beam two reflections.

3-3-2 Physical Description of the Interferometer

The measurements of phase and optical density are carried out simultaneously on the interferometer, but the requirements for the phase measurements are much more severe. The path difference within the interferometer must be kept constant to within a small fraction of a wavelength for a time interval long enough for the measurement to be made. The interferometer must be well isolated from vibration transmitted from the floor through the stand or from internal sources, from airborn acoustic vibration, air currents, thermal drifts and stray light.

The interferometer was placed on a massive granite slab which sat on vibration isolation spring mounts[39] on a steel frame table. The spring mounts were chosen to provide critical damping with the loading on them, and damp out frequencies greater than ~3.5 Hz very quickly. The table legs rest on a stack of alternating layers of thin plywood and felt/rubber shock mount pads, and these in turn sit in sand boxes. As a measure of the success of this approach, a person could walk near the apparatus with no apparent effect on its operation. Transients generated by a sharp blow would die out in a small fraction of a second.

A box of two inch foam rubber placed over the granite slab provided thermal stability and blocked air currents. It was spray painted black on the inside to reduce stray light. Two panels cut in the box could be removed for easy mounting of the samples and to facilitate alignment. Light entered through a small hole cut in one side of the box. The external vibration precautions and sponge box are shown in Fig. 10.

The layout of the interferometer components is shown in Fig. 9. The two beamsplitters and mirror M1 are mounted on a common heavy brass plate. The mirror is rigidly attached to it, and the beamsplitters are

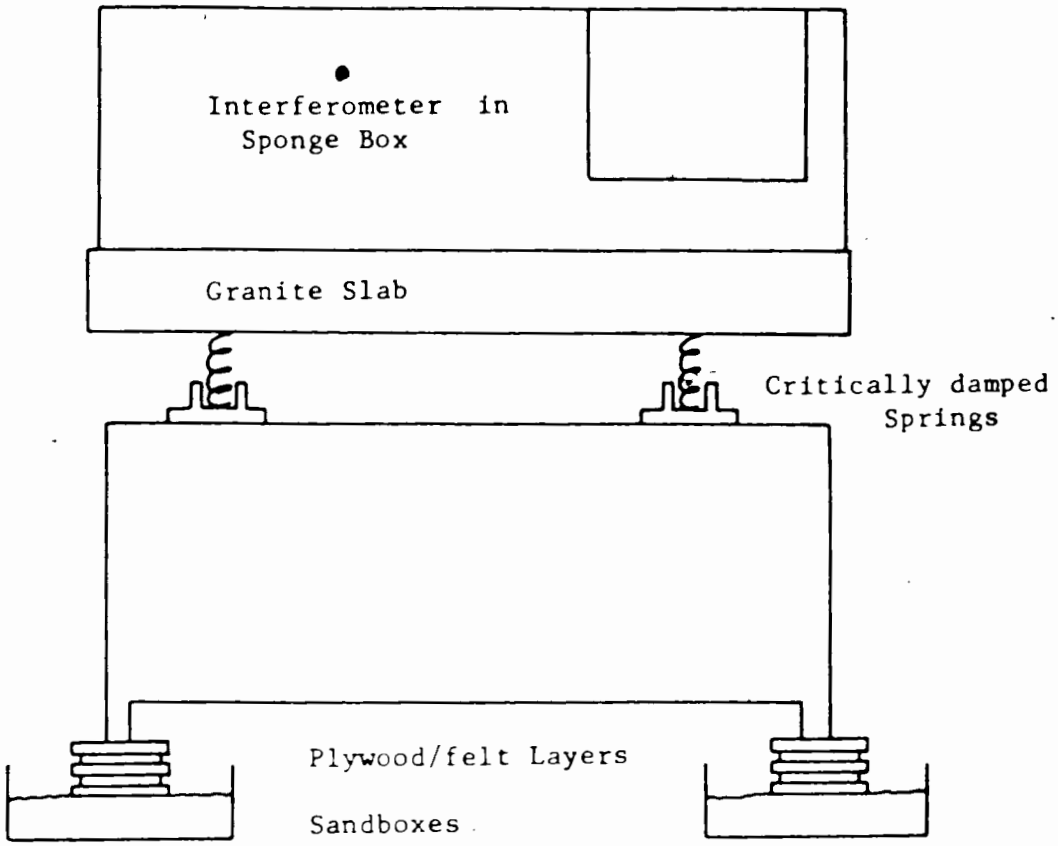

Fig. 10. The precautions taken to isolate the interferometer from external vibration, thermal gradients, and stray light.

on three-screw mounts for aligning. The brass base sits on rubber pads on a concrete block, which rests on more rubber pads on the granite slab. Mirror M2 is rigidly attached to the piezoelectric translation unit, which is clamped to a heavy metal stand which rests on three points on the granite slab. This isolation of the PZT mirror from the rest of the interferometer was found to be necessary to reduce the effects of vibration caused by the movement of the mirror.

A long focal length lens placed ahead of the first beam splitter focusses the laser beam to roughly a 10 μm diameter spot at the sample location. If used, mirror M3 is mounted on a three-screw alignment stand on the granite slab. The beam expanding telescope and the photomultiplier tube are mounted on an optical rail which is fastened to the granite slab with double-sided tape. The telescope stand has vertical and lateral horizontal movements for alignment. Neutral density filters were often placed just ahead of the photomultiplier

As described above, the samples were permanently mounted on brass foils or glass slides for easy handling. The brass foils are clamped onto a sample holder with two holes matching those on the foils, as shown in Fig. 11. The gold films on glass slides are clamped in slots on a similar holder. The holder slides in a groove in a tray which is mounted on a pedestal on the granite slab, and extends into one arm of the interferometer. The tray position can be adjusted vertically, and limiting screws on each end of the tray are adjusted so that the focussed beam passes cleanly through one or other of the holes when the holder is slid to either end of the tray. The tray can also be tilted about horizontal and vertical axes to ensure that the mount is perpendicular to the beam. The holder is moved by a handle which extends through a small hole in the sponge box.

Several sample holders were made, for measurements at normal incidence or at 30 or 45 degrees. The oblique incidence holders are tilted at fixed angles from vertical. For oblique incidence measurements, a Glan-Thomson polarizer is placed ahead of the first beam spliter and aligned to keep the incident polarization vertical, i.e. in the plane of incidence.

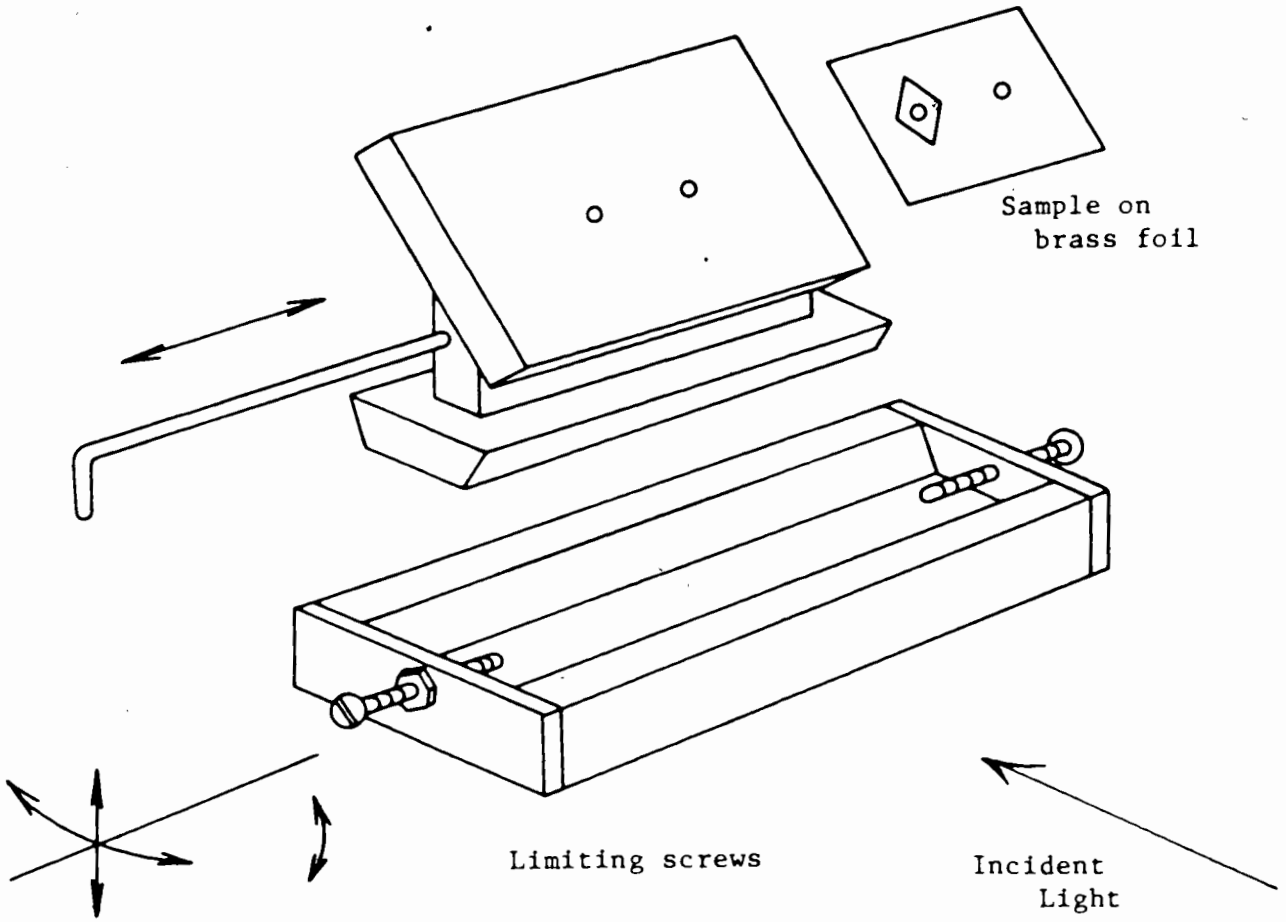

Fig. 11. The sample holder, showing the directions of motion and alignment.

Light from the laser source was directed into the interferometer through two internal reflection prisms in a periscope arrangement clamped to the granite slab outside the sponge box. Both prisms were on three screw mounts so the input beam could be easily aligned with the interferometer.

3-3-3 Electronics

During operation the data was recorded and partially analysed on a PDP 11/10 computer using an interface built by Dr. R.A.D. Hewko. The electronics are shown schematically in Fig. 12.

A 0-10 V ramp is generated by passing pulses from a 6.55 MHz clock through a 12-bit digital to analog converter. The ramp signal is amplified and fed to the Burleigh PZ-81 translator, thus providing a linear shift in the path length of the reference arm of the interferometer. The resulting sinusoidal signal from the IP28 photomultiplier passes through a filter amplifier (using the AC input) and is displayed on an oscilloscope. By varying the bias and gain on the PZT amplifier the initial phase and length of the phase sweep can be controlled. The ramp generator also provides a slow rather than rapid return to reduce the vibration caused by the movement of mirror M2.

The amplitude of the filtered sine wave is monitored on a digital voltmeter, and is periodically recorded and stored in the computer through Interface B. In Interface A the filtered sine wave is amplified and clipped by a high gain amplifier, producing a square wave whose edges correspond to the zero crossings of the sine wave. This square wave is also displayed on the oscilloscope. A second square wave is produced by monitoring the most significant bit on the digital to analog converter in the ramp generator; its edges correspond to the points half way down the ramp and half way up on the return. This wave is used to trigger the oscilloscope sweep and to gate Interface A. Two counters in Interface A continuously count pulses from a 1MHz clock, and these counters are reset to zero by the gate pulse. The first two positive-going edges from the squared sine wave cause latches to be set

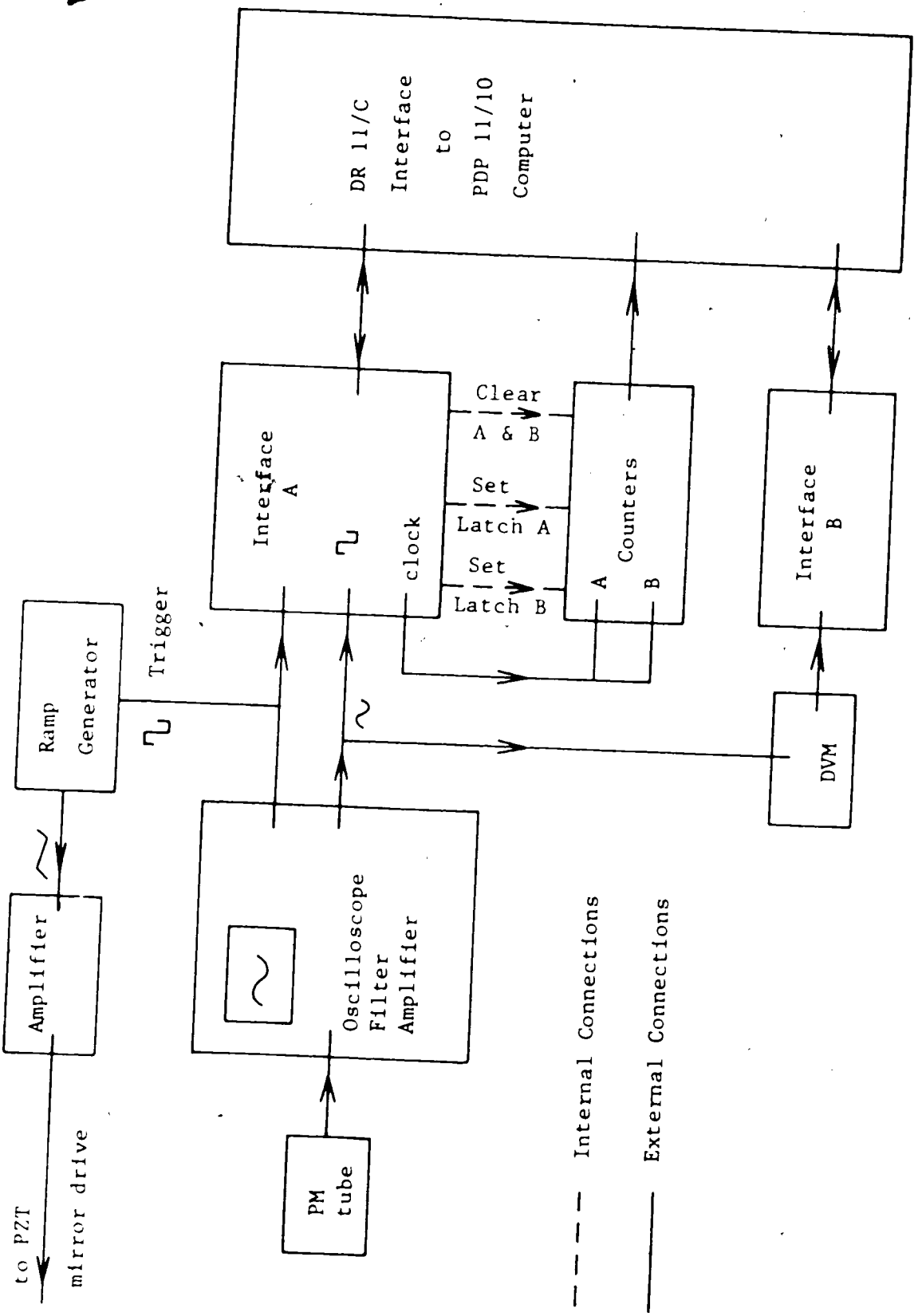

Fig. 12. A schematic diagram of the electronics.

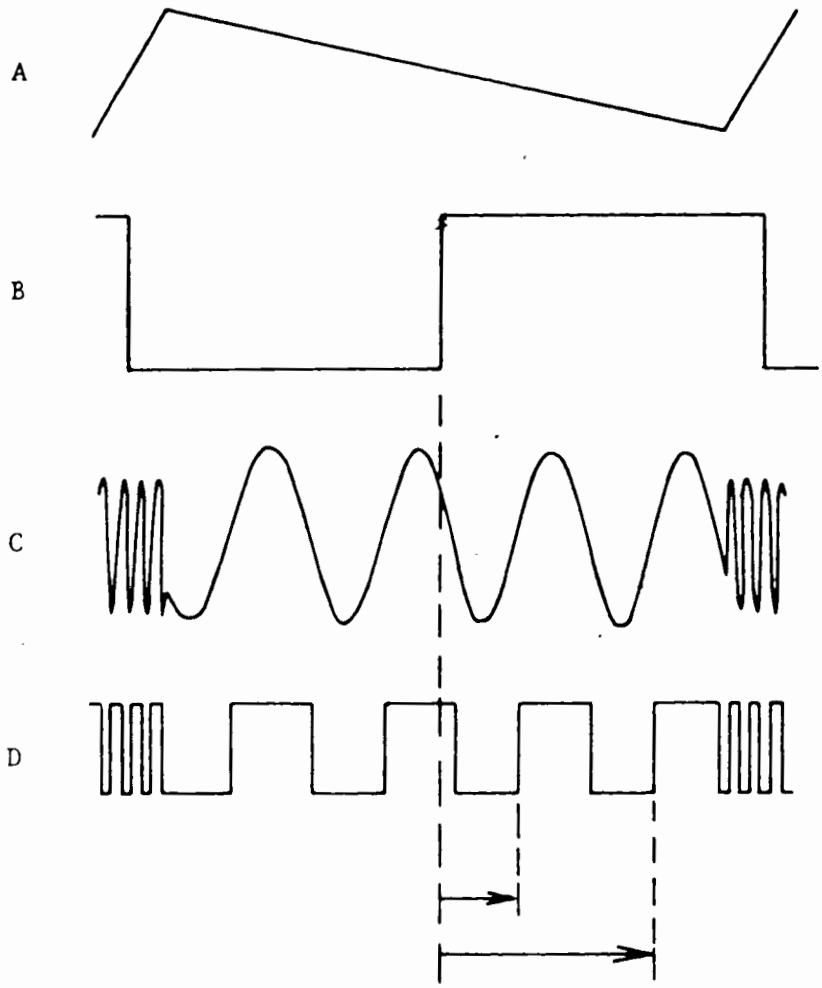

Fig. 13. Signals seen at various points in the electronic circuit. (A) is the ramp, (B) the trigger pulse, (C) the signal as seen on the oscilloscope, and (D) the squared signal in Interface A. The two time intervals measured are also shown.

on the two counters. The counter readings are recorded by the computer, and correspond to the time intervals between the trigger pulse and the next two zero crossings of the sine wave. The difference between the readings thus corresponds to the time interval for a 2π phase shift in the interferometer signal, and the individual readings give phase measurements with respect to a fixed point on the ramp. If the sample is alternately inserted and withdrawn from the sample beam, the 2π phase interval does not change, but the phase with respect to the trigger pulse does. The difference between the individual readings with the sample in and out of the beam gives the phase difference (modulo 2π) for light passing through the sample and through an equivalent thickness of air.

The ramp, sine wave signal, and the square waves are shown in Fig. 13 along with the phase intervals measured.

3-3-4 Operating Procedure

To align the interferometer, the incident beam is directed onto the periscope, and the prisms adjusted until the beam enters the system cleanly. The first beam splitter is adjusted to bring the sample and reference beams into coincidence at the surface of the second beam splitter, which is then adjusted to bring the two beams into alignment at the entrance to the beam expanding telescope. The alignment is fine tuned by adjusting the beam splitters and the telescope position to maximize the signal seen on the oscilloscope.

The sample is then inserted into the interferometer and the holder tray angles are adjusted to align the reflected beam with the incident beam, thus ensuring normal incidence. For oblique incidence measurements this is checked periodically using a normal incidence holder. The tray vertical position and the limiting screws are then adjusted to ensure that the beam passes cleanly through each of the holes in the sample holder.

Data collection and analysis are controlled by the BASIC program FILMS5. The wavelength, angle of incidence, and sample identification are stored in the program, and the vertical gain scales for the oscilloscope filter amplifier with the sample in and out of the beam are then selected and stored. These scales are used in the determination of the optical density. The program is then begun with the sample holder on the "air" side, i.e. with the beam passing through the open hole. The period of the phase shift scan is determined from the difference between the two zero crossing phases, averaged over 1000 ramp sweeps. The phase and optical density measurements begin immediately. The time intervals from the trigger pulse to the next two positive-going zero crossings (corresponding to δ and $\delta + 2\pi$) are averaged for 60 ramp sweeps and converted to phase, then the program stops. At the beginning of this cycle and after every 10 ramp sweeps the AC intensity is read and recorded. The sample holder is then manually moved to the "sample" position, and the oscilloscope gain reset if necessary, and the program is restarted. This cycle is repeated twenty times, with the sample alternately inserted and withdrawn, finishing up on the "air" side again. Immediately after the last cycle the period of the phase shift scan is remeasured, and the measured phase shifts corrected on the assumption that any change in the period occurred linearly with time.

After each cycle, the averaged phase, difference from the last averaged phase, averaged intensity, and optical density (ratio to the last averaged intensity) are printed. The final phase shift and optical density values are obtained by averaging the values obtained between successive cycles. These values are printed out along with the standard deviations of their means. The next sample is mounted and the process repeated.

The sequence is begun on the "air" side so that the determination of the period of the phase sweep is always made on the cleanest signal possible, since the signals for transmission through strongly attenuating samples were much noisier. This is also the reason for measuring the period before and after the phase measurements and using

the second zero crossing to double the number of phase measurements made in a given time, rather than measuring the phase and period simultaneously.

The measured phase with the sample either in or out was found to drift slowly with time, with a period of hours or days before the direction of drift reversed. By repeating the sample in/out sequence any linear drift with time is automatically corrected for when the measurements are averaged. Usually the drift was small and presented no problem. The program contained a test which rejected any phase value more than 90 degrees different from the running average value. Because of this, signals were not allowed to drift within 20 degrees of 0 or 360 degrees. If this did occur, the run was terminated and repeated.

It was found that the results were most consistant if all of the samples were measured at one wavelength in as short a time period as possible. This was particularly true for the dye laser as retuning it to exactly the same wavelength is not easy. When the dye laser source was used, wavelength was measured on a Spex 1401 double grating spectrometer at the beginning of the run and after every two samples to check for any drift in wavelength. Allowing for time to mount samples, measure wavelength, touch up the alignment etc. a set of 8 samples could be measured in 2 to 2.5 hours. This gives the information necessary to calculate n and k at one wavelength.

3-3-5 Associated Procedures, Calibrations, and Accuracy

Results were found to be more consistant if the phase sweep length was adjusted to an integral number of cycles. This is adjusted by varying the gain of the PZT amplifier. We adopted the practice of always setting the gain so that the phase swept through 4 complete cycles. The same ramp generator settings were always used, and the resulting sine wave signal displayed had a frequency of about 100 Hz as seen on the oscilloscope. The 3-db settings on the filter amplifier were also kept constant at 10 and 1000 Hz. One possible reason for any sensitivity to the phase sweep length is that the ramp return was much

faster (~800 Hz) than the sweep, and a longer sweep would produce higher frequencies in the return part of the cycle, which would be differently effected by the filter amplifier. In particular, the digital voltmeter averages over all input frequencies, and so the intensity measurements would be affected by increased attenuation of the higher frequencies. Varying the initial phase setting has no effect on the phase measuements, but can alter the DVM readings by about 1%. However as the optical density is the logarithm of the ratio of these readings this variation is not significant.

The errors calculated by FILMS5 were the standard deviations of the means of the values determined. The accuracy was largely determined by the laser source. With the HeNe line or the stronger Ar laser lines phase shifts could be measured accurately and reproduceably to within 1 degree. With the dye laser source the phase error was a few degrees, and the optical density error about .02. Superimposed signal traces with the sample in and out are shown in Fig. 14, with a HeNe source and the RhB dye laser source. These traces are typical of the best and worst signals handled.

The line width of the RhB dye laser was about 2 cm^{-1}, corresponding to a coherence length of about 0.5 cm. Line width was improved to better than 1 cm^{-1} with the R6G dye by using a Fabry-Perot etalon in the laser cavity. The etalon reduced intensity too much to be used with the less efficient RhB dye. With all of the laser sources exact retroreflection from the sample had to be avoided as it produced interference in the laser cavity, resulting in a very noisy signal.

Optical density measurements were calibrated using a high quality set of neutral density filters. The intensity of the sine wave signal was measured with the filters placed in turn at the sample location: the test was repeated with the filters placed after the beam expanding telescope. Both tests gave the same result. A plot of observed vs. expected O.D. was approximately linear for the less opaque filters, but the observed O.D. was slightly lower than expected with the highly opaque filters (O.D.>~4). This was attributed to the characteristics of the photomultiplier tube.

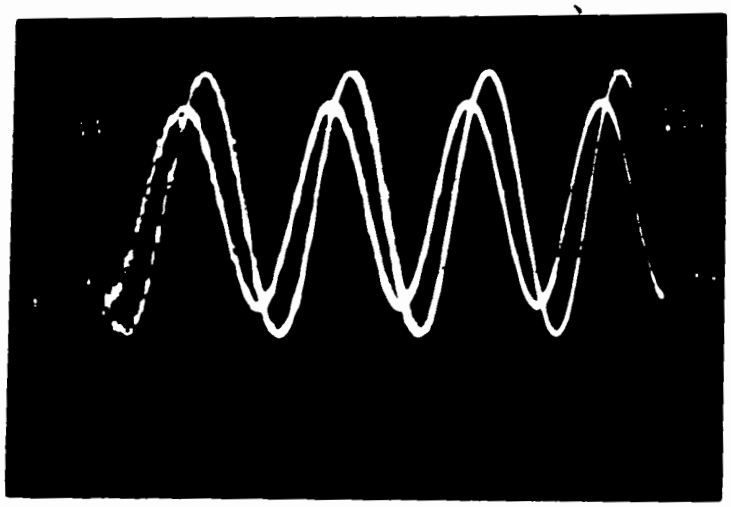

Source HeNe laser (632.8 nm)
Sample GaSe 23 Phase Shift 58.7 ±.5 degrees
Optical Density 0.264 ±.005

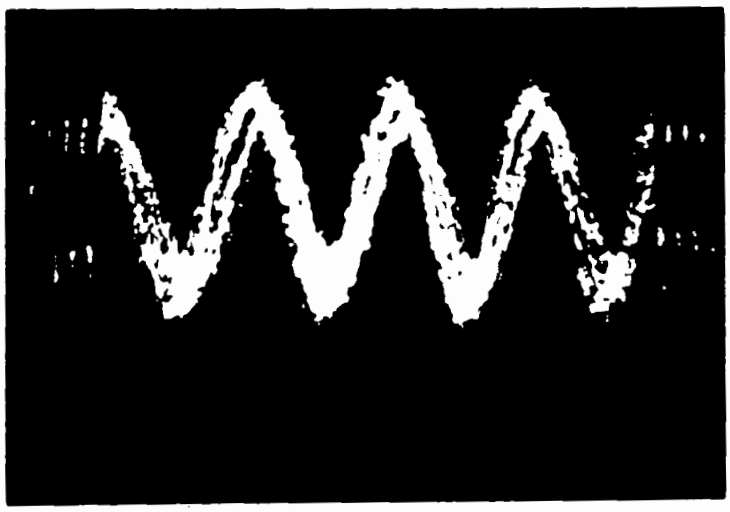

Source RhB dye laser (645 nm)
Sample GaSe 22 Phase Shift -49.5 ±4.6 degrees
Optical Density 0.219 ±.012

Fig. 14. Typical photomultiplier signals, showing superimposed traces with the sample in and out of the laser beam.

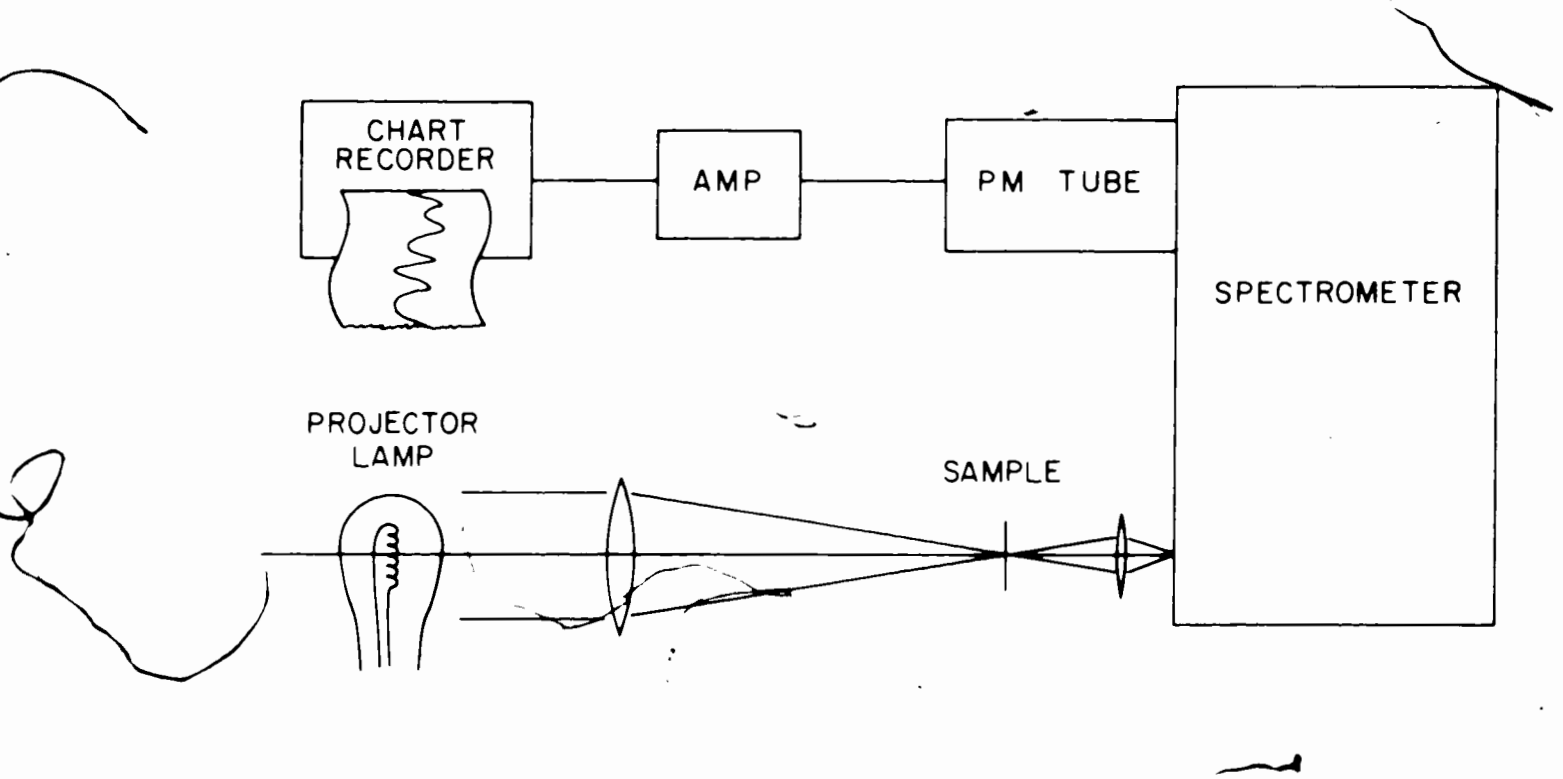

Fig. 15. A schematic diagram of the apparatus used for the Butler fringe measurements.

3-4 Butler Fringe Measurements

The intensity of light transmitted through the samples was measured with the apparatus shown in Fig. 15. White light from a projector lamp was focussed with a long focal length lens on the sample, and the transmitted light was refocussed on the entrance slit of a Spex 1400 double grating spectrometer. The signal from a FW-130 photomultiplier placed at the output slit of the spectrometer was amplified, then recorded on a strip chart recorder. As described above, fringes are obtained if either the wavelength or angle of incidence is varied. Spectral lines from a Ne or Hg lamp superimposed on the input were used to calibrate the wavelength scans. Coloured glass filters were used to prevent light from different grating orders from interfering with the desired signal in certain wavelength ranges.

The samples were mounted on the normal incidence sample holder from the interferometer. For oblique incidence measurements the sample holder table was rotated about a vertical axis. Since converging light results in different path lengths through the sample, thus changing the fringe condition, the maximum range of incident angles was restricted to $\pm$20 mrad. for normal incidence measurements. For oblique angle measurements collimating slits were placed at the lens to further restrict the range of angles to $\pm$1 mrad. A Nicol prism polarizer was used for oblique incidence measurements.

To measure transmission as a function of the angle of incidence, the wavelength was chosen and fixed on the spectrometer. The sample holder table was slowly rotated by means of a clock motor, and the signal recorded as above. Slits were cut every 10 degrees around the edge of the table, and a lamp/photodiode pair on opposite sides of the table edge produced marker pulses for angle measurements.

The following measurements were made with each sample. First wavelength scans were made over as wide a range as possible at normal incidence; this confirmed the sample quality as well as providing data for the ordinary dispersion curves. Next rotational scans at two

different wavelengths were made, with polarization perpendicular to the plane of incidence to maintain the ordinary refractive index. These runs were used with the normal incidence wavelength scan to determine the sample thickness and order of interference, and to determine the ordinary dispersion curve. A rotational scan with polarization in the plane of incidence was made to correlate the interference order for oblique incidence wavelength scans with the normal incidence scan, and finally wavelength scans at one or more angles of incidence were made.

The ordinary dispersion curves from the different samples were averaged to give a final ordinary dispersion curve. This curve was then used with the sample thickness, interference order, and oblique incidence scan data to produce extraordinary dispersion curves, which were then averaged to give the final extraordinary dispersion curve.

CHAPTER 4
RESULTS AND DISCUSSION

4-1 Gold Analysis - Thick Film Limit

Phase and optical density measurements were made on the thin gold films, using the interferometer as outlined in Section 3-3-4. All the measurements were made at normal incidence and at room temperature, and covered the spectral range from 459.7 to 632.8 nm. The values of the refractive index and extinction coefficient can be easily obtained from these measurements if the films are in the thick film regime, i.e. they are thick enough that absorption makes the effects of multiple internal reflection negligible. Under these circumstances, the observed phase shift (from Equation (51)) and optical density can be expressed

$$\psi = \phi_{air} - \phi_{sample}$$
$$= -\frac{2\pi d}{\lambda} - \phi + \frac{2\pi nd}{\lambda} \qquad (131)$$

$$O.D. = \log_{10}(\text{constants}) - \frac{4\pi kd}{\lambda}\log_{10}e \qquad (52)$$

If the phase shift and optical density data are plotted as functions of sample thickness at constant wavelength, the values of n and k are derived from the slopes of the curves. Taking the derivatives of Equations (131) and (52) and rearranging,

$$n = 1 + \frac{\lambda}{2\pi}\frac{\partial\psi}{\partial d} \qquad (132)$$

$$k = \frac{\lambda}{4\pi\log_{10}e}\frac{\partial O.D.}{\partial d} \qquad (133)$$

Since only the slopes of the curves are used, any effects due to the surfaces cancel out of the expressions. The thickness at which the thick film limit is reached can be specified by the criterion[30] $\exp(-4\pi kd/\lambda) < .01$ (this gives a limit thickness of 70 nm at 632.8 nm or 100 nm at 488 nm), or can be determined qualitatively from the linearity of the data with d. A family of curves of observed phase shift versus thickness at 488 nm is shown in Fig. 16; in these curves, k is held constant and n varied. A similar family of curves of optical density versus d in which n is held constant and k varied is shown in

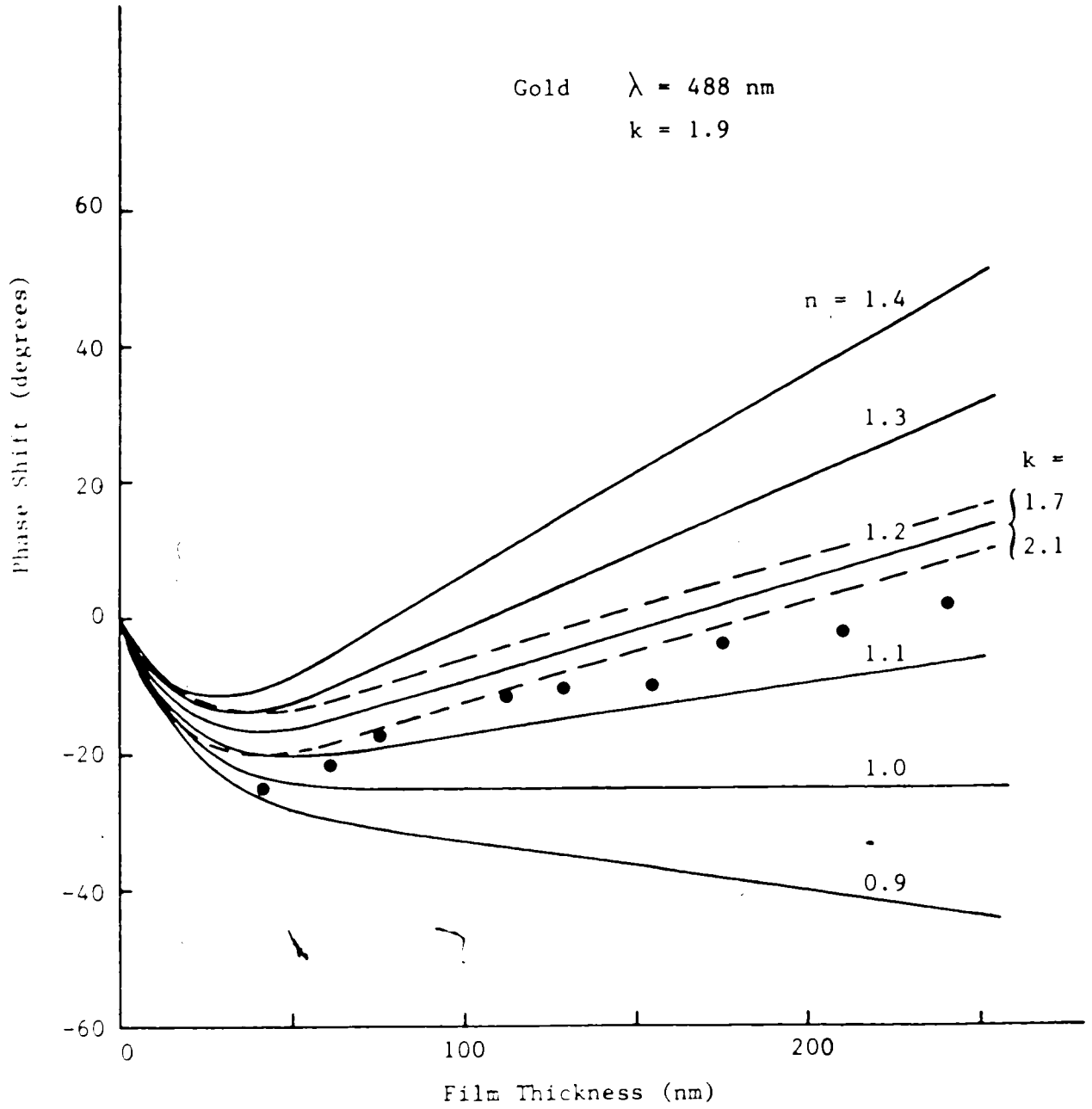

Fig. 16. Calculated curves of phase shift (air - sample) as a function of sample thickness.

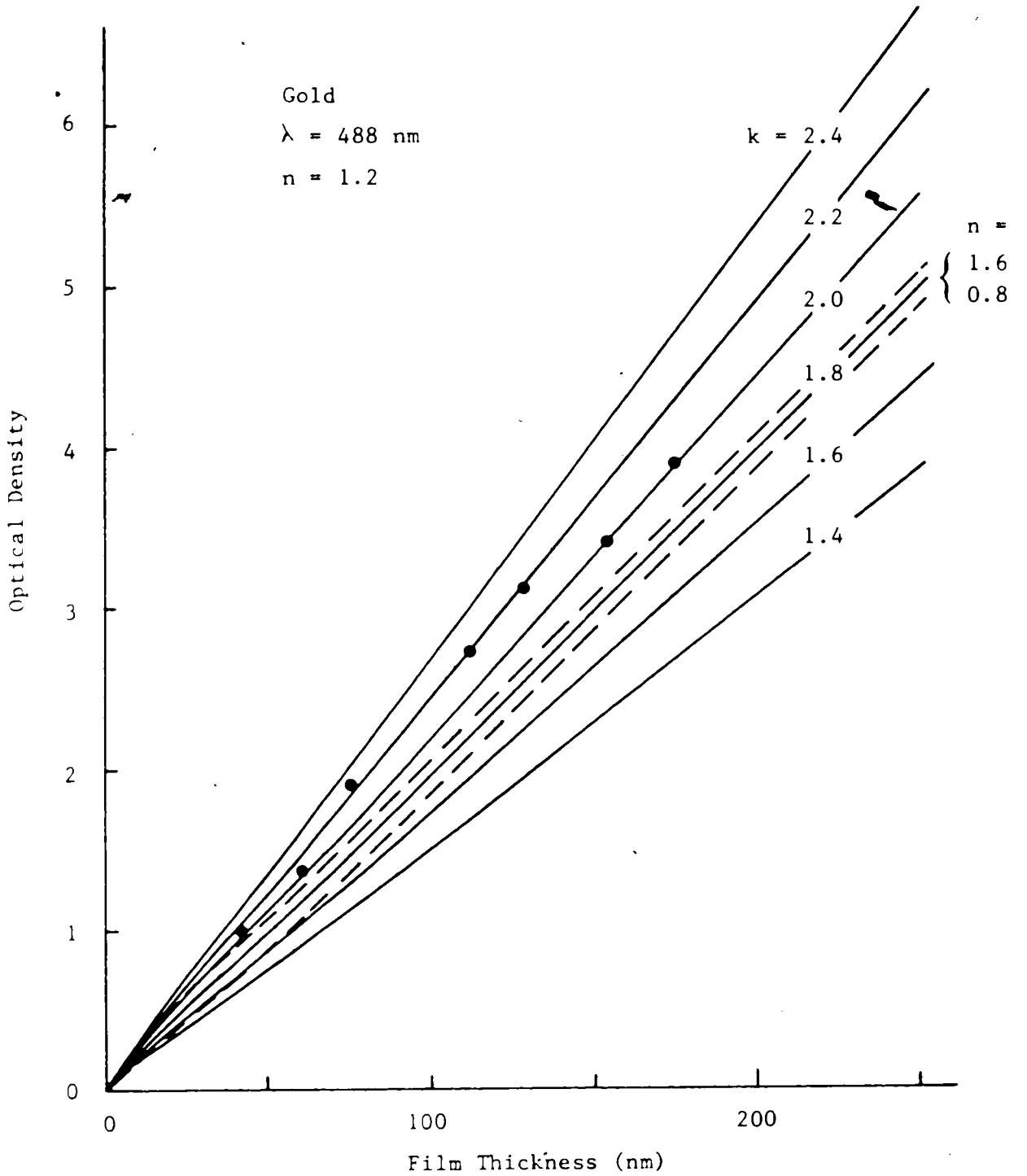

Fig. 17. Calculated curves of optical density as a function of sample thickness.

Fig. 17. Both sets of curves become linear for thickness greater than about 50 nm, corresponding to an attenuation factor $\exp(-4\pi kd/\lambda)$ of .05. These and similar sets of curves at other wavelengths suggest that .05 is a more reasonable criterion than .01 for the thick film limit.

The phase and optical density data obtained at 488 nm are superimposed on the curves of Figs. 16 and 17. The phase data were accurate and reproduceable to about 1 degree, and shows the predicted linearity with thickness. The optical density data was reproduceable to within a few percent. At that stage of the research the optical density data was obtained by reading the DVM by eye with the sample in and out of the beam. The DVM we had at that time was considerable less stable than the one we later acquired, and the instability was compounded by the deterioration Also the Argon laser was in serious need of repair at that time, with the result that the weakest lines (459.7, 476.5, and 501.7 nm) were very noisy. Thus the derived values of k do not show the accuracy which the procedure is capable of achieving.

The values of n and k were obtained by linear regression fits of the phase and optical density data. The results are listed in Table I and shown along with the results of a more detailed analysis and results from the literature in Figs. 18 and 19. The results will be discussed after the next section.

Table I -- The optical constants of gold, as determined from analysis in the thick film limit and by computer programs KNSEQ and KNCSEQ (pp 66-68). The errors shown are the statistical fitting errors. Values marked with an asterisk are considered less reliable because of weak and noisy laser lines. Values of the real and imaginary parts of the dielectric constant calculated from the KNCSEQ results are also shown.

wavelength (nm)	thick film	KNSEQ	KNCSEQ
	Refractive Index		
459.7	1.44 ±.09	1.49 ±.02	1.54 ±.004
476.5	1.38 ±.04	1.29 ±.02	1.37 ±.006
488.0	1.18 ±.015	1.13 ±.02	1.18 ±.005
496.5	1.04 ±.01	0.95 ±.04	1.06 ±.005
501.7	0.88 ±.02	0.86 ±.025	0.90 ±.02
514.5	0.65 ±.02	0.65 ±.02	0.70 ±.01
632.8	0.20 ±.04	0.31 ±.01	0.26 ±.005
	Extinction Coefficient		
495.7 *	1.57 ±.2	2.01 ±.2	1.59 ±.2
476.5 *	1.63 ±.2	1.81 ±.2	1.57 ±.2
488.0	1.87 ±.03	2.01 ±.04	1.88 ±.03
496.5	1.79 ±.04	2.02 ±.06	1.82 ±.05
501.7 *	1.63 ±.2	1.80 ±.2	1.59 ±.2
514.5	2.02 ±.03	2.18 ±.04	1.98 ±.02
632.8	3.40 ±.04	3.72 ±.08	3.27 ±.03

	Dielectric Constant	
	ϵ_1	ϵ_2
488.0	-2.14 ±.13	4.44 ±.08
496.5	-2.19 ±.20	3.86 ±.12
514.5	-3.43 ±.10	2.77 ±.07
632.8	-10.63 ±.18	1.70 ±.05

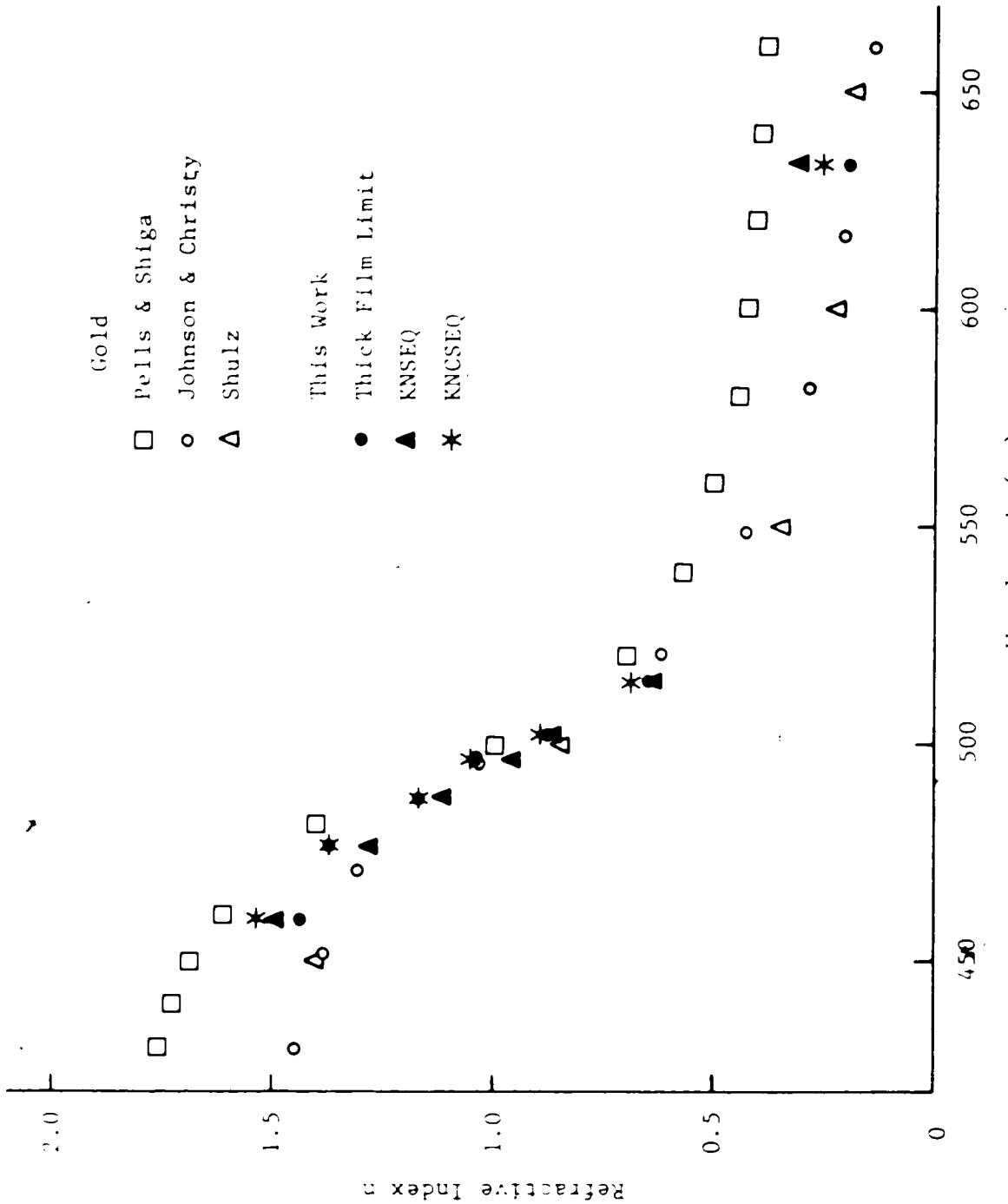

Fig. 18. The real part of the refractive index of gold, as a function of wavelength.

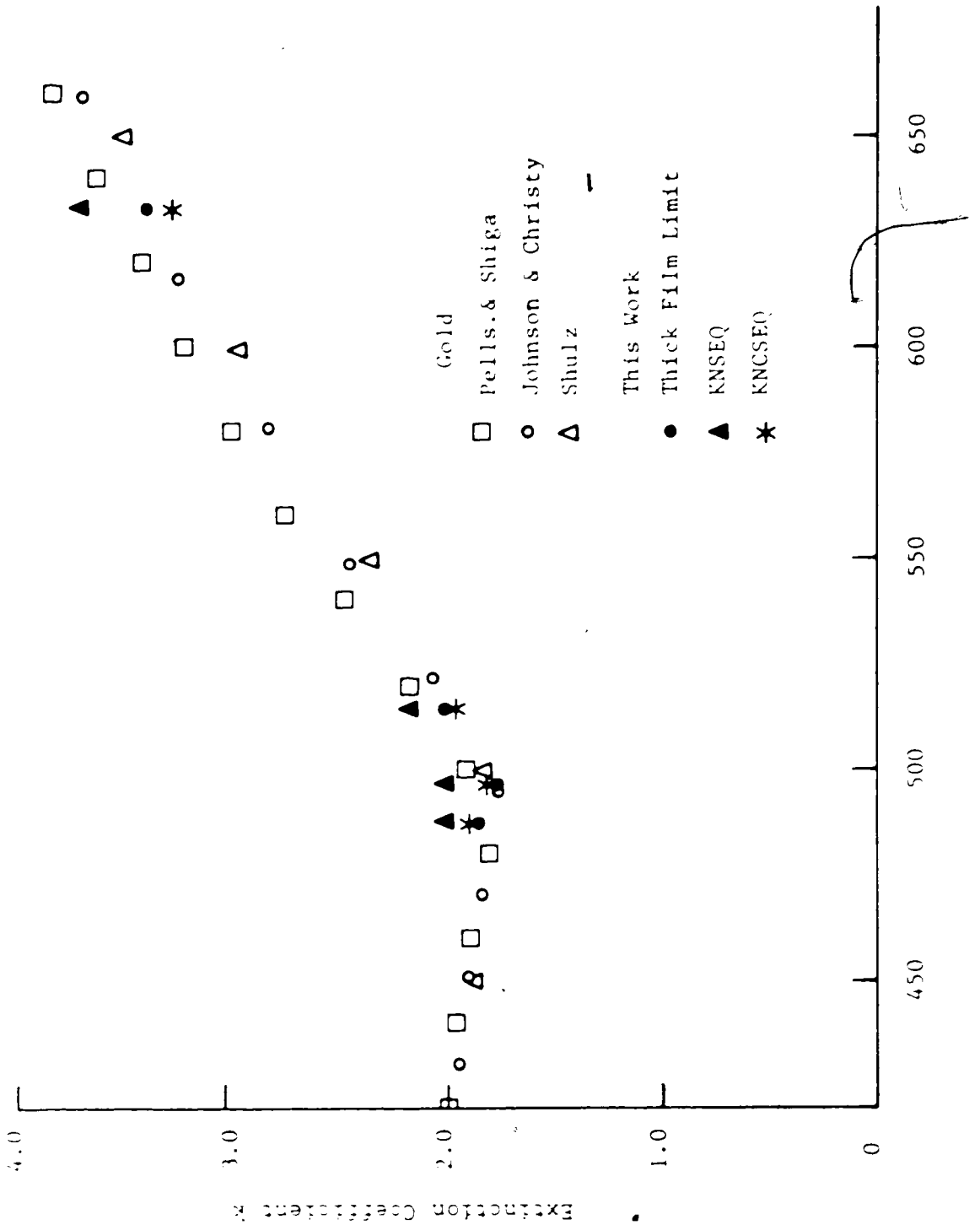

Fig. 19. The imaginary part of the refractive index of gold, as a function of wavelength.

4-2 Gold Analysis - Full Expressions

The gold data were also fitted using the full expressions for the phase shift and optical density, i.e. Equations (46) and (52) using (39). Since there was no program available that could do a least squares fit to an equation of this complexity, the fitting was done by working out the least squares condition explicitly and solving the resulting expression numerically.

If x_d represents a set of data for samples of different thickness and $X_d(z)$ is a theoretical expression to be fitted as a function of z to the data, then the least squares condition for the best fit is that the sum of squares of the deviations be a minimum, or equivalently that the derivative of the sum be zero:

$$\sum_d [x_d - X_d(z)]^2 = \min$$

$$\sum_d [x_d - X_d(z)] \frac{\partial X_d(z)}{\partial z} = 0 \qquad (134)$$

Equations (46) and (52) were fitted to the phase and optical density data in this way. Both of Equations (46) and (39) depend on both n and k and thus in principle both parameters could be obtained by fitting either expression. However, the optical density expression is much more sensitive to k than to n, and the phase expression to n than to k. This can be seen on Figs. 16 and 17, where auxilliary curves (dashed) show the effects of varying the less sensitive parameter. Varying k shifts the phase curves up or down slightly, but for most of the range the curves are parallel to the original. Varying n has a similar slight effect on the optical density curves. This is not surprising, since most of the range shown is in the thick film regime. The extinction coefficient is associated with absorption, and thus largely determines the optical density, whereas the refractive index is associated with the wavelength of the light in the material, and thus determines the phase.

Because of these considerations, the phase shift expression was fitted by varying n only, and the optical density expression by varying k only. The expressions were fitted alternately and iteratively, using the updated values of n and k. The fitting was done by the FORTRAN program KNSEQ. The thick film limit values of n and k were used as initial values, and since the n values were considered to be more reliable the optical density expression was fitted first to obtain k. For each fit the value of phase shift or optical density and the appropriate derivative is calculated for each sample thickness and subtracted from the data, and the products of the deviation and derivative are summed, as in Equation (134). The sum is then solved numerically for the value of n or k by the IMSL[40] subroutine ZSYSTM. This subroutine solves a set of simultaneous non-linear equations by iterating until the roots converge to within a specified number of significant figures or until a preset number of iterations is reached.

For an isotropic medium and normal incidence, the observed phase shift ψ and optical density are given by (from (46) and (52) with (39a))

$$\psi = -\frac{2\pi d}{\lambda} - \arctan {}^{P_1}/_{P_2} \tag{135}$$

$$O.D. = \log_{10} \frac{P_0}{16(n^2+k^2)} \tag{136}$$

The final expressions for the derivatives with respect to n and k are

$$\frac{\partial \psi}{\partial n} = \frac{1}{(P_1^2+P_2^2)}\left[\left(\frac{2\pi d}{\lambda} Q_1 + kF_1(F_2-2)\right)e^{2K} - \left(\frac{2\pi d}{\lambda} Q_2 - kF_2(F_1-2)\right)e^{-2K} + (Q_4+8k^2)\sin 2N + 2k\,4n^2-F_3(F_3+2)\cos 2N\right] \tag{137}$$

$$\frac{\partial O.D.}{\partial k} = \log_{10}e\left[\frac{1}{P_0}\left(4F_1(k+\frac{\pi d}{\lambda}F_1)e^{2K} + 4F_2(k-\frac{\pi d}{\lambda}F_2)e^{-2K} + 8(n^2-1+3k^2)\sin 2N - 8k(n^2-3+k^2)\cos 2N\right) - \frac{(n^2+2k)}{(n^2+k^2)}\right] \tag{138}$$

where $Q_1 = (nF_1 + 2k^2)^2 + k^2F_3^2$ (139)

$Q_2 = (nF_2 - 2k^2)^2 + k^2F_3^2$ (140)

$Q_3 = (nF_1 + 2k^2)(nF_2 - 2k^2) + k^2F_3^2$ (141)

$Q_4 = 4F_3(F_3+1)$ (142)

The phase and optical density expressions were each fitted three times for each data set. The results were usually very close to the final values after the second fit. Each fit required typically 4 or 5 iterations to converge to 4 significant figures. The fitting process was very insensitive to the input values of n and k, which could be changed by $\pm.2$ and still give the same answer at the first fit. It was necessary to use double precision to obtain reliable results. The KNSEQ results are listed in Table I and shown in Figs. 18 and 19.

Unlike the thick film approach, the KNSEQ fit does not eliminate surface effects, nor does it account for them since the theory assumes abrupt interfaces. Oxide layers or adsorbed layers of contaminants such as water could cause optical behaviour which is not characteristic of the bulk material. The differences between the thick film limit and KNSEQ results suggests that such effects may be present. As a means of compensating for possible surface effects, it was assumed that any such effect would be consistent from sample to sample, and the fits were repeated with a fixed phase or optical density term which was independent of sample thickness but could vary with wavelength added to each datum. For both phase shift and optical density the program fitted two equations of the form

$$\sum_d [x_d + c - X_d(z)] \frac{\partial(\text{dev})}{\partial z, c} = 0 \qquad (134a)$$

where the derivative of the deviation with respect to the constant c is 1. An input value of $c = 0$ was used. The fits were just as insensitive to the input values of n and k as were the KNSEQ fits, but the statistical errors were about half as large. The results, labelled KNCSEQ, are listed in Table I and shown in Figs. 18 and 19.

As an alternative approach, the fits were repeated assuming an effective thickness $d_{eff} = d_{meas} + d_o$ with the term d_o being independent of sample thickness. The program then fitted two equations

$$\sum_d [x_d - X_d(z,d_o)] \frac{\partial X_d(z,d_o)}{\partial z, d_0} = 0 \qquad (134b)$$

The derivatives of phase and optical density with respect to d_o were of similar complexity to equations (137) and (138). The results for n and k were similar to those from KNSEQ and KNCSEQ but the fits were less satisfactory; more iterations were required, and sometimes the fit did not converge to the required number of significant figures within the specified number of iterations. Furthermore the fitted values of d_o, which ranged from 0 to 100 nm, were not at all systematic. This approach was not pursued.

4-3 Gold Results

As seen in Figs. 18 and 19, the three analyses of the data give at least good qualitative agreement with each other and with measurements reported in the literature, with the possible exception of the k values obtained with the three weakest laser lines. The thick film limit values are in particularly good agreement with Johnson and Christy[16]. The values obtained with KNSEQ tend to be slightly lower for n and higher for k. The KNCSEQ values are in much better agreement with the thick film limit values. This approaches is considered to be the most reliable. The reduction of the statistical errors indicates that some addition to the theory to account for surface effects is realistic. The KNCSEQ results at the shorter wavelengths are closer to those of Pells and Shiga[22]. The results are also in good agreement with the measurements of Joensen et al [17,18].

The fitted values of the constants are shown in Fig. 20 as a function of wavelength. There is a suggestion of a systematic variation, with the constant phase term being largest and the constant optical density term smallest in the range where the dispersion curve is

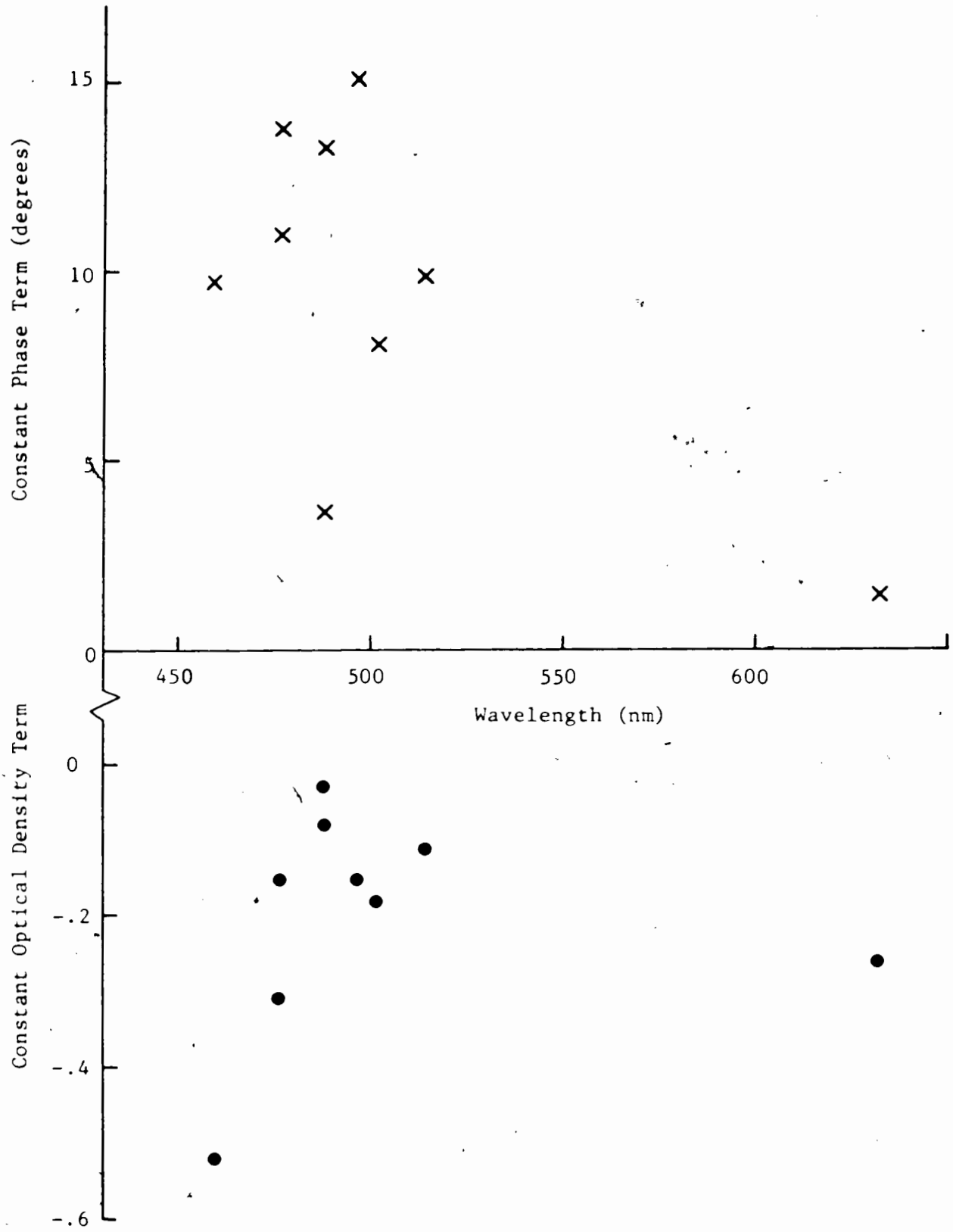

Fig. 20. The values of the fitted constants as a function of wavelength.

steepest. The treatment here is purely phenomenological. Better data, particularly for the optical density, would be required for a meaningful analysis of these effects. The final system with the DVM interfaced to the computer would probably be good enough for this purpose. A much more quantitative assessment of sample quality would be required, and a detailed study of the effects of contaminant layers would probably also be necessary. This is beyond the scope of this work.

The errors quoted for n and k in Table I are the standard deviations of the means of the final fitted values. When possible systematic errors in the determination of sample thickness are taken into account, the values of n are felt to be accurate to $\pm .01\%$ and the values of k to within a few percent. The values for the three weakest lines are somewhat less reliable.

4-4 GaSe - Butler Fringe Results

Transmission was recorded as a function of wavelength for a set of GaSe samples, and dispersion curves for each sample were obtained from the fringe data by the method outlined in section 3-4. The results for the ordinary index for the five thickest samples (18 to 320 μm) were averaged by combining all the data points, weighting each point according to the total number of points for that sample, and fitting a third order polynomial in $1/\lambda^2$. To check for any small systematic features on the curve, the values of thickness and interference order for each sample were then adjusted for best fit to the average curve and the individual curves recalculated and superimposed. No features were seen other than a slight deviation from the general shape of the curve on either side of the small gap in the data which appeared at the band edge. This gap in the data was the result of the rapid change in absorption at the exciton line, which made it very difficult to resolve the fringes over a narrow wavelength interval.

For samples thicker than about 50 μm, no fringes could be seen for energies greater than the band gap energy (~2 eV, or λ = 620 nm).

Three thinner samples (1.5 to 6 μm) were used to extend the curve well into the absorbing region. The normal incidence fringe patterns for these samples were obtained, and their thickness and interference orders were determined by comparing the data in the transparent region with the initial average curve. Using these values, the dispersion curves were calculated, and combined with the previous data to give the final averaged ordinary dispersion curve.

The fitted polynmials provide a convenient and accurate means of reproducing the data. Separate polynomials were fitted to the data in the regions above and below the band gap. Since the polynomials could not reproduce the small hooks near the band edge, only data for wavelengths more than 10 nm from the edge were fitted. The coefficients obtained are listed in Table II.

A similar approach was used to obtain the extraordinary dispersion curve. Measurements were made at 30 and 45 degrees incidence with the light polarized in the plane of incidence. The extraordinary index for each point was calculated using Equation (121), taking the value of the ordinary index at that wavelength from the averaged ordinary polynomial. The results were fitted to polynomials as for the ordinary index: the values of the coefficients are listed in Table II.

Table II -- Coefficients of the fitted polynomial dispersion curves for GaSe. With wavelength λ in μm,

$$n = A + B/\lambda^2 + C/\lambda^4 + D/\lambda^6$$

	λ range	A	B $(\mu m)^2$	C $(\mu m)^4$	D $(\mu m)^6$
n_o	.408 - .609	2.647	0.134	-0.0155	2.58×10^{-3}
	.621 - 1.02	2.678	0.121	-0.0215	5.41×10^{-3}
n_e	.425 - .600	2.406	0.166	-0.044	5.48×10^{-3}
	.640 - .955	2.004	0.645	-0.335	0.072

The resulting ordinary and extraordinary dispersion curves are shown in Fig. 21, in which the data from several samples is shown superimposed. The relative accuracy is indicated by the scatter in the points. The absolute accuracy is about $\pm.01$ to .015 for the ordinary index, $\pm.025$ for the extraordinary index in the transparent region, and about $\pm.07$ for the extraordinary index in the absorbing region. The results for $n_{\parallel}$ in the absorbing region showed more sample variation than in the other regions. Some samples gave smooth data, others noisy data, but all data sets showed the same wavelength dependence. The fitted polynomial in this region is also shown.

These results are in excellent agreement with those of Wasscher and Dieleman[11]. The present results extend the range of measurement considerably, and establish the proper shape of the $n_{\parallel}$ curve in the absorbing region. Much less structure is seen on the curves near the band edge than was reported by Brebner and Deverin[25] or Akhundov et al[26], and the extraordinary dispersion curve is substantially higher than that reported by Akhundov et al[26].

4-5 GaSe - Interferometer Results

The interferometer was used to measure a set of GaSe films of thickness 0.5 to 2.5 μm over a wavelength range 514.5 to 650 nm. This was done to test the performance of the interferometer with weakly absorbing films by comparing the results with the Butler fringe results, and also to examine the region near the band edge in detail. The measurements were made at oblique as well as normal incidence to obtain the extraordinary parameters. For the measurements near the band edge the DVM was interfaced to the computer. For the other measurements it was read by eye as before.

The analysis also followed the same pattern as before, with the optical density and phase data being fitted alternately, adjusting k only for the optical density fit and n only for the phase fit. The justification for this procedure is somewhat different here. Curves

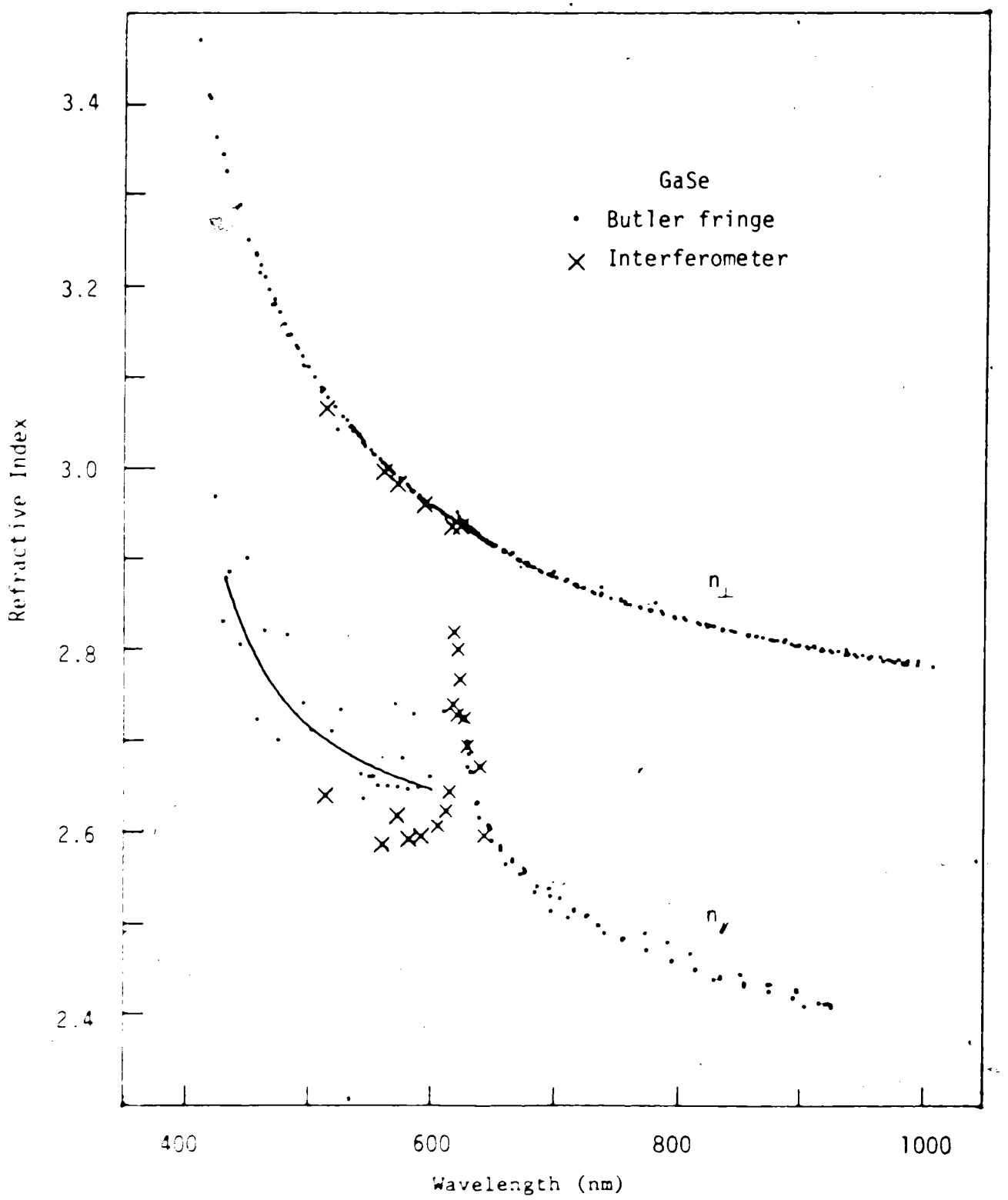

Fig. 21. The refractive indices of GaSe.

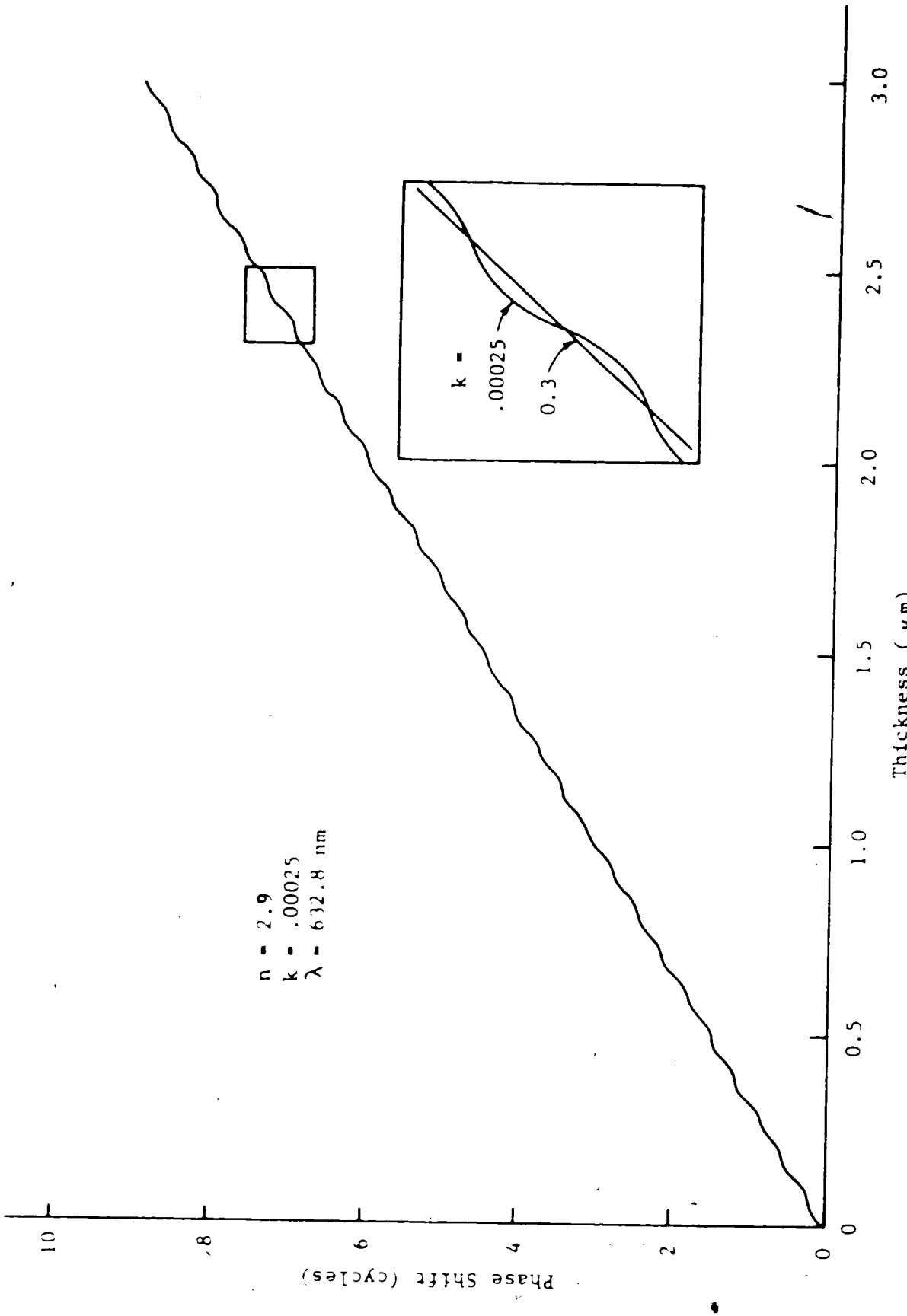

Fig. 22. A calculated curve of phase shift as a function of sample thickness for GaSe.

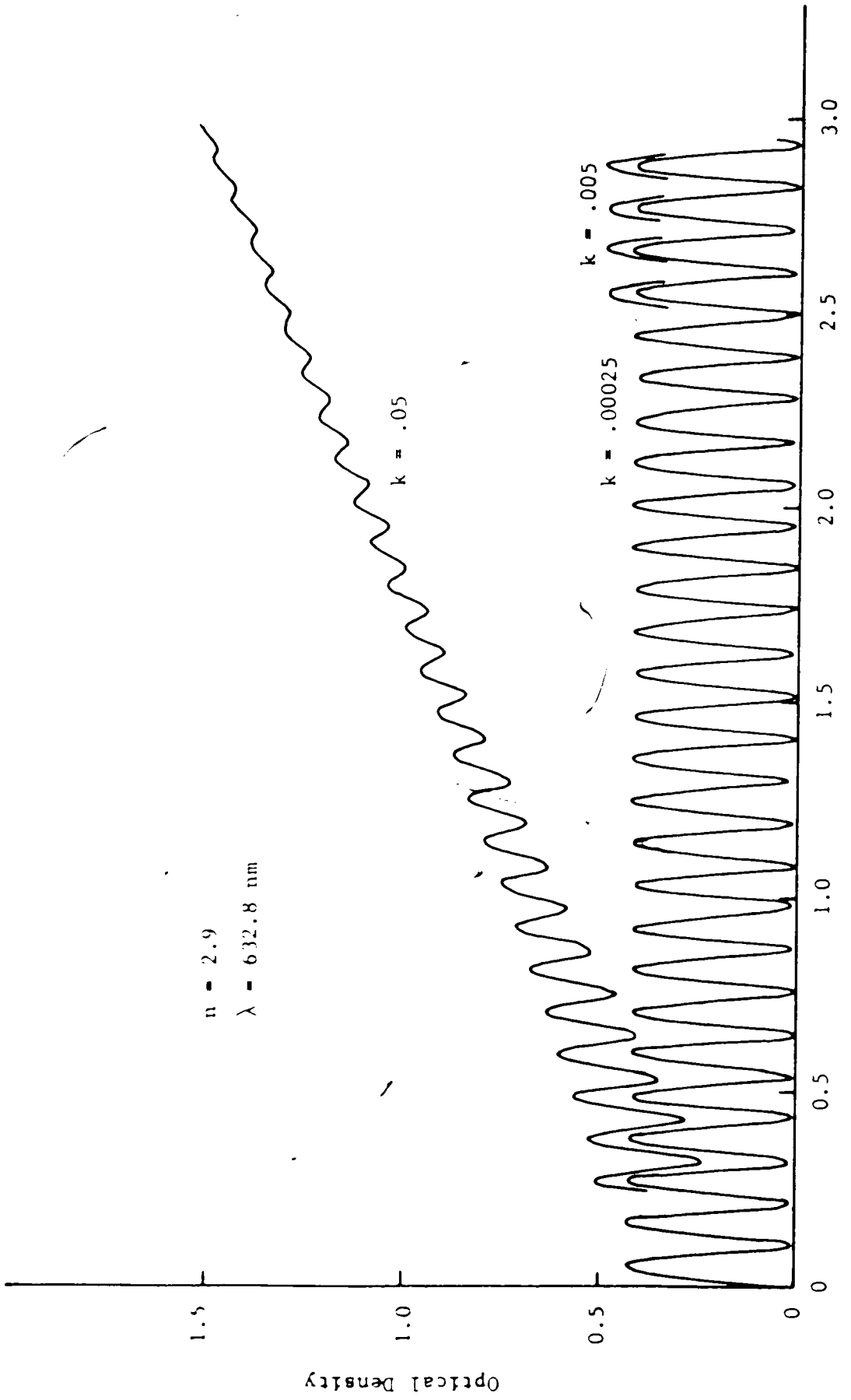

Fig. 23. Calculated curves of optical density as a function of sample thickness, for GaSe.

showing the expected variation of the observed phase shift and optical density with sample thickness calculated using parameters representative of GaSe are shown in Figs. 22 and 23. As before, the curves of phase shift with thickness are determined primarily by the refractive index; k determines the amplitude of the oscillation, which is reduced as k increases. The mean slope and amplitude of the oscillation in the optical density curve is determined by the value of k and the periodicity of the oscillation by n. However in the thickness range of the present measurements the oscillations are much more important than is the mean slope, and thus if the optical density data is fitted by varying both n and k the variation of n would dominate. Thus it was felt that more reliable values of k would be obtained if the n values were obtained from a fit of the phase data and used as a fixed input parameter for the optical density fits.

No attempt was made to incorporate constant vaules of phase or optical density to account for surface effects as with the gold data. These effects should be very small, since the phase shift invloves many full cycles (though it is measured modulo 2π) and because of the weak dependence of the optical density on k.

The normal incidence measurements were fitted using KNSEQ in exactly the same manner as with the gold films. The initial values of n were taken from the Butler fringe results, interpolating across the small gap in the data at the band edge, and the initial k values were taken from Wasscher and Dieleman[11]. The oblique incidence data was fitted by the program EKNSEQ, which functions in exactly the same manner as KNSEQ. This program fits the more complicated oblique incidence expressions, as given by Equations (103) and (117). Initial values of n were taken from the Butler fringe results, and k again from Wasscher and Dieleman[11]. Values of $n_\perp$ and $k_\perp$ provided as fixed input data were taken from the KNSEQ results.

The derivatives of the phase shift and optical density expressions with respect to $n_{//}$ and $k_{//}$ are again obtained by straightforward, tedious calculus: the final expressions are

$$\frac{\partial \psi}{\partial n_{//}} = \frac{1}{(P_1^2+P_2^2)}\left(P_1\frac{\partial P_2}{\partial n_{//}} - P_2\frac{\partial P_1}{\partial n_{//}}\right) \qquad (143)$$

$$\frac{\partial O.D.}{\partial k_{//}} = \log_{10}e\left(\frac{1}{P_0}\frac{\partial P_0}{\partial k_{//}} - \frac{J_{1k}}{J_1}\right) \qquad (144)$$

where the derivatives

$$\frac{\partial P_0}{\partial k} = (G_{1k}+2G_1K_{//k})e^{2K_{//}} + (G_{2k}-2G_2K_{//k})e^{-2K_{//}} + (G_{3k}-2G_4N_{//k})\sin 2N_{//} + (G_{4k}+2G_3N_{//k})\cos 2N_{//} \qquad (145)$$

$$\frac{\partial P_1}{\partial n} = (e^{-K_{//}}-e^{K_{//}})\left[2J_{1n}\cos\theta\sin N_{//} - J_{4n}\cos N_{//} + 2J_1N_{//n}\cos\theta\cos N_{//} + J_4N_{//n}\sin N_{//} + J_3K_{//n}\sin N_{//}\right] - (e^{K_{//}}+e^{-K_{//}})\left[J_{3n}\sin N_{//} + 2J_1K_{//n}\cos\theta\sin N_{//} + J_3N_{//n}\cos N_{//} - J_4K_{//n}\cos N_{//}\right] \qquad (146)$$

$$\frac{\partial P_2}{\partial n} = (e^{K_{//}}+e^{-K_{//}})\left[2J_{1n}\cos\theta\cos N_{//} + J_{4n}\sin N_{//} - 2J_1N_{//n}\cos\theta\sin N_{//} + J_4N_{//n}\cos N_{//} + J_3K_{//n}\cos N_{//}\right] + (e^{K_{//}}-e^{-K_{//}})\left[J_{3n}\cos N_{//} + 2J_1K_{//n}\cos\theta\cos N_{//} - J_3N_{//n}\sin N_{//} + J_4K_{//n}\sin N_{//}\right] \qquad (147)$$

In these expressions, the subscripts n and k denote derivatives with respect to $n_{//}$ and $k_{//}$ respectively. The G, J, and P expressions are defined in Equations (103) to (117) in section 2-5-2. Also defining

$$c = n_{//}^2 + k_{//}^2 \qquad (148)$$

$$f = \sqrt{c^2 + 4n_{//}^2k_{//}^2} \qquad (149)$$

we have

$$N_{//n} = \frac{\partial N_{//}}{\partial n_{//}} = \frac{2\pi d}{c^2\lambda}\left\{\frac{c}{f}\left[\frac{n_{//}}{a}(k_{//}^2+a^2)(n_\perp n_{//}+k_\perp k_{//}) + \frac{n_{//}}{b}(k_{//}^2-b^2)(n_\perp k_{//}-n_{//}k_\perp)\right] - (n_{//}^2-k_{//}^2)(an_\perp-bk_\perp) - 2n_{//}k_{//}(ak_\perp+bn_\perp)\right\} \qquad (150)$$

$$N_{//k} = \frac{\partial N_{//}}{\partial k_{//}} = \frac{2\pi d}{c^2\lambda}\left\{\frac{c}{f}\left[\frac{k_{//}}{a}(n_{//}^2-a^2)(n_\perp n_{//}+k_\perp k_{//}) + \frac{k_{//}}{b}(n_{//}^2+b^2)(n_\perp k_{//}-n_{//}k_\perp)\right] + (n_{//}^2-k_{//}^2)(ak_\perp+bn_\perp) - 2n_{//}k_{//}(an_\perp-bk_\perp)\right\} \qquad (151)$$

$$K_{\perp n} = \frac{\partial K_\perp}{\partial n_\perp} = \frac{2\pi d}{c^2\lambda}\left\{\frac{c}{f}\left[\frac{n_\perp}{b}(k_\perp^2-b^2)(n_\perp n_\perp + k_\perp k_\perp) - \frac{n_\perp}{a}(k_\perp^2+a^2)(n_\perp k_\perp - n_\perp k_\perp)\right]\right.$$
$$\left. - (n_\perp^2-k_\perp^2)(ak_\perp + bn_\perp) + 2n_\perp k_\perp(an_\perp - bk_\perp)\right\} \qquad (152)$$

$$K_{\perp k} = \frac{\partial K_\perp}{\partial k_\perp} = \frac{2\pi d}{c^2\lambda}\left\{\frac{c}{f}\left[\frac{k_\perp}{b}(n_\perp^2+b^2)(n_\perp n_\perp + k_\perp k_\perp) - \frac{k_\perp}{a}(n_\perp^2-a^2)(n_\perp k_\perp - n_\perp k_\perp)\right]\right.$$
$$\left. - (n_\perp^2-k_\perp^2)(an_\perp - bk_\perp) - 2n_\perp k_\perp(ak_\perp + bn_\perp)\right\} \qquad (153)$$

Using these expressions,

$$J_{1n} = \frac{\lambda}{\pi d}(\eta N_{\perp n} + \nu K_{\perp n}) \qquad (154)$$

$$J_{1k} = \frac{\lambda}{\pi d}(\eta N_{\perp k} + \nu K_{\perp k}) \qquad (155)$$

$$J_{2n} = \frac{4\sin^2\theta}{c^3}\left[\alpha n_\perp(n_\perp^2-3k_\perp^2) - \beta k_\perp(3n_\perp^2-k_\perp^2)\right] \qquad (156)$$

$$J_{2k} = \frac{4\sin^2\theta}{c^3}\left[\alpha k_\perp(3n_\perp^2-k_\perp^2) + \beta n_\perp(n_\perp^2-3k_\perp^2)\right] \qquad (157)$$

$$J_{3n} = \frac{\lambda}{2\pi d}(\alpha N_{\perp n} + \beta K_{\perp n}) + \frac{2\sin^2\theta}{c^3}\left[\eta n_\perp(n_\perp^2-3k_\perp^2) - \nu k_\perp(3n_\perp^2-k_\perp^2)\right] \qquad (158)$$

$$J_{3k} = \frac{\lambda}{2\pi d}(\alpha N_{\perp k} + \beta K_{\perp k}) + \frac{2\sin^2\theta}{c^3}\left[\eta k_\perp(3n_\perp^2-k_\perp^2) + \nu n_\perp(n_\perp^2-3k_\perp^2)\right] \qquad (159)$$

$$J_{4n} = \frac{\lambda}{2\pi d}(\beta N_{\perp n} - \alpha K_{\perp n}) - \frac{2\sin^2\theta}{c^3}\left[\eta k_\perp(3n_\perp^2-k_\perp^2) + \nu n_\perp(n_\perp^2-3k_\perp^2)\right] \qquad (160)$$

$$J_{4k} = \frac{\lambda}{2\pi d}(\beta N_{\perp k} - \alpha K_{\perp k}) + \frac{2\sin^2\theta}{c^3}\left[\eta n_\perp(n_\perp^2-3k_\perp^2) - \nu k_\perp(3n_\perp^2-k_\perp^2)\right] \qquad (161)$$

and $G_{1k} = 4J_{1k}\cos^2\theta + 4J_{3k}\cos\theta + J_{2k}$ (162)

$$G_{2k} = 4J_{1k}\cos^2\theta - 4J_{3k}\cos\theta + J_{2k} \qquad (163)$$

$$G_{3k} = 8J_{4k}\cos\theta \qquad (164)$$

$$G_{4k} = 8J_{1k}\cos^2\theta - 2J_{2k} \qquad (165)$$

The values of the refractive indices obtained from the interferometer measurements are shown in Fig. 21, and in greater detail near the band edge in Figs. 24 and 25. The values of the extinction coefficients are shown in Fig. 26, compared to the values obtained by Wasscher and Dieleman[11]. These values are listed in Table III.

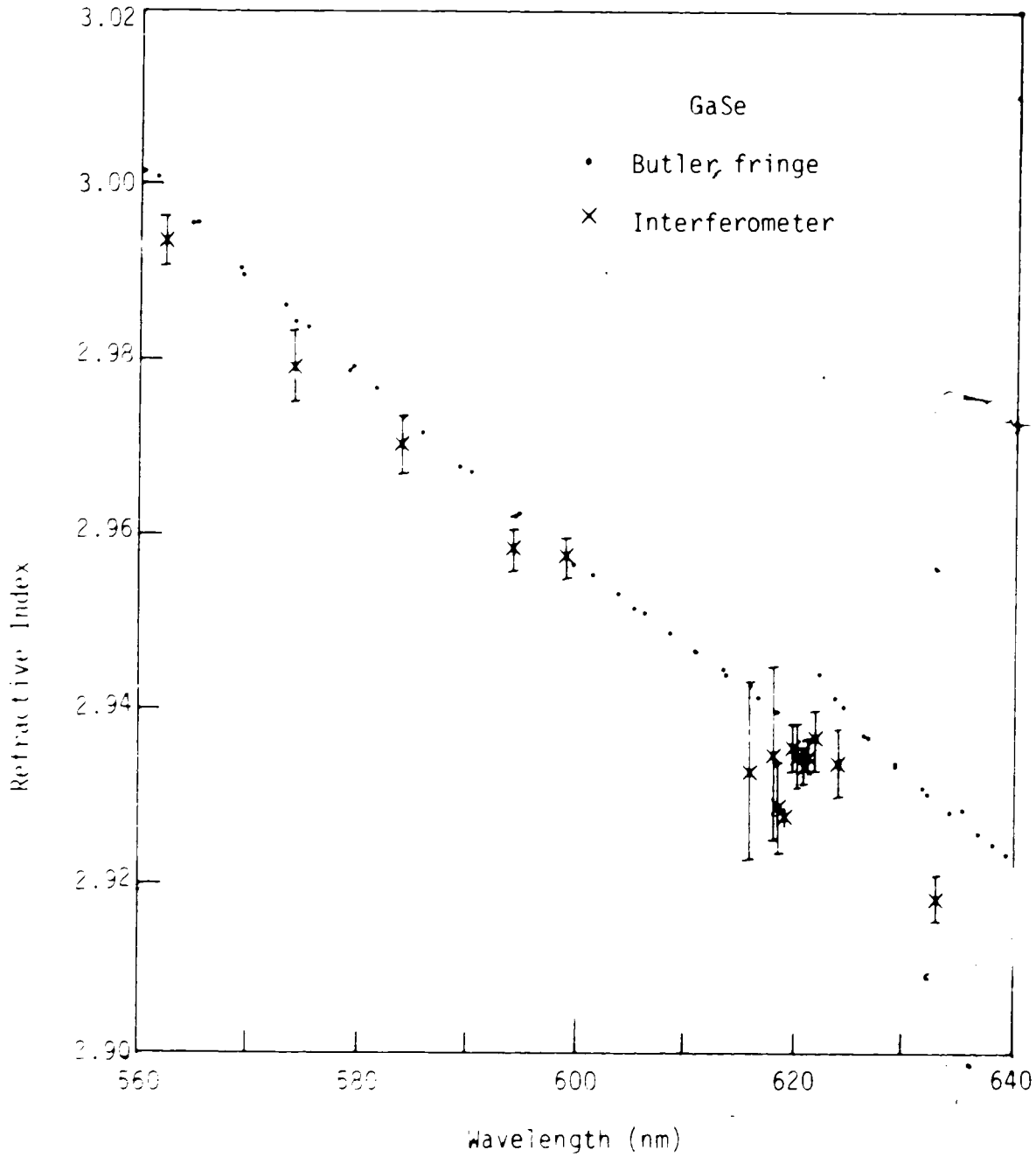

Fig. 3-. The ordinary refractive index $n_{\perp}$ of GaSe near the band edge.

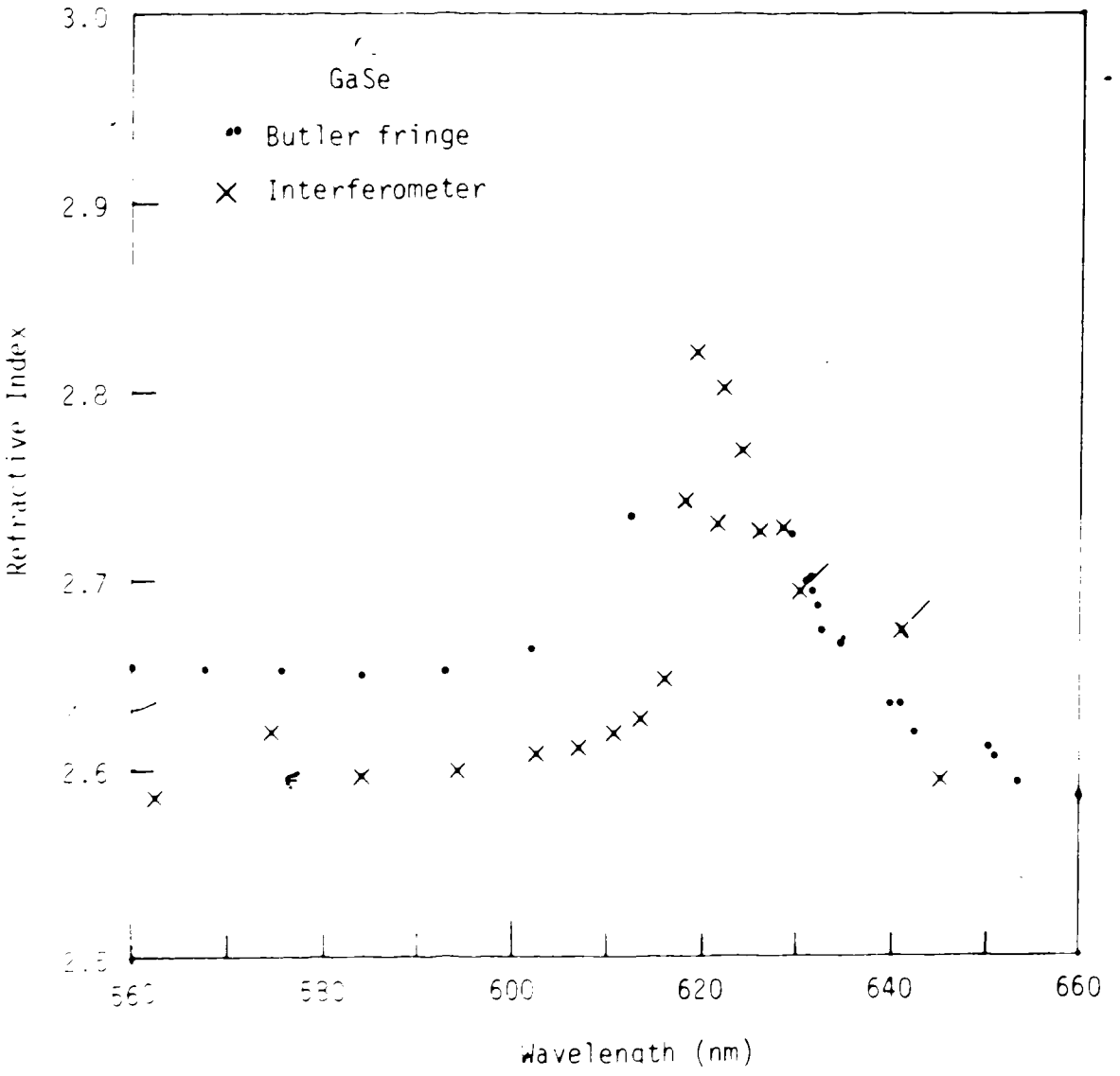

Fig. 25. The extraordinary refractive index n_e of GaSe near the band edge. The interferometer points marked with a slash are values which did not converge properly within the specified number of iterations.

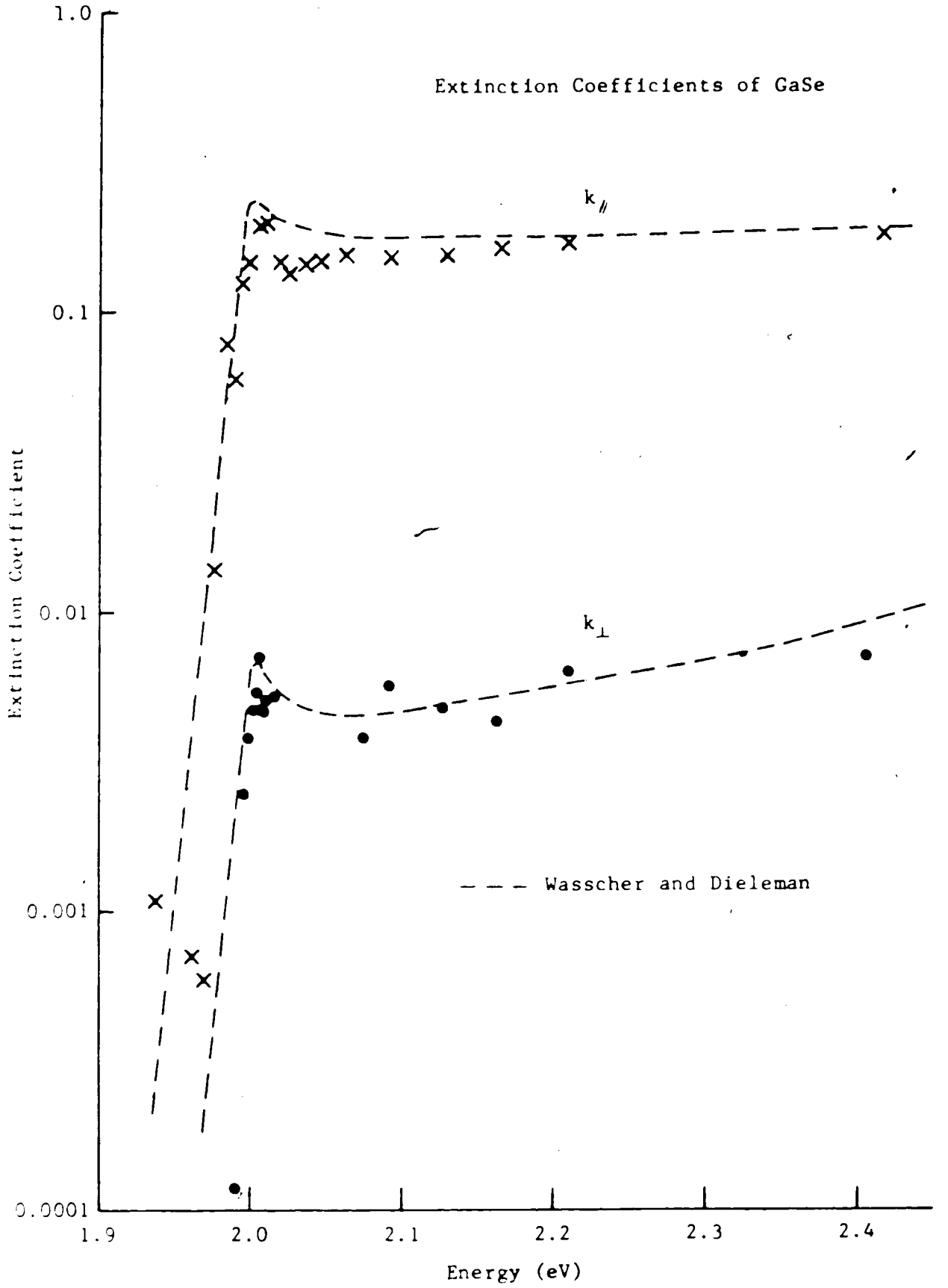

Fig. 26. The extinction coefficients of GaSe.

Table III -- The optical constants of GaSe as determined from the interferometer measurements. Values marked with an asterisk did not converge to within four significant figures in 30 iterations. The errors shown are the statistical fitting errors.

Wavelength (nm)	Energy (eV)	Ordinary n	Ordinary k
514.5	2.414	3.063 ±.002	.00716
562.3	2.209	2.993 ±.003	.00632
574.3	2.163	2.979 ±.004	.00429
584.0	2.127	2.970 ±.003	.00480
594.2	2.090	2.958 ±.002	.00562
599.2	2.073	2.957 ±.002	.00380
616.1	2.017	2.932 ±.010	.00524
618.1	2.010	2.934 ±.010	.00504
618.7	2.008	2.928 ±.005	.00468
619.2	2.006	2.927 ±.001	.00702
619.9	2.004	2.935 ±.003	.00474
620.3	2.003	2.934 ±.004	.00528
620.9	2.001	2.932 ±.002	.00470
621.4	1.999	2.934 ±.002	.00374
622.1	1.997	2.936 ±.003	.00245
624.1	1.990	2.933 ±.004	.00012
632.8	1.963	2.918 ±.002	-.00108 (?)
		extraordinary	
514.5	2.414	2.640	0.181
562.3	2.209	2.586	0.170
574.4	2.163	2.619	0.161
584.0	2.127	2.594	0.153
594.3	2.090	2.597	0.153
602.5	2.062	2.606	0.156
607.0	2.046	2.609	0.149
610.7	2.034	2.617	0.146
613.6	2.024	2.625	0.134
616.0	2.017	2.646	0.147
618.3	2.009	2.741	0.199
619.5	2.005	2.819	0.191
621.7	1.998	2.728	0.146
622.5	1.995	2.800	0.125
624.4	1.990	2.767	0.0594
626.2	1.984	2.722	0.0782
628.6	1.976	2.726	0.0139
630.5	1.970	2.693 *	0.00059
632.8	1.963	2.817 *	0.00071
641.0	1.938	2.672 *	0.00109
645.3	1.925	2.595	0.0221

The ordinary refractive index values are in very good agreement with the Butler fringe values, and confirm that the structure on the ordinary dispersion curve near the band edge is small. The ordinary extinction coefficient values are in good agreement with Wasscher and Dieleman's results[11], but the results are rather noisy, and do not show much detail of the band edge or exciton line. This is due to the very low level of absorption in the thin samples used, and to the amount of noise on the dye laser lines. The data near the band edge, obtained with the DVM interfaced to the computer, are noticeably smoother than the data for which the DVM was read by eye.

The extraordinary refractive index values obtained from the interferometer measurements clearly show the peak in the dispersion curve at the band edge. The results are in good agreement with the Butler fringe values on the long wavelength side of the peak, but are systematically lower by about .05 on the short wavelength side. The interferometer results also show a slightly narrower peak, with the short wavelength side being shifted to longer wavelengths while the long wavelength side is uneffected. The data points marked with a slash did not converge to four significant figures within thirty iterations, so their accuracy is less certain. The $n_{/\!/}$ and $k_{/\!/}$ values are listed in Table III.

The extinction coefficient values are in good agreement with Wasscher and Dieleman[11], and show more detail at the band edge. The band edge appears to be resolved from the exciton line. According to Schluter's model[41] for the electronic band structure of GaSe the same transition (Γ_4^- to Γ_3^+) is responsible for band edge absorption in both polarizations. This transition is allowed for E//c and forbidden for E⊥c, but becomes weakly allowed for E⊥c if spin orbit coupling is taken into account. Furthermore, the bands are three dimensional at the Γ point, so no spurious effects such as two dimensional excitons are expected. Thus the present results obtained with the extraordinary polarization can be compared to measurements made at normal incidence, i.e. with ordinary polarization. An indirect

transition at slightly lower energy than the direct transition has also been observed[42,43], but the absorption is very much weaker and was not observed here.

Grandolfo et al[44] obtained good agreement between experimental absorption data obtained at normal incidence and a theoretical model using values for E_g = 2.025 eV, an exciton binding energy of 14.3 meV, and the Lorentzian parameter Γ (the half width at half maximum height of the exciton peak) of 9.1 meV at 280.5 K. These numbers were obtained by fitting a curve of a series of sharp exciton lines and an abrupt band edge convoluted with a Lorentzian lifetime broadening function to experimental absorption data obtained at normal incidence. The theoretical curve calculated on the basis of this model is shown in Fig. 27 compared to the present $k_{//}$ data. The curve has been corrected for a 13 degree temperature difference using their value of .414 meV/degree, then scaled upward by a factor of 31 to match the data at the absorption peak. (The unscaled curve is slightly higher than our $k_\perp$ data. A ratio of 35 for absorption in the two polarizations is expected[11,45].) The agreement between the data and curve give strong support to the model and values used in the calculations in Ref. [41].

Several authors[46,47] have reported a variation of the absorption of the exciton peak with sample thickness when studying thin GaSe crystals at low temperature. The effect was attributed to surface polaritons[47]. Since in the present method the variation of data with sample thickness is fitted, any such effect could have serious consequences; however, curves given by Bosacchi et al[47] indicate that no effect is expected at room temperature.

The error bars in Fig. 24 show the standard deviations of the mean (fitted) values of $n_\perp$. When the uncertainty in sample thickness is taken into account, the $n_\perp$ values are accurate to about $\pm$.005. The observed phase shift is almost entirely dependent on $n_\perp$ at normal incidence. In contrast, the optical density expression is very strongly dependent on $n_\perp$ although only $k_\perp$ was adjusted in the fit. Under these circumstances it is difficult to extract a meaningful value for the

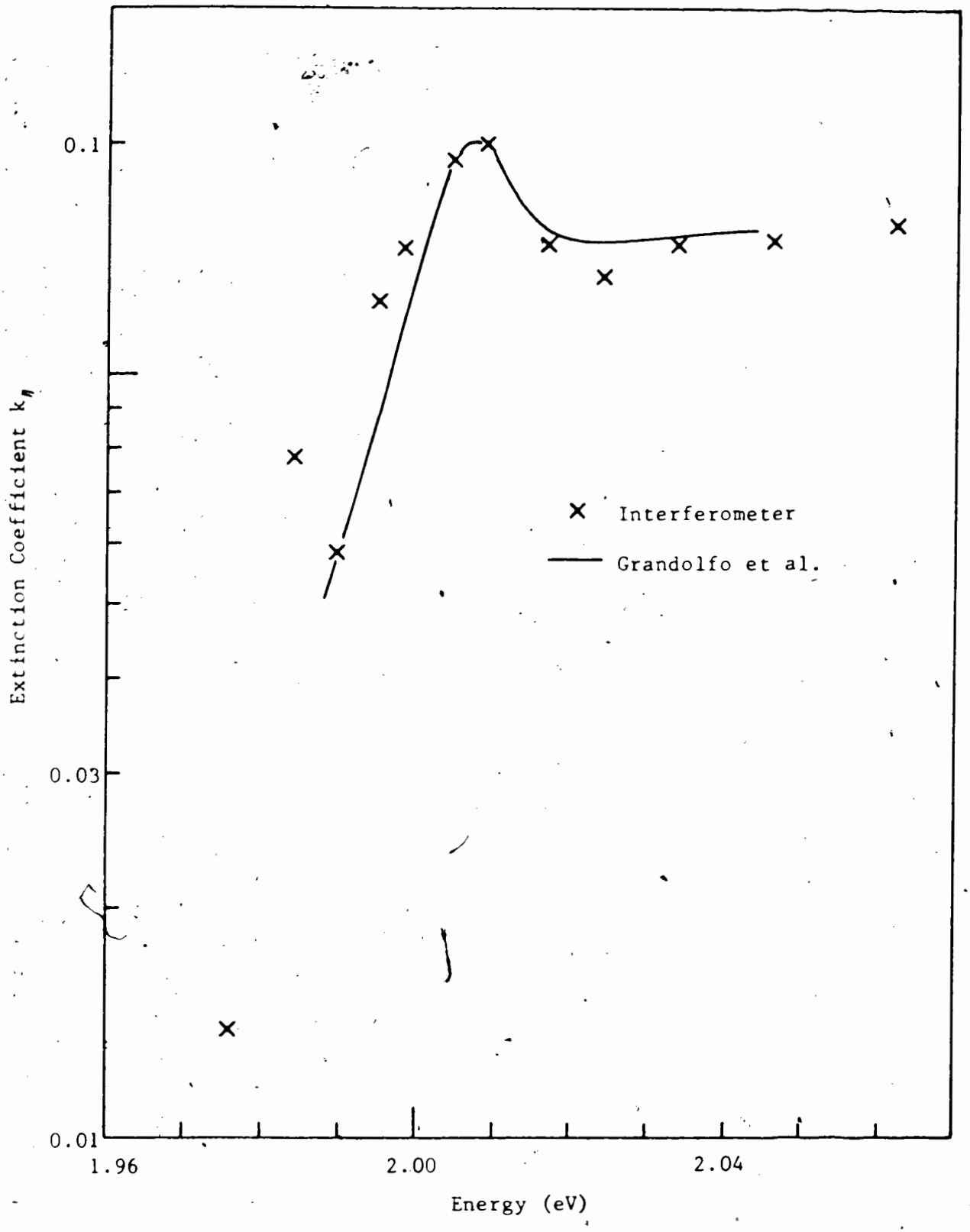

Fig. 27. The extraordinary extinction coefficient $k_{\parallel}$ compared to the theory of Grandolfo et al [44].

uncertainty of $k_\perp$. If only the non-oscillating part of the optical density equation is considered, fits to the data of $\pm.003$ to .007 are obtained. However the scatter on the data points indicates that these values are very pessimistic. Some idea of the accuracy of the fit can be obtained from the standard deviation of the optical density data from the fitted curve. For these measurements, the standard deviation was typically .04 on an average value of about .25. The accuracy of the fitted $k_\perp$ values is estimated to be about 10%. (The corresponding rms deviation for the phase shift data is about 6 degrees in 2 to 8 cycles.) The fits are quite sensitive to the initial value of $n_\perp$, which must be within about 5% of the final value to ensure convergence. Within these limits the same values of $n_\perp$ and $k_\perp$ were always obtained. The fits were very insensitive to the initial values of $k_\perp$. All of the fitted values of $n_\perp$ and $k_\perp$ converged properly.

The uncertainty of the extraordinary parameters is more difficult to estimate. The rms deviations of the phase shift data were about the same as for the normal incidence data, and the deviations of the optical density were slightly better (.025 in an average value of about .3). The standard deviation of the mean $n_{//}$ values was also about the same as for the $n_\perp$ values, indicating that the curves were equally well fitted to the data. However, the fitted values of $n_{//}$ were very sensitive to the input values of $n_\perp$; a shift in $n_\perp$ would produce an opposite shift in $n_{//}$ about ten times as large. When the uncertainty in sample thickness is included, the absolute error on the fitted $n_{//}$ values is estimated to be $\pm.11$ although the relative error is less than $\pm.01$. The initial value of $n_\perp$ also had a small effect on the fitted value of $k_{//}$. The fitted values were sensitive to the initial values of $n_{//}$ which for this range of parameters must be within about 10% of the final value to ensure convergence. The fitted values were not sensitive to the initial value of $k_{//}$, but an increase in the initial $k_\perp$ produces a slight decrease in the fitted value of $k_{//}$. The accuracy of the final values of $k_{//}$ is estimated to be a few percent. Any values of k below about .001 are considered to be unreliable.

CHAPTER 5
CONCLUSIONS

5-1 Assessment of the techniques

A transmission interferometric technique using a laser as a light source has been developed for studying the optical properties of thin solid films. The optical densities and phase changes on transmission through a set of films are measured, and the measured values are fitted as a function of sample thickness. If the samples are thick enough that multiple internal reflections can be neglected, this procedure eliminates the effects due to the sample surfaces, and the resulting values of the optical constants are characteristic of the bulk material. The method has been evaluated by making measurements on gold films, which have high absorption but a low refractive index, and on thin GaSe single crystals, which are weakly absorbing but have a high refractive index, and comparing the results with values reported in the literature[11,16].

The refractive index values obtained were fitted to the data with a statistical accuracy of typically $\pm.01$ for the gold films and $\pm.003$ for the GaSe films. Greater accuracy was possible with the weakly absorbing GaSe because much thicker samples were used and the measured phases covered a range of several cycles, whereas with the strongly absorbing gold films the phase shifts were less than one cycle. Taking into account possible systematic errors in the values of for example the sample thicknesses, the absolute accuracy of the refractive index measurements is better than $\pm.015$ for gold and $\pm.005$ for the ordinary refractive index of GaSe. The extraordinary refractive index of GaSe was also determined, but because the values obtained are very sensitive to the values of the ordinary refractive index the absolute accuracy of the $n_{//}$ results is about $\pm.11$, with a relative error of less than $\pm.01$. For comparison, Johnson and Christy[16] estimate the accuracy of their determinations of both n and k for the noble metals to be $\pm.02$. Butler

fringe measurements of the refractive indices of GaSe are accurate to ±.01 to ±.015 for the ordinary index (this work and Ref. [11]), and ±.07 for the extraordinary index.

The accuracy of the determination of the extinction coefficient is more difficult to establish. With the strongly absorbing gold films, the extinction coefficient values were estimated to be accurate to within a few percent for the strong laser lines, and to ±.2 with the weak noisy lines. These values were all obtained before the digital voltmeter was interfaced to the computer, and it is felt that with the statistical averaging of a large number of readings the system should be capable of measuring the extinction coefficient to better than 1%. The DVM was interfaced to the computer for some of the measurements on the thin GaSe crystals. The results shown in Figs. 25 and 26 indicate that the relative accuracy is very good, but since the expression which is fitted to the data is much more sensitive to the refractive index than to the extinction coefficient the absolute accuracy cannot be obtained easily. Absolute accuracy is felt to be in the 5-10% range.. The values of k which were less than .001 are not considered to be reliable.

Measurement with the interferometric technique is most difficult when either n or k is large and the other small. Strong absorption prohibits the use of thick films, and thus the variation of phase and optical density must be determined over a narrower range of sample thickness. Although the uncertainties of our measurements on gold do not seem to vary with the actual values obtained, this means that the fractional error becomes very large for small n. Silver, with n = .05 and k = 4.2 at 632.8 nm, has been suggested[18] as the "worst case" test. The closest the present measurements came to these values was with gold at 632.8 nm, where values of n = .26 ±.015 and k = 3.3 ±.1 were obtained. For silver, the technique should be capable of similar accuracy for n and much better accuracy for k because of the improvements made in the measurement of optical density. At the other extreme, with very weakly absorbing materials such as GaSe in the transparent region, the lack of sensitivity of the optical density data

to k results in poor fitted values of k, although the values of n are accurately determined. Thicker samples could be used to increase the absorption but since the phase data is measured modulo 2π, it must be fitted by a piecewise continuous curve, and data would have to be taken at enough thickness values over the full range of thicknesses to ensure an unambiguous fit.

The optical properties of highly opaque materials have generally been determined using reflectivity techniques. Compared to these techniques, the transmission technique has the advantage of being very much less sensitive to surface effects; thus the preparation and handling of samples is much less critical, and the results are more likely to be representative of the bulk properties of the material. The prime disadvantage of the transmission interferometric technique is the need for an intense coherent source. Lasers must be used, and thus the measurements are restricted to the laser lines or the range of the dyes available. A much greater range of wavelengths is available for the reflectivity measurements. The present method is also very time consuming. Measurements must be made at each wavelength on a set of six or more samples of different thickness, which probably have to be prepared separately. Typically four data points can be obtained in one day.

For measurements on weakly absorbing materials, other techniques are probably more suitable for most purposes. The Butler fringe method is more direct, and produces reliable dispersion curves over a wide wavelength range. Values of the refractive indices are obtained at discrete wavelengths corresponding to the maxima of the fringe pattern obtained with each sample. Thinner samples, and hence more widely spread data points, are required to study the absorption region, and there may be a small gap at an abrupt absorption edge where data cannot be obtained reliably. A reasonable interpolation can probably be made through this region. If the response of the system on which the transmission vs. wavelength curves were obtained is well known the same curves can be used to obtain the optical densities at any wavelength.

The programs used to analyse the interferometer data could easily be modified to provide the k values, with refractive index values from the Butler fringe dispersion curves as input data. The region of greatest interest for the absorption measurements is the region near the band edge where the gap in the refractive index data occurs, so there is some reliance on the interpolated part of the dispersion curve. This approach would probably be more accurate than present techniques in which reflectivity corrections are made to a simplified transmission expression. The only advantage that the interferometer has to offer is the ability to step through the band edge region in very small steps, and thus its utility would come if the details of the curves in this region are desired.

The use of an interferometer for the measurement of optical density has the great potential advantage that the output signal is proportional to the amplitude rather than the intensity of the transmitted beam, and thus measurements can be made on much thicker films than would be possible with noncoherent techniques. This advantage is not fully realized with a noisy light source, but the technique still provides accurate results. Moreover, the simultaneous measurement of phase shift and optical density ensures that these values are obtained under identical conditions from the same spot on the sample.

The greatest potential of the interferometric technique is its ability to provide accurate values of the optical properties of thin films of highly absorbing materials. These measurements are not highly sensitive to the condition of the surfaces of the films, and could thus be used as reference points for, or independent confirmation of, reflectivity measurements over part of their measurement range. This would be particularly useful if it could be assumed that surface conditions effect the absolute values of the optical constants to a much greater degree than the features of their variation with wavelength. The technique is sufficiently accurate that it could also be used for a detailed study of surface effects.

5-2 Improvements, Extensions, and Suggestions for Further Work

There are several simple improvements which could be made to the apparatus or technique to improve its performance. The interferometer was designed to include an electro-optic light modulator in the sample arm, but this was found to be unnecessary. The path lengths of the interferometer arms could be substantially reduced, and the beam splitters and fixed mirror could be mounted much closer to their common base. Both of these steps would probably reduce the slow phase drift with time which, although not a serious problem, was annoying.

With a redesign of the sample holder, either a cryostat or a hot finger in an evacuated chamber could be incorporated into the system for measurements in different temperature ranges. If only the sample holder were moved as in the present system, the presence of windows would be compensated for by the sample in/out technique. A cryostat could lead to instabilities due to thermal gradients, and the interferometer loop might have to be placed in an evacuated chamber to avoid this. If semiconductors were to be studied at low temperatures, the possibility of a dependence of the exciton absorption on the sample thickness would have to be taken into account. The technique could also be modified to observe the variation of the optical constants as electrostatic or magnetic field were applied across the sample. For studying films of an easily oxidized material it would be beneficial to fill the interferometer chamber with an inert gas. Even the present sponge box might be suitable for this purpose.

The interferometric technique is sufficiently accurate to make possible an extensive study of surface effects. The measurements reported in the text showed that better agreement between the experimental data and the theory was obtained if surface effects were taken into account, by assuming that surface conditions were the same on all samples and attaching a constant term to each data point. It was shown that by fitting the variation of the phase shift and optical density data as a function of sample thickness, surface effects could be

eliminated in the thick film limit, i.e. with samples thick enough that the effects of multiple internal reflections are negligible. Surface effects can similarly be eliminated in the thin film limit: with very weakly absorbing films, the relative strengths of the successive internally reflected components of the light are almost independent of sample thickness, and any surface effects on these components will also remain constant. The phase and intensity of the emerging beam thus depends only on the relative phases of the components, which are determined by the sample thickness. Weak absorption is a perturbation on this idealized system, but as such it can also be measured. If measurements are made on samples in the intermediate range, in which the relative strengths of the internally reflected components depend on the sample thickness, then the effects due to surface layers would vary, and greater care would be required in the interpretation of the results.

Although the transmission measurements can provide information on surface effects, more accurate information could be gained by modifying the system to measure reflectivity as well as transmissivity. If mirror M1 were replaced by a beam splitter (probably a fairly highly reflecting one) the intensity of the back reflected beam from the sample could be measured directly, or it could be used with the part of the reference beam transmitted by beam splitter BS2 to set up a second interferometer loop. A good quality and well characterized mirror mounted on the sample holder between the sample and "air" positions would be used for comparison in the reflectivity measurements. The same PZT would create the phase sweep in both loops, but the rest of the equipment and part of computer interfacing would have to be doubled, and the programs and procedures changed. A third alternative, which would permit the use of the present equipment and procedures at the cost of simultaneous measurements, would be to rotate the new beam splitter (at M1) by 90 degrees and mount the samples behind it, outside the present interferometer loop, and do separate reflectivity runs. The path lengths of the sample and reference beams in the reflectivity loop would have to be equalized, particularly if the dye laser were to be used.

Samples in the thick film regime would be measured. The true values of the optical constants would be obtained from the transmission measurements, and the differences between measured reflectivity values and those calculated using the "true" optical constants would be attributable to the surface effects. In the thick film limit all samples should have the same reflectivity. The values obtained with a two-loop system would provide a check on reproduceability, and again this procedure would ensure that all measurements were obtained under identical conditions. Phase measurements for the reflectd beam would probably not be possible, since it would be extremely difficult to reproduce the sample position to within a small fraction of a wavelength. However, phase measurements might be useful for studying the changes with time of the surface conditions of a single sample of a highly reactive material.

Initially surface effects in reflectivity could probably be treated phenomenologically, by attaching constant terms to the data as was done with the transmission measurements. Ultimately the proper equations would have to be developed, treating the surfaces as layers of unknown but sample independent thickness and optical constants.

Appendix A

On Butler Fringe Determination of Refractive Index

Under some circumstances, the equation $m\lambda = 2nd$ (120) leads to a very simple method of determining the refractive index from the multiple internal reflection fringe pattern observed at normal incidence. The wavelengths λ and $\lambda + \Delta\lambda$ of two adjacent fringes, with interference orders m and m-1 respectively, are measured. If the wavelength difference between the fringes is small, and if it can be assumed that the variation of n over this small interval is negligible, then applying Equation (120) to the two fringes and eliminating m between them leads to the expression for the refractive index:

$$n = \frac{(\lambda + \Delta\lambda)}{2d\,\Delta\lambda} \approx \frac{\lambda^2}{2d\,\Delta\lambda} \qquad (166)$$

Here only the two wavelengths and the sample thickness must be known. However, the assumption that the variation of n over the wavelength interval is negligible must be treated very carefully[48], a fact that is not always recognized[27]. If the same approach is followed but different values n and $n + \Delta n$ for the refractive index at the two wavelengths are used, the expression for n becomes

$$n = \frac{(\lambda + \Delta\lambda)}{2d\,\Delta\lambda} - \lambda\frac{\partial n}{\partial \lambda} \approx \frac{\lambda^2}{2d\Delta\lambda} + \lambda\frac{\partial n}{\partial \lambda} \qquad (167)$$

This shows that Equation (166) is only strictly valid for a dispersionless material.

A reasonable approximation to the dispersion curve for which knowledge of the interference order is still unnecessary might be obtained as follows. Equation (166) would first be used in a region of low dispersion to generate an initial value of n. This value would be used with (120) to find the interference order, then a dispersion curve would be generated in the region around the initial readings. The slope

of this curve would be used with (167) to obtain a corrected value of n, then the correct value of ω and the final dispersion curve would be generated using (120). The correction would not be exact since the initial dispersion curve would not be correct, but if the procedure were carried out in a region of low dispersion the final dispersion curve should be a reasonable approximation to the true curve.

Appendix B

Programs for the Analysis of Butler Fringe Data

The following set of programs has been developed for the determination of the dispersion curves of weakly absorbing materials from the interference fringes caused by multiple internal reflection in thin parallel-sided samples, as seen in transmission. They were developed for the specific case of uniaxial crystals with the optic axis perpendicular to the surfaces. The locations of transmission fringe maxima are determined, either as wavelength is scanned at constant angle of incidence (normal incidence or oblique incidence with polarization in or perpendicular to the plane of incidence), or as the angle of incidence is varied with the wavelength constant, and with the appropriate polarization.

The programs outlined here are written in BASIC for use with a PDP 11/10 computer equipped with a TU60 Cassette unit and a Decwriter for input. The programs contain options to input and edit new data, read old data, analyse, and store data or results on cassette. They prompt the user for the appropppriate input information, including some information which is no longer relevant but which has been retained so that old data can still be used without changing its format. Entering a set of zeroes terminates data input. All wavelengths are in Angstroms. The programs are stored on cassette.

NENOLI is now used only for entering, editing, and storing new data for wavelength scans at constant angle of incidence. All data sets contain one line for sample identification comments, the number of data points (counted and entered automatically), and a set of eight parameters: 1) ordinary(0) or extraordinary(1) index data, 2) sample thickness (μm), 3) angle of incidence (degrees), and the uncertainties in 4) thickness, 5) angle of incidence, 6) interference order, and 7) wavelength. The final parameter was originally used to identify the material being studied, but is now used to store the correction to the relative interference order which is initially recorded. The data is then entered in pairs, relative interference

order and wavelength, for the successive fringes.

MDROT calculates the sample thickness and interference order from the angles corresponding to fringe maxima obtained when the sample is rotated as wavelength is held constant, with polarization perpendicular to the plane of incidence so that only the ordinary index of refraction is involved. Runs are required at at least two wavelengths, and the difference in m for the two wavelengths must also be known (this is obtained from the wavelength scan at normal incidence). The input information is the identification comment, and for each run, the wavelength, difference in m from the first run, and pairs of the interference order relative to normal incidence and the angle of the fringe. The program fits Equation (124) to all possible pairs of data at each wavelength, as outlined in Section 3-2-2, and prints out thickness with its fitting error, interference order with its error, and the ordinary index with error at the wavelengths of each run. The interference order printed out is for the first normal incidence fringe at wavelength shorter than that of the first run.

NORT calculates the ordinary index from normal incidence wavelength scan data sets stored by NENOLI, using Equation (120). The data is read from cassette, but parameters such as the relative interference order can be corrected if desired. It prints out the sample identification and parameters, then calculates and prints out a table of interference order, wavelength and energy in eV, and ordinary index with uncertainty for each of the stored data points. The results can be stored on cassette.

NAV2L averages the results from several NORT or NERT runs, and fits a third order polynomial in $1/\lambda^2$ to the data. The wavelength range of the fit can be specified, and the input result sets can be weighted. Separate fits above and below a specified wavelength can be obtained. A data proximity limit can be specified, which prevents any region from becoming too heavily weighted (for example if many fringes were recorded near a band edge to check for details of the dispersion curve. With our thickest samples, every 50th or 100th

fringe was normally recorded.) Up to eight result sets can be averaged; if there are less than eight enter 00 to proceed. The program prints out the result sets used, the polynomial parameters, and a table of n at intervals of 100 Å over the range of the data. The result sets and polynmial parameters are stored on cassette.

NERT calculates the extraordinary dispersion curve from oblique incidence wavelength scan data, using a modification of Equation (121):

$$n_{\parallel} = \frac{\sin\theta}{\sqrt{1 - \left(\frac{m\lambda}{2n_{\perp}d}\right)^2}} \qquad (168)$$

It reads a NENOLI data set stored on cassette, then permits a change of the input parameters. It also reads a NAV2L averaged result set for normal incidence results, which it uses to calculate the ordinary index at each wavelength required. It prints out the identification, parameters, and a table of interference order, wavelength and energy, ordinary index, and extraordinary index with uncertainty, and stores the results on cassette.

BTHK2M and BTHN2M calculate sample thickness and the correction to the relative interference order by adjusting them for best fit of a NENOLI data set to a specified NAV2L averaged set, over a specified wavelength range. BTHK2M fits data for wavelengths longer that the absorption edge if the NAV2L averaged results were split at a band edge. BTHN2M fits data at wavelengths shorter than the edge, and is used for the thinnest samples.

N2PLOT plots NORT or NERT results as points, or NAV2L averaged results as continuous curves, on an XY plotter interfaced to the computer. The wavelength and refractive index ranges can be specified.

REFERENCES

[1] F. Abeles, ed., Optical Properties of Solids, North Holland, Amsterdam (1972)

[2] O.S. Heavens, Optical Properties of Thin Solid Films, Dover Publications, New York (1965)

[3] F. Abeles, in Physics of Thin Films Vol. 6, ed. G. Hass and R.T. Thun, Academic Press, New York (1971)

[4] J.E. Nestell and R.W. Christy, Appl. Optics 11, 643, (1972)

[5] M.-L. Theye, Phys. Rev. B 2, 3060 (1970)

[6] Paul H. Smith, Surface Science 16, 34 (1969)

[7] D. den Engelsen, J. Opt. Soc. Amer. 61, 1460 (1971)

[8] F. Meyer, E.E. de Kluizenaar, and D. den Engelsen, J. Opt. Soc. Amer. 65, 529 (1973)

[9] D.J. de Smet, J. Opt. Soc. Amer. 64, 631 (1974)

[10] J.L. Brebner, J. Phys. Chem. Sol. 25, 1427 (1964)

[11] J.D. Wasscher and J. Dieleman, Phys. Lett. A 39, 279 (1972)

[12] F. Goos, Z. Phys. 100, 95 (1936)

[13] F. Goos, Z. Phys. 106, 606 (1937)

[14] C.F.E. Simons, Physica (Utr.) 10, 141 (1943)

[15] L.G. Shulz, Adv. Phys. 6, 102 (1956)

[16] P.B. Johnson and R.W. Christy, Phys. Rev. B 6, 4370 (1972)

[17] P. Joensen, J.C. Irwin, J.F. Cochran, and A.E. Curzon, J. Opt. Soc. Amer. 63, 1556 (1973)

[18] Per Joensen, M.Sc. Thesis, Simon Fraser University (1973)

[19] T.A. McMath, R.A.D. Hewko, O. Singh, A.E. Curzon, and J.C. Irwin, J. Opt. Soc. Amer. 67, 630 (1976)

[20] L.G. Shulz, J. Opt. Soc. Amer. 44, 357 (1954)

[21] L.G. Shulz and I.R. Tangherlini, J. Opt. Soc. Amer. 44, 362 (1954)

[22] G.P. Pells and M. Shiga, J. Phys. C 2, 1835 (1969)

[23] T.A. McMath and J.C. Irwin, Phys. Stat. Sol. a 38, 731 (1976)

[24] T.A. McMath, G. Jackle, and J.C. Irwin, Phys. Stat. Sol. a 43, K151, (1977)

[25] J.L. Brebner and J.-A. Deverin, Helv. Phys. Acta 38, 650 (1965)

[26] G.A. Akhundov, S.A. Musaev, A.E. Bakhyshev, N.M. Gasanly, and L.G. Musaeva, Sov. Phys. Semicond. 9, 94 (1975)

[27] G.A. Akhundov, L.G. Musaeva, and M.D. Khomutova, Opt. Spektrosk. 39, 700 (1975)

[28] A.I. Malik, Z.D. Kovalyuk, and G.B. Delevskii, Sov. Phys. Sol. State 18, 420 (1975)

[29] John David Jackson, Classical Electrodynamics, John Wiley and Sons, New York (1962)

[30] Max Born and Emil Wolf, Principles of Optics, Pergamon Press, Oxford (1964)

[31] L.P. Mosteller Jr. and F. Wooten, J. Opt. Soc. Amer. 58, 511 (1968)

[32] L.N. Hadley and D.M. Dennison, J. Opt. Soc. Amer. 37, 451 (1947)

[33] L.D. Landau and E.M. Lifshitz, Electrodynamics of Continuous Media, Addison-Wesley Publ. Co., Reading, Mass. (1960)

[34] R.M.A. Azzam and N.M. Bashara, Ellipsometry and Polarized Light, North Holland Publ. Co., New York (1977)

[35] Handbook of Chemistry and Physics, 47th Edition, Robert C. Weast ed. The Chemical Rubber Co., Cleveland (1966)

[36] K. Schubert, E. Dove, and M. Kluge, Z. Metallk. 46, 216 (1955)

[37] Z.S. Basinski, D.B. Dove, and E. Mooser, Helv. Phys. Acta 34, 373 (1961)

[38] J.C. Irwin, R.M. Hoff, B.P. Clayman, and R.A. Bromley, Solid State Comm. 13, 1531 (1973)

[39] Model UR1-EL vibration isolators, Lo-Rez Vibration Control Ltd. Vancouver

[40] "International Mathematical and Statistical Library", IMSL Inc., Houston, Texas. These subroutines are permanently stored and available on call in the University's main computer.

[41] M. Schluter, Il Nuovo Cimento 13B N2, 313 (1973)

[42] Gaston Fischer, Helv. Phys. Acta 36, 317 (1963)

[43] H. Kamimura, K. Nakao, and Y. Nishina, Phys. Rev. Lett. 22, 1086 (1969)

[44] M. Grandolfo, E. Gratton, F. Anfosso Somma, and P. Vecchia, Phys. Stat. Sol. b 48, 729 (1971)

[45] A. Bourdon and F. Khelladi, Solid State Comm. 9, 1715 (1971)

[46] M.V. Kurik, A.I. Savchuk, and I.M. Rarenko, Sov. Phys. Opt. and Spectr. 24, 536 (1968)

[47] A. Bosacchi, B. Bosacchi, and S. Franchi, Phys. Rev. Lett. 36, 1086 (1976)

[48] A. Anedda, Appl. Optics 13, 1595 (1974)